

SEA-LEVEL RISE FLOODING AND RELATED IMPACTS: PRIMARY URBAN CORE,  
HONOLULU, HAWAI'I

A DISSERTATION SUBMITTED TO THE GRADUATE DIVISION OF THE  
UNIVERSITY OF HAWAI'I AT MĀNOA IN PARTIAL FULFILLMENT OF THE  
REQUIREMENTS FOR THE DEGREE OF

DOCTOR OF PHILOSOPHY

IN

GEOLOGY AND GEOPHYSICS

December 2019

By

Shellie L. Habel

Dissertation Committee:

Charles Fletcher III, Chairperson

Kolja Rotzoll

Aly I. El-Kadi

Delwyn Oki

Thomas Giambelluca

Keywords: Sea-Level Rise, Groundwater Inundation, Groundwater Modeling, Hazard  
Assessment, Flood Simulations

© 2019, Shellie L. Habel

## ACKNOWLEDGMENTS

*Sea-level rise is like aging. You can't stop it, you can only do it better or worse.*

-Thomas Ruppert, Coastal Planning Specialist, Sea Grant Florida

The challenges brought on by sea-level rise are imminent and in response, communities across the world are taking unique stances towards facing this reality. Overall, the spectrum of responses varies from communities accepting and efficiently managing these challenges over time, to ignoring the issue entirely.

Hawai'i can be proud that it is shooting for the former. Our community is well informed and acknowledging of a complicated future, and the people instrumental in illuminating this reality are talented and tireless in their respective roles. I would like to thank them all. It is impossible to thank them enough.

Specifically, I would like to thank my advisor, Chip Fletcher. For decades he has insisted that we move forward intelligently in our efforts to tackle sea-level rise and climate change related challenges. With all that he does it is remarkable that he finds time to encourage the educational and personal growth of his students. He is a force to be reckoned with and I am so lucky to have his guidance. I would like to thank Kolja Rotzoll for being so generous with his time, his expertise, and his drive for perfection. In addition to establishing the field of research in which this dissertation embodies, he has made this contribution to it much stronger. I am thankful to Delwyn Oki and Aly El-Kadi for providing their expertise and patience, for extending their knowledge of hydrology, and for helping to refine the methods developed in this dissertation. I am thankful to Tom Giambelluca for sharing his expertise regarding the intricate interconnections between surface water and groundwater. I am also very grateful for the assistance from the Hawai'i State Department of Health Leaky Underground Storage Tank Division. The groundwater model presented in this dissertation would not have been as robust without the data provided by their patient staff.

I am also thankful to have collaborated with current, former, and honorary members of the University of Hawai'i Coastal Geology Group. They not only contributed to this research, but also made up the overall wonderful workplace environment of the Nerd Nest and Dork Den. They include Matthew Barbee, Tiffany Anderson, Haunani Kane, Brad Romine, Kristian McDonald, Kammie Tavares, Jin-si Over, Alisha Summers, Anne Mikkelsen, Hannah Cooper, Laura Corley, and Trista McKenzie. I am particularly indebted to Matthew Barbee for so thoroughly sharing his knowledge regarding cartographic mapping methods and analysis of geospatial data. Also, thank you to the staff and faculty who embody the School of Ocean and Earth Science and Technology. This research institution is renowned for both its quality of research and academics. To provide both is rare and commendable.

I am thankful to my colleagues at the University of Hawai'i Sea Grant including Darren Lerner, Darren Okimoto, members of the Dukes of Hazards, and all the amazing members of the UH Sea Grant Staff. I am also thankful to my colleagues at the State Office of Conservation and Coastal Lands. Your endless diligence and creativity help to ensure thoughtful management of Hawai'i's natural resources.

Funding was provided by the Honolulu Board of Water Supply [Award Number C16545003] and the University of Hawai'i Sea Grant Program [Award Number NA140AR4170071]. Critical partnerships also include the U.S. Geological Survey, the Department of Land and Natural Resources Office of Conservation and Coastal Lands, the H.K.L. Castle Foundation, the Honolulu Police Department, the Pacific Islands Climate Science Center, and the City and County Honolulu Office of Climate Change, Sustainability and Resiliency.

Finally, I would like to thank my friends and family. I'd especially like to thank Dan Habel for being the best thing about life and for making it beautiful and sweet. I'd like to thank my Dad, for his service and bravery in Vietnam, and for being the best father he could despite facing his own struggles. Lastly, I would like to thank my Mom, a talented scientist who set aside her own research ambitions so that her children could grow-up somewhere beautiful. I could not have done any of this without her guidance and I attribute any success I have had to her.

## ABSTRACT

Sea-level rise (SLR) induced impacts in Honolulu, Hawai‘i are becoming increasingly apparent such that local government offices are recognizing the need to implement management strategies. Action has been initiated towards exploring local applicability of various adaptation measures; however, such efforts require site-specific data regarding a suite of SLR related vulnerabilities. This dissertation seeks to streamline methods used to identify where, when, and from what source flooding is expected to occur, and in turn, reveal likely impacts to critical infrastructure. Flood sources considered here include narrowing of vertical unsaturated space and groundwater inundation (GWI), storm-drain backflow, and passive direct marine flooding. For proof of concept, the methods are applied to the Primary Urban Core (PUC) of Honolulu; however, the methods are universal such that they can be applied to generally any urban coastal region. The methods explored in this dissertation do not simulate dynamic coastal processes (i.e., coastal erosion, sediment accretion or changes in land cover) and thus are most appropriately applied to regions that host heavily armored shorelines such as the PUC.

Arguably the most challenging source of SLR induced flooding to manage is GWI, as groundwater progressively inundates infrastructure from below the ground surface, and thus requires a separate set of adaptation strategies to manage. Impacts related to SLR induced lifting of coastal groundwater were first revealed as a major threat by Rotzoll and Fletcher (2013). In their study, 1D regression modeling was employed to simulate groundwater elevation as a function of the distance inland, and compared to digital-elevation models to reveal locations vulnerable to GWI. In the first part of this dissertation their method was refined by employing a 3D modeling method (MODFLOW-2005) to simulate water-table elevation, and by using an expanded observation dataset for model calibration. To illustrate the value of the methodology a damage analysis is conducted. Results indicate that SLR of 1 m generates GWI across 23% of the study area encompassing the Waikīkī area and threatens \$5 billion of taxable real estate and 48 km of roadway. Results further reveal that 86% of the 259 active cesspool sites are likely inundated at present, suggesting that cesspool effluent is currently entering coastal groundwater.

In the second part of this dissertation a simpler method of simulating SLR induced GWI is explored. This is accomplished by comparing simulations of groundwater elevation generated using hydrostatic modeling with those generated using the 3D numerical groundwater modeling

approach developed in part one. The study area considered in the second part of this dissertation is expanded relative to that considered in part one, and represents the entire PUC. The specific intent of the study is to explore the effectiveness of the hydrostatic approach in simulating equilibrium aquifer effects of multi-decadal SLR, and in-turn GWI for the study area. Further, the intent here is to spur preliminary understanding of GWI impacts in municipalities that lack the required data to conduct rigorous groundwater-modeling investigations. Results show that hydrostatic modeling in the study area yields similar results to numerical modeling when referencing the local mean higher-high water tide datum (generally typical of flood studies). Thus, the more simplified method can be used to produce preliminary simulations of GWI and in turn to analyze related impacts.

The third part of this dissertation develops a method to identify locations in which SLR induced flooding will result from a combination of mechanisms including 1) direct marine flooding, 2) storm-drain backflow, and 3) groundwater inundation. Using the methods of Thompson et al. (2019), annual flood threshold exceedances are assessed over coming decades considering secular local mean sea level (LMSL) rise, annual LMSL variability, and the annual 99th percentile of astronomical tidal height. With the combined method, near-term scenarios of flooding are produced that consist of high-resolution, site-specific raster datasets featuring water depth generated by the three flood mechanisms. Further, locations vulnerable to infrastructure failure are assessed by superimposing geospatial data that characterize locations of drainage, roadway, and cesspools on flood simulations. Results suggest that flood-management strategies will likely require site-specific engineering that consider multiple flood mechanisms, and that failure to attend to each mechanism individually may render such strategies ineffective. This may lead to a false sense by key decision makers that SLR adaptation has been achieved.

## TABLE OF CONTENTS

ACKNOWLEDGMENTS .....	iii
ABSTRACT.....	v
LIST OF FIGURES .....	ix
LIST OF TABLES.....	xi
Chapter 1 : Introduction .....	1-1
1.1 Value of Sea-Level Rise Flood Simulations and Mapping.....	1-2
1.2 Local Sea-Level Rise .....	1-3
1.3 Study Area.....	1-4
1.4 Objectives and Future Directions .....	1-5
Chapter 2 : Development of a Model to Simulate Groundwater Inundation Induced by Sea-Level Rise and High Tides in Honolulu, Hawai‘i.....	2-7
2.1 Introduction .....	2-7
2.1.1 Study Area: Waikīkī, O‘ahu, Hawai‘i .....	2-10
2.2 Methods.....	2-13
2.2.1 Compilation of Water-Level Measurements: Continuous Water Level Monitoring.....	2-13
2.2.2 Compilation of Water-Level Measurements: Discrete Observations.....	2-15
2.2.3 Groundwater Model Construction and Calibration .....	2-16
2.2.4 GWI Map Generation .....	2-20
2.2.5 Uncertainty .....	2-22
2.2.6 Damage Assessment.....	2-22
2.3 Results .....	2-24
2.3.1 Monitoring Results .....	2-24
2.3.2 Hydrologic Modeling Results.....	2-26
2.3.3 Results of GWI Mapping.....	2-28
2.3.4 Vulnerability Assessment.....	2-29
2.4 Discussion .....	2-30
2.5 Conclusion.....	2-31
Chapter 3 : Comparison of a Simple Hydrostatic and a Data-Intensive 3D Numerical Modeling Method of Simulating Sea-Level Rise Induced Groundwater Inundation for Honolulu, Hawai‘i, USA.....	3-34
3.1 Introduction .....	3-34

3.1.1 Study Area .....	3-37
3.1.2 Sea-Level Rise Projections.....	3-38
3.2 Methods.....	3-38
3.2.1 Groundwater Elevation Data and Subsets .....	3-39
3.2.2 Summary of Modeling Methods.....	3-40
3.3 Results .....	3-45
3.3.1 Test of Model.....	3-45
3.3.2 SLR Flood Simulations .....	3-46
3.4 Discussion .....	3-48
3.5 Summary and Conclusion .....	3-49
Chapter 4 : Compound Flooding Related to Sea-Level Rise and Urban Infrastructure .....	4-51
4.1 Introduction .....	4-51
4.1.1 Study Area .....	4-54
4.1.2 Sea-Level Rise Projections.....	4-56
4.2 Methods.....	4-57
4.2.1 Identification of Flood Thresholds .....	4-57
4.2.2 Flood-Frequency Prediction .....	4-58
4.2.3 Flood Mapping .....	4-58
4.2.4 Damage Assessment.....	4-60
4.3 Results .....	4-61
4.3.1 Results of Mapping Analysis.....	4-61
4.3.2 Frequency Analysis .....	4-67
4.4 Discussion .....	4-68
4.5 Summary and Conclusion .....	4-72
4.6 Appendix .....	4-73
4.6.1 Supplementary Information on the Geohydrology of the Study Area.....	4-73
4.6.2 Supplementary Information on Groundwater-Level Simulation.....	4-74
References Cited.....	4-78

## LIST OF FIGURES

Figure 2-1 : Study area of Waikīkī and surrounding commercial and residential districts on the island of O‘ahu, Hawai‘i.....	2-11
Figure 2-2 : Conceptual model of the freshwater lens located in the basalt aquifer and overlying caprock sediments of O‘ahu’s southeastern coastal plain.....	2-12
Figure 2-3 : Spatial distribution of parameter zones that characterize variations in hydraulic conductivity across the study area. ....	2-18
Figure 2-4 : a) Calibration plot showing observed vs. computed water levels and b) corresponding plot of residual vs. computed water levels.....	2-19
Figure 2-5 : Groundwater level observations at the four monitored well sites in order of shoreline proximity.....	2-25
Figure 2-6 : Simulated water levels reported in meters relative to LMSL representing current conditions with average annual recharge and a 0-m tide stage.....	2-27
Figure 2-7 : Raster visualizations of simulated GWI and narrowed unsaturated space for simulations representing a) current conditions and b) 0.32, c) 0.60, and d) 0.98 m increases in sea-level for a tide height representative of the MMT datum (0.49 m above LMSL). ....	2-28
Figure 2-8 : Spatial calculations of study area percentages considering regions with unsaturated space narrower than 0.33 m, regions with GWI, and the sum of both.....	2-29
Figure 3-1 : Primary Urban Center of Honolulu on the island of O‘ahu, Hawai‘i. ....	3-38
Figure 3-2 : Diagram of model construction.....	3-42
Figure 3-3 : Composite water table simulations considering the influence of MSL and MHHW generated using hydrostatic and 3D numerical simulations, along shore-normal transects (see Figure 3-1 for location).....	3-46
Figure 3-4 : Simulations of 1 m SLR at MSL and MHHW showing GWI. ....	3-47

Figure 4-1 : Observations and illustrations of direct marine flooding, drainage backflow, and groundwater inundation within Honolulu..... 4-54

Figure 4-2 : Infrastructure locations including Class V OSDS (cesspools), storm water conduits and roadway..... 4-56

Figure 4-3 : Flooding and infrastructure failure across the PUC considering minor and moderate flood thresholds..... 4-63

Figure 4-4 : Qualitative comparison of the 35 cm flood scenario in the Māpunapuna industrial area and observations during 2017 king tide events..... 4-65

Figure 4-5 : Days per year of exceedance for minor and moderate flooding per decade. .... 4-67

Figure 4-6 : a) Hawai‘i State Department of Health website (State of Hawai‘i Department of Health, 2019) showing the number of leaking underground storage tanks identified across the State; b) photo showing a construction trench in which contaminated groundwater containing liquid petroleum hydrocarbon was unearthed..... 4-70

## LIST OF TABLES

Table 2-1: For each monitored well site, values of site distance from the coastline, vertical offset from LMSL, tidal lag, and tidal and sea-level anomaly efficiency ..... 2-26

Table 2-2: Results of the damage assessment including taxable parcel and structure real estate considering damages to the ground floor, kilometers of inundated roadway, percentage of the total number of active OSDS sites not compliant with current construction regulations, and the number of OSDS sites fully submerged to the ground surface. .... 2-30

Table 3-1 : Comparison of error statistics calculated for model residuals. Simulations considering MSL and MHHW scenarios are analyzed. Calculations include root mean squared error (RMSE), mean ( $\mu$ ), median, skew, standard deviation ( $\sigma$ ), minimum and maximum residual values. .... 3-45

Table 4-1: Areas of flooding by individual and compound flood mechanisms consisting of direct marine inundation, drainage backflow, and groundwater inundation at four flood thresholds: 2017 flood observations, minor, moderate, and major flood thresholds (William V. Sweet et al., 2018). ..... 4-64

Table 4-2: Failed infrastructure: length of roadway (km) featuring dangerous driving conditions; length of roadway impassable by 4 wheel drive vehicles; number of drainage inlets that have no capacity for storm water and instead act as conduits for additional flooding; number of cesspools that are non-functional at filtering effluent and/or are fully flooded to the ground surface. .... 4-64

## **Chapter 1 : Introduction**

Sea-level rise (SLR) related impacts are emerging and aggregating such that planners and managers of coastal municipalities are becoming increasingly aware of the potential consequences. The main intent of this dissertation is to provide decision makers with detailed information about SLR induced flooding and associated impacts to urban infrastructure. With a more thorough understanding of the location, the timing, and the cause of flooding, adaptation efforts can be more effectively streamlined. Here, such information is generated as part of three individual studies that expand upon the body of knowledge regarding SLR induced flood simulation.

As part of the studies presented here, methods are developed that simulate SLR induced groundwater inundation (GWI) and storm-drain backflow. Results are superimposed atop simulations of more commonly considered direct marine inundation to illustrate that SLR induced flooding will result from multiple mechanisms. To identify vulnerable municipal assets, flood simulations are compared to geospatial data that characterize locations of critical infrastructure. The increasing frequency in which simulated flooding is likely to occur is determined by coupling results with analyses produced by Thompson et al. (2019) that describe increasing annual instances of flood-threshold exceedance. For proof of concept, the methods developed as part of this dissertation were applied to the Primary Urban Core (PUC) of Honolulu, which hosts a considerable concentration of municipal assets in low-lying coastal areas.

This dissertation is organized such that the second chapter describes the development of a 3D modeling approach (MODFLOW-2005) that can be used to simulate SLR induced changes in water-table elevation, and in turn, narrowing of vertical unsaturated space and GWI. The methods presented in chapter 2 are data and time intensive, thus the third chapter explores the applicability of the comparatively simple hydrostatic (i.e., bathtub) approach in simulating SLR induced GWI. The fourth and final chapter combines simulations of multiple flood sources (GWI, drainage backflow, and direct marine inundation) and incorporates the results of Thompson et al. (2019) as previously stated. The three chapters were written for publication in peer reviewed journals such that similar information is included in introductions for chapters 2, 3, and 4, and in the sections below that provide general background.

## 1.1 Value of Sea-Level Rise Flood Simulations and Mapping

Over the past century, coastal urbanization has been maximized through implementation of engineering strategies such as shoreline armoring, land reclamation, and gravity-flow drainage. Honolulu, Hawai‘i is a prime example of such activity, as limited tidal ranges have allowed for densification of development in areas featuring minimal elevations. As a result, the tidal elevation required to produce urban flooding is among the lowest in the United States (Sweet et al., 2017) and the potential for SLR related economic losses are the highest in the State of Hawai‘i (Hawai‘i Climate Change Mitigation and Adaptation Commission, 2017).

Over the 20th century, the global mean sea level rose at a rate of  $1.2 \pm 0.2$  mm/yr, and from 1993 to 2016 that rate accelerated to  $3.4 \pm 0.4$  mm/yr (Nerem et al., 2010). Associated flooding from SLR is expected to increase in frequency and magnitude over the remaining century, such that by 2040 it is projected that Honolulu will experience 100 tidal floods per year, not considering the contribution from rainfall (Thompson et al., 2019).

Flooding concerns are further complicated by the influence of sea-level oscillations on coastal groundwater levels, and by the overheight of coastal groundwater elevations relative to sea level. Mainly due to these two factors, coastal groundwater is expected to be the source of substantially more flooding in Honolulu than flooding produced solely by direct marine inundation (Rotzoll and Fletcher, 2013). Flood vulnerability for coastal municipalities hinges largely on freeboard and vertical unsaturated space (Sweet and Park, 2014); the former describes the vertical distance between infrastructure and sea level, while the latter describes vertical unsaturated distance between infrastructure and tidally influenced coastal groundwater. As sea level rises, these distances will narrow and, in some places, become lost altogether. This is expected to produce various mechanisms of flooding (i.e., GWI, drainage backflow, and direct marine inundation) in the form of increasingly severe periodic localized immersion that will be exacerbated during periods of extreme high tide (Firing and Merrifield, 2004). Flooding from heavy rainfall is also likely to be exacerbated due to reduced unsaturated space available for infiltration and reduced options of drainage and runoff (Horton, 1933).

As SLR induced flooding inevitably breaches the elevation of built infrastructure, flood damage will ensue. Various components of underground infrastructure will be, and in some locations already are, the first utilities to be compromised by inundation (Sterling and Nelson, 2013; Veiga, 2014). The array of essential utilities affected includes sewer mains, storm-drain

systems, vented utility corridors, roadway, and on-site sewage disposal systems (OSDS). The potential for inundation of corroded sewer mains and OSDS is especially concerning due to the likelihood of sewage-based contamination of groundwater and thus nearshore waters, to which groundwater eventually flows. In regions such as the Hawaiian Islands where OSDS constitute a major component of sewage treatment, the coastal discharge of contaminated groundwater already presents a serious public health concern (Whittier and El-Kadi, 2014). Thus, in addition to the direct impacts of SLR induced flooding, contamination will likely expand across the ground surface, providing increased opportunity for public exposure as flooding becomes more widespread (Balaraman, 2016).

## **1.2 Local Sea-Level Rise**

In Honolulu, the semi-diurnal tide range is 0.58 m and the local rate of SLR is  $1.41 \pm 0.21$  mm/yr based on monthly mean sea-level measurements at the Honolulu tide station from 1905 to 2015 (National Oceanic and Atmospheric Administration (NOAA), 2017a). Future acceleration in the rate of local SLR is expected to occur; however, the timing and magnitude of acceleration remain uncertain. Projections provided by the Fifth Assessment Report of the Intergovernmental Panel on Climate Change (IPCC) suggest that global mean sea level could rise 0.18 to 0.32 m by mid-century, 0.33 to 0.60 m by 2075, and 0.52 to 0.98 m by 2100 under Representative Concentration Pathway 8.5, the “business as usual” scenario (Church et al., 2013). However, simulations of globally relative rates of future SLR indicate that the component representing the redistribution of ice melt reaches the highest magnitude across the equatorial Pacific, resulting in rates of simulated local SLR in Honolulu exceeding 8 mm/yr over the second half of the century (Spada et al., 2013). Additionally, the contribution of ice melt solely from Antarctica has been reported as having the potential to contribute more than 1 m of SLR by 2100 (DeConto and Pollard, 2016). These, and additional findings that global ice loss is exceeding researchers’ expectations, and that the tropical Pacific region is subject to SLR that will exceed global mean SLR, led Sweet et al. (2017) to develop regional SLR scenarios that significantly exceed IPCC projections. For example, the Sweet et al. (2017) “Intermediate High” scenario for global mean SLR is 1.5 m by the end of the century, with an additional rise of approximately 0.5 m for the Hawai‘i region. Because global IPCC SLR projections likely underestimate future rates of local SLR in the Honolulu area, and are out of date with respect to sea-level studies that have been completed since the most recent IPCC report, the upper ranges of the IPCC projections are considered in the present

case study and are referred to in terms of their magnitudes to preserve the relevance of simulation results as SLR projections evolve.

### **1.3 Study Area**

The study area considered in this dissertation encompasses the PUC on the southeastern coastal plain of O‘ahu, Hawai‘i. The city represents a major hub for tourism, international business and military defense; it is estimated that 76% of O‘ahu’s employment is concentrated within the PUC (Hawai‘i Climate Change Mitigation and Adaptation Commission, 2017). The Honolulu metropolitan area features the 4th highest population density in the United States behind Los Angeles, New York City, and San Francisco (Dillinger, 2019), in which 9% of its population reside in the floodplain (NOAA Office for Coastal Management, 2019). The PUC hosts the majority of O‘ahu’s critical infrastructure, including Daniel K. Inouye International Airport, Hickam Field, Honolulu Harbor, Ke‘ehi Lagoon, Honolulu Power Plant, five solid waste collection locations, Hawai‘i bio-waste system, the Māpunapuna industrial area and a sewage treatment plant. Further, the area includes locations popular to residents and visitors including Ala Moana Mall, the Honolulu Convention center and the Waikīkī area. The Waikīkī area is especially vital to the State’s economy as it represents the core of Hawai‘i’s tourism industry, hosting 49,000 jobs and 39% of total Statewide visitor spending (Hawai‘i State Department of Business Economic Development & Tourism, 2018). Owing to the high density of population and economic assets, Honolulu faces the highest potential of economic loss in the State, representing 66% of the total statewide losses resulting from approximately 1 m of SLR (Hawai‘i Climate Change Mitigation and Adaptation Commission, 2017). Further, the area hosts a shallow grade such that small increments of SLR will cause relatively large lateral shifts in the extent of inundation (Kane et al., 2015).

Large swaths of the dense urban network in Honolulu have been developed atop land that was filled over the 19th and 20th centuries. This occurred as part of large-scale land reclamation projects that dramatically altered shoreline locations and topography. Filling of low-lying areas such as shallow coral reef, marshes and salt ponds was undertaken in Kaka‘ako, Kewalo, Honolulu, Waikīkī, and Sand Island, as well as the runway of the Daniel K. Inouye International Airport (Department of Transportation, n.d.; Honolulu Dredging Construction Company, n.d.; Wiegel, 2008). These reclamation projects were spurred by rapid growth in tourism and the military-based economy, such that the PUC has now become intensely developed to the point that

nearly the entire coastline has been engineered or otherwise altered and armored. Interestingly, the State Sea-Level Rise Report has identified many of the areas constructed atop fill as being most vulnerable to SLR related economic impacts (Hawai'i Climate Change Mitigation and Adaptation Commission, 2017); this is the result of projects generally elevating the topography only a few meters above mean sea level.

#### **1.4 Objectives and Future Directions**

The overall objective of this dissertation is to establish a foundation for foresighted planning and policymaking through the development of methods that expand upon SLR-induced flood simulation. The methodologies developed mainly require publicly available data including topographic and bathymetric LiDAR, locations of drainage and other critical infrastructure, water-level measurements, rates of groundwater withdrawals and recharge, and subsurface geology. The flood simulations can be seamlessly incorporated into geospatial platforms to compare with municipal geospatial data sets, toward identification of threatened infrastructure. The simulations can be displayed visually, providing decision makers with a perspective of future scenarios.

Main limitations of the methods presented and avenues for future work are listed below:

- Simulations are steady-state and thus do not assess time-dependent hydrological processes such as variations in recharge, pumping rates, boundary flows and groundwater storage, and aperiodic short-term changes in sea level by phenomena such as storm-surges, tsunamis, etc. Future approaches would benefit from being transient so that variations in these processes could be simulated.
- MODFLOW-2005 assumes a uniform density of water, and thus does not incorporate the influence of density-driven fluid flow such as mixed seawater and freshwater flows. Future approaches could be refined to include consideration of density using modeling systems such as SEAWAT (Langevin et al., 2003).
- Simulations do not consider flow that occurs in the unsaturated zone or surface-water flow, evaporation from surface-water sources, and ponding or routing of waters that occurs once groundwater has breached the ground surface. Future approaches could be expanded to include such processes.
- The simulations do not consider dynamic changes in landscape (i.e., erosion) produced by SLR. Honolulu's coastline within the PUC is unique relative to the more natural

coastlines featured among the Hawaiian Islands in that it is heavily developed and armored. Such changes have been simulated by Anderson et al. (2018). Future work may include combining mapping products so that the method could account for vulnerabilities to erosion in locations that lack coastal armoring.

- Simulations do not include simulation of rainfall induced flooding. Future approaches would benefit from incorporation of this flood component and would require development of dynamic modeling that accounts for the influence of land use on infiltration, exfiltration, and runoff.

Many of the potential avenues of study listed would require additional data for model calibration. Collection of such data could be accomplished through the installation of a monitoring network designed for continuous measurement of salinity, water level, contamination, etc. Studies that explore the various sources of groundwater contamination would also be beneficial for efforts related to remediation, land-use changes, and public welfare.

## **Chapter 2 : Development of a Model to Simulate Groundwater Inundation Induced by Sea-Level Rise and High Tides in Honolulu, Hawai‘i**

Published as: Habel, S., Fletcher, C.H., Rotzoll, K., El-Kadi, A.I., 2017. Development of a model to simulate groundwater inundation induced by sea-level rise and high tides in Honolulu, Hawai‘i. *Water Res.* 114, 122–134. doi:10.1016/j.watres.2017.02.035

*Abstract* - Many of the world’s largest cities face risk of sea-level rise (SLR) induced flooding owing to their limited elevations and proximities to the coastline. Within this century, global mean sea level is expected to reach magnitudes that will exceed the ground elevation of some built infrastructure. The concurrent rise of coastal groundwater will produce additional sources of inundation resulting from narrowing and loss of the vertical unsaturated subsurface space. This has implications for the dense network of buried and low-lying infrastructure that exists across urban coastal zones.

Here, we describe a modeling approach that simulates narrowing of the unsaturated space and groundwater inundation (GWI) generated by SLR-induced lifting of coastal groundwater. The method combines terrain modeling, groundwater monitoring, estimation of tidal influence, and numerical groundwater-flow modeling to simulate future flood scenarios considering user-specified tide stages and magnitudes of SLR.

We illustrate the value of the method by applying it to the heavily urbanized and low-lying Waikīkī area of Honolulu, Hawai‘i. Results indicate that SLR of nearly 1 m generates GWI across 23% of the 13 km<sup>2</sup> study area, threatening \$5 billion of taxable real estate and 48 km of roadway. Analysis of current conditions reveals that 86% of 259 cesspool sites in the study area, identified as active in 2009, are likely inundated. This suggests that cesspool effluent is currently entering coastal groundwater, which not only leads to degradation of coastal environments, but also presents a future threat to public health as GWI would introduce effluent at the ground surface.

### **2.1 Introduction**

Ongoing sea-level rise (SLR) poses a significant threat to evolving coastal municipalities and mega-cities initially developed under the misconception that sea level would remain approximately stationary (Gornitz et al., 2001; Nicholls, 1995; Spanger-Siegfried et al., 2014).

However, it is now understood that even marginal increases in sea level are cause for concern as, in the United States alone, 3.7 million people live within 1 m elevation of their respective local high tide datum (Strauss et al., 2012). Over the 20th century, sea-level rose at a rate of 1.2 +/- 0.2 mm/yr, and from 1993 to 2016 accelerated to a rate of 3.4 +/- 0.4 mm/yr (Nerem et al., 2010). Initial ramifications are already being observed in the form of tidal flooding and decreased drainage. In parts of New York City, streets flood so regularly that residents joke about giving children wading boots as gifts, and cars require regular brake and muffler changes due to frequent contact with saltwater (Gregory, 2013). In Norfolk, Virginia, vertical rulers have been installed along low-lying streets so that drivers can assess flood-water depth (Gillis, 2016). And in Miami, Florida, some businesses have noted a 15% drop in revenue due to traffic rerouting around flooded areas (Prothero, 2013; Spanger-Siegfried et al., 2014). Such flooding is expected to increase in frequency and magnitude; for instance, by 2040 it is projected that Washington D.C. will experience 388 tidal floods per year, not considering the contribution from rainfall, amounting to multiple flood events per day (Spanger-Siegfried et al., 2014).

Flooding concerns are further complicated by the interaction of coastal groundwater levels with sea level. Because coastal groundwater tables are generally above mean sea level and oscillations are closely tied to those of the ocean surface, groundwater tables rise by a similar magnitude as sea level rises, causing more flooding than predicted by hydrostatic modeling (Rotzoll and Fletcher, 2013). For example, a scenario of 1-m SLR considering groundwater inundation (GWI) is expected to more than double the amount of flooding in Honolulu, Hawai'i produced solely by marine inundation (Rotzoll and Fletcher, 2013). The threat of flooding is unique for each coastal municipality, hinging largely on the vertical extent of unsaturated space between built infrastructure and tidally influenced coastal groundwater (Sweet and Park, 2014). As sea level rises, this space will narrow and, in some places, will be lost altogether. This will produce GWI in the form of increasingly severe periodic localized flooding (Rotzoll and Fletcher, 2013) that will be exacerbated during periods of extreme high tide (Firing and Merrifield, 2004). Heavy rainfall is also likely to cause more extensive flooding owing to reduced unsaturated space available for infiltration and reduced surface drainage pathways (Horton, 1933).

As coastal groundwater levels rise with sea level and inevitably breach the elevation of built infrastructure, flood damage will ensue. Various components of underground infrastructure

will be, and in some locations already are, the first utilities to be compromised by inundation (Sterling and Nelson, 2013; Veiga, 2014). The array of essential utilities affected includes sewer mains, storm-drain systems, vented utility corridors, and on-site sewage disposal systems (OSDS). Storm-drain systems are subject to high water flooding that can impact urban activities. The potential for inundation of corroded sewer mains and OSDS is especially concerning owing to the likelihood of sewage-based contamination of groundwater. In regions such as the Hawaiian Islands where OSDS constitute a major component of sewage treatment, the coastal discharge of contaminated groundwater already presents a serious public health concern (Whittier and El-Kadi, 2014). As GWI becomes more widespread, contamination will be present at the ground surface, providing increased opportunity for public exposure (Balaraman, 2016).

Various offices in local and state government recognize that ongoing SLR will necessitate the development of adaptive design standards with regard to land-use policy, infrastructure, and hazard mitigation (National Research Council (NRC), 2011; New Jersey Department of Environmental Protection (NJDEP), 2013; Savonis et al., 2008; US Army Corps of Engineers (USACE), 2013). Adopting such standards is judicious; however, the lack of available hazard projections and site-specific mapping is a limiting factor and has been cited as one of the principal impediments to adaptation related policy (Bierbaum et al., 2013). The production of such hazard maps requires consideration of numerous distinct, yet interrelated regional characteristics that pertain to a municipality's SLR related flood risk. These include locally unique rates of SLR, tidal range, topography, subsurface geology, water-table elevation, groundwater flow, and tidal-influence on groundwater.

The purpose of this study is to develop a method that can be used to simulate flood scenarios in urban municipalities resulting from inundation by tidally influenced groundwater. The method goes beyond simple hydrostatic modeling that assumes flooding based solely on ground elevation relative to sea level. Here we account for the over-height of the groundwater table with respect to sea level and consider the decay of tidal effects with increasing distance from the coastline, which is generally overlooked in hydrostatic modeling. Further, we employ a quasi-three-dimensional groundwater model calibrated with a comprehensive collection of water-level observations, which allows simulated water levels to vary in the cross-shore direction, an improvement compared to the one-dimensional simulation of water levels produced by Rotzoll

and Fletcher (2013). The method mainly requires data that is publicly available for many regions including topographic and bathymetric LiDAR, water-level measurements, rates of groundwater withdrawals and recharge, and subsurface geology.

The model output can be seamlessly incorporated into geospatial platforms to compare with municipal geospatial data sets, toward identification of threatened infrastructure and quantification of future damage considering threatened taxable real estate. The output can also be displayed visually, providing decision-makers with a perspective of future scenarios. Specifically, the objectives of this method are to 1) gain an understanding of the hydrologic effects of SLR on coastal water-table elevations across a site-specific dense urban setting, 2) estimate the areal extent of GWI and expected narrowing of unsaturated space resulting from SLR-induced groundwater lift, and 3) produce maps that illustrate localized regions at risk of GWI resulting from SLR at a specified tide stage.

### **2.1.1 Study Area: Waikīkī, O‘ahu, Hawai‘i**

For proof of concept, the method was applied to the Waikīkī area on the island of O‘ahu, Hawai‘i. Waikīkī is the gateway of Hawaiian tourism, accounting for nearly half of tourism statewide, supplying more than 72,000 jobs, and providing 8% of the gross state product (Department of Business: Economic Development and Tourism, 2003). At present, the Waikīkī coastal zone has generally narrow unsaturated space such that many construction projects working below the ground surface require dewatering of worksites. The conjunction of tidally influenced groundwater and narrow unsaturated space produces localized temporary flooding during extreme tide events (Firing and Merrifield, 2004), requiring only a 20 cm tide above the mean higher high water (MHHW) datum to produce such flooding (Sweet, 2014). It follows that as SLR continues, unsaturated space will become progressively narrowed or eliminated altogether, resulting in chronic GWI.

#### **2.1.1.1 Background**

The study area is located on the southeastern side of the island of O‘ahu, Hawai‘i (Fig. 2-1). It is situated atop a low-lying coastal platform that is bounded to the northeast by an eroded and fragmented shield volcano known as the Ko‘olau Volcano, to the east by a volcanic tuff cone known as Diamond Head Crater, to the west by Honolulu’s principal seaport, Honolulu Harbor, and to the south by the coastline.

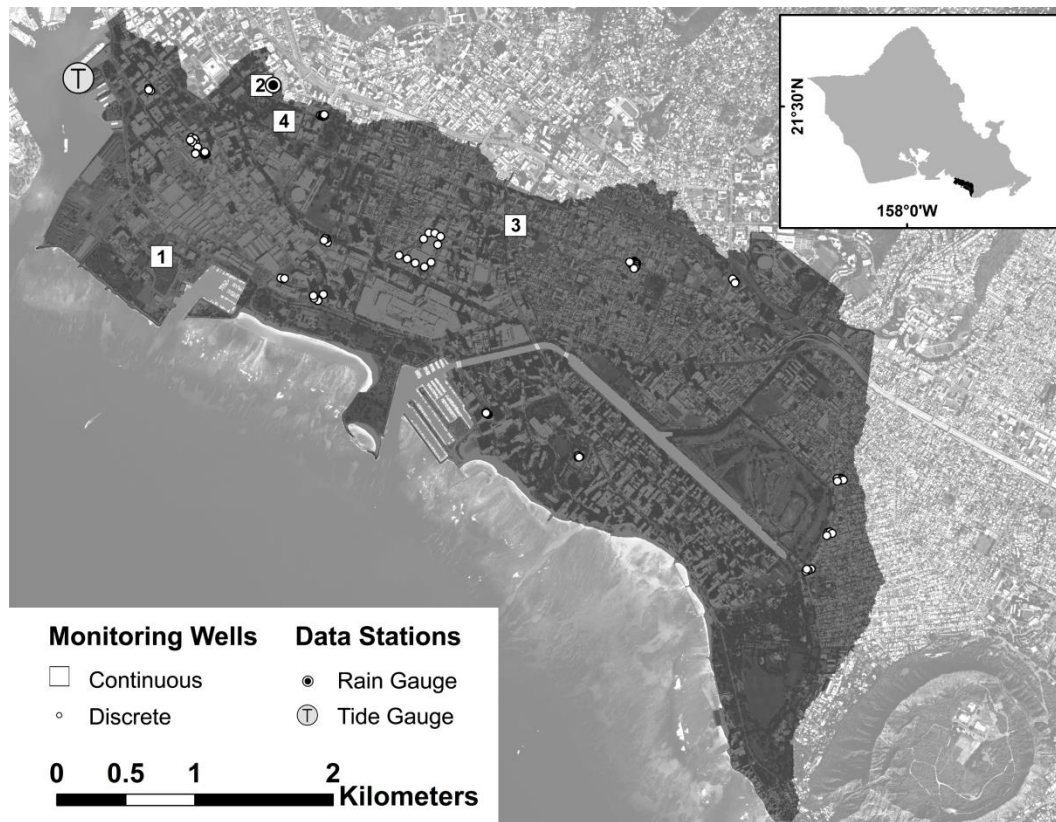


**Figure 2-1** : Study area of Waikīkī and surrounding commercial and residential districts on the island of O‘ahu, Hawai‘i. The shaded area shows the study region. Locations of wells from which water-level observations were obtained are shown.

The southeastern coastal plain of O‘ahu is composed of a mixture of post-erosional volcanics, eroded alluvial debris from the Ko‘olau Volcano and sedimentary deposits produced by Pleistocene sea-level variations including lagoonal deposits, coral debris, and coral ledges. These materials make up the geologic unit referred to as caprock, which lie atop the basalt of the Ko‘olau Volcano (Finstick, 1996; Oki et al., 1998; Stearns and Vaksvik, 1935). Nearly the entire study area has been further overlain by heterogeneous human-placed fill consisting mainly of coralline sand and gravel (Finstick, 1996).

Groundwater within O‘ahu’s southeastern coastal plain occurs primarily in the freshwater lens located in the basalt aquifer, and secondarily in caprock sediments (Gingerich and Oki, 2000). The freshwater lens floats atop saltwater due to density differences between salt and freshwater (Fig. 2-2) and with an interface that is roughly approximated by the Ghyben-Herzberg principle (Macdonald et al., 1983). Groundwater from the lens system migrates from inland recharge areas to coastal discharge areas (Souza and Voss, 1987).

Lower permeability caprock acts as a semi-confining layer to the freshwater lens along the coastline by partially obstructing flow (Stearns, 1935).

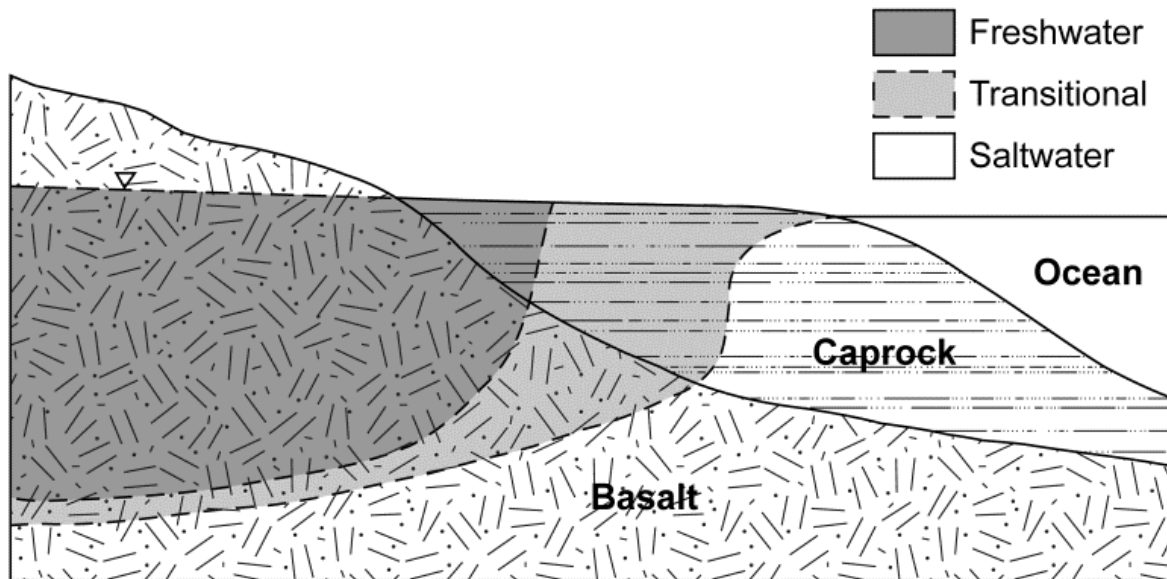


**Figure 2-2 :** Conceptual model of the freshwater lens located in the basalt aquifer and overlying caprock sediments of O‘ahu’s southeastern coastal plain. The lens floats atop higher density saltwater and a transitional brackish-water boundary.

Within the caprock aquifer, the uppermost limestone unit is unconfined and contains mainly brackish non-potable water that is highly vulnerable to contamination from the adjacent urban setting (Visher and Mink, 1964) Well withdrawal from the caprock aquifer is mainly employed for small-scale irrigation and for use in cooling towers (Whittier et al., 2010). Groundwater in the caprock aquifer is influenced by rainfall and marine oscillations generated by the tide and seasonal sea-level anomalies (Gonneea et al., 2013; Ponte, 1994; Wu et al., 1996; Yin et al., 2001). Marine oscillations become damped, decreasing in amplitude and increasing in lag as oscillations propagate further inland (Li and Barry, 2000).

Groundwater flow to the caprock aquifer occurs as water moves down-gradient from underlying basalt aquifers and discharges into the caprock and the ocean. Surficial recharge to the caprock aquifer stems from infiltration of rainfall, water main leakage, septic leachate, seepage from reservoirs and cesspools, and irrigation (Engott et al., 2017).

### **2.1.1.2 Local Sea-Level Rise**

In Honolulu, the semi-diurnal tide range is 0.58 m and the local rate of SLR is 1.41 +/- 0.21 mm/yr based on monthly mean sea-level measurements at the Honolulu tide station from 1905 to

2015 (National Oceanic and Atmospheric Administration (NOAA), 2017a). Future acceleration in the rate of local sea level is expected to occur; however, the timing and magnitude of acceleration remain uncertain. Projections provided by the Fifth Assessment Report of the Intergovernmental Panel on Climate Change (IPCC) suggest that global mean sea level could reach 0.18 to 0.32 m by mid-century, 0.33 to 0.60 m by 2075, and 0.52 to 0.98 m by 2100 under Representative Concentration Pathway (RCP) 8.5, the “business as usual” scenario (Church et al., 2013). However, simulations of globally relative rates of future SLR indicate that the component representing the redistribution of ice melt reaches the highest magnitude across the equatorial Pacific, resulting in rates of simulated local SLR in Honolulu exceeding 8 mm/yr over the second half of the century (Spada et al., 2013). Additionally, the contribution of ice melt solely from Antarctica has been reported as having the potential to contribute more than 1 m of SLR by 2100 (DeConto and Pollard, 2016). Since global IPCC SLR projections likely underestimate future rates of local SLR in the Honolulu area, and are out of date with respect to sea-level studies that have been completed since the most recent IPCC report, the upper ranges of the IPCC projections are considered in the present case study and are referred to in terms of their magnitudes to preserve the relevance of simulation results as SLR projections evolve.

## **2.2 Methods**

Our method toward assessing the effect of SLR on tidally influenced water-table elevations and associated GWI includes six main components; 1) continuous groundwater-level monitoring, 2) compilation of discrete groundwater-level measurements, 3) estimation of tidal efficiency, 4) development and calibration of a groundwater-flow model, 5) generation of flood maps, and 6) completion of a damage assessment. The following sections detail each component of the method.

### **2.2.1 Compilation of Water-Level Measurements: Continuous Water Level Monitoring**

Continuous observations of water level were taken to evaluate the influence of ocean oscillations on coastal water levels within the study area. Monitoring was accomplished at existing well sites established by the Department of Health Underground Storage Tank program. This federally mandated program manages privately and publicly owned underground storage tanks and installs shallow observation wells upon detection of contaminant leaks. The presence of these wells provides a unique opportunity to monitor water levels in heavily urbanized areas where monitoring opportunities would otherwise be limited.

The monitoring network employed in this study consisted of four shallow (<10 m depth) wells (Fig. 2-1), penetrating only the caprock, that were monitored for several months at intervals ranging from 5 to 15 minutes. Data acquired during monitoring included groundwater pressure changes and temperature. The readings were converted from pressure measurements to water levels (m). The elevation of the ground surface at each well location was obtained using the nearest data point represented in 2013 NOAA LiDAR data (National Oceanic and Atmospheric Administration (NOAA), 2017b). Elevations were not obtained through leveling due to the poor condition and control of benchmarks near well locations, which would have provided reduced accuracy relative to the 2013 NOAA LiDAR dataset, which has 1 m horizontal resolution and 0.15 m vertical resolution. Ground elevations were used to reference groundwater levels relative to local mean sea level (LMSL).

Groundwater levels were compared to ocean levels to evaluate the influence of long-period (sea-level anomaly) and short-period (tidal) ocean oscillations at inland locations. Sea-level anomaly is the deviation of the non-tidal ocean level from LMSL that occurs over weeks and months. Ocean-oscillation data were recorded at six-minute intervals at the NOAA Honolulu, Hawai'i tide station (Station 1612340) and referenced to LMSL (National Oceanic and Atmospheric Administration (NOAA), 2017a) (Fig. 2-1). To separate tidal from sea-level anomaly oscillations, a weekly-moving average was applied to the tide-gage and groundwater data, which effectively removes the semi-diurnal and diurnal oscillations associated with the ocean tide. The weekly-moving average represents the sea-level anomaly, while the pure tidal signal is calculated by subtracting the sea-level anomaly from the tide-gage data. Groundwater levels were additionally compared to rainfall data for analysis of potential relations to groundwater elevation. Rainfall data were acquired for the Beretania Pump Station (Network ID GHCND:USC00510211) (National Oceanic and Atmospheric Administration (NOAA), 2016), located within approximately 2 km of all monitoring sites.

The influence of ocean oscillations was quantified for each well by calculating tidal phase lag, and tidal and sea-level anomaly efficiency. The tidal phase lag was evaluated by cross correlating tidal signals at the Honolulu tide station with tidal signals observed in the groundwater data. Tidal efficiency, which describes the amplitude ratio between groundwater-level oscillations and ocean oscillations, was found using linear least-squares regression of lag-corrected

groundwater time series to tidal-signal data. The slope of the regressed line quantifies tidal efficiency, while the y-intercept quantifies mean elevation of the groundwater level relative to mean ocean level.

Long-period oscillations of sea-level anomaly efficiency were found similarly using linear least-squares regression of weekly-moving averaged groundwater time series to sea-level anomaly data. The lag of the groundwater data to sea-level anomaly was too small to be considered. The tidal and sea-level anomaly efficiencies were used to remove both oscillations at the discrete measurements. For that purpose, a linear least-squares regression of lag as a function of distance of the observations from the coastline and exponential regressions of tidal and sea-level anomaly efficiencies as a function of distance from the coastline were completed.

### 2.2.2 Compilation of Water-Level Measurements: Discrete Observations

Ninety-five discrete water-level measurements (Fig. 2-1) that include information regarding time of measurement and surveyed elevation were acquired from Department of Health Leaky Underground Storage Tank records; measurements were taken between 1992 and 2008. Groundwater-level data were corrected with respect to the tidal efficiency, sea-level anomaly efficiency, and tidal lag as a function of distance from the coastline to represent the mean water level at that location. Groundwater levels corrected for ocean oscillations ( $wl_{corr}$ ) at the lag corrected time of measurement were calculated by:

$$wl_{corr} = wl - sl_{tide @ time T-Lx} e^{ax} - sl_{anom} e^{bx},$$

where

$wl$  is the measured groundwater level (m relative to LMSL),

$sl_{tide}$  is the tidal signal (sea-level anomaly removed) at the time of the groundwater measurement corrected for tidal lag (m relative to LMSL),

$sl_{anom}$  is the sea-level anomaly (weekly moving average ocean oscillation) (m above LMSL),

$a$  is the slope of the exponential relation between tidal efficiency and distance from the shoreline,

$b$  is the slope of the exponential relation between sea-level anomaly efficiency and distance from the shoreline,

$x$  is the distance from the shoreline (m).

$T$  is the time the groundwater measurement was taken (local standard time: year, month, day, hour, min)

$L$  is the slope of the linear relation between tidal lag and distance from the shoreline (min/m)

### **2.2.3 Groundwater Model Construction and Calibration**

A groundwater-flow model was developed to simulate steady-state water levels at LMSL in the unconfined caprock aquifer considering the current elevation of sea level and increases in sea level of 32 cm, 60 cm, and 98cm. Hydrologic characteristics used to construct the model were based on regional hydrologic studies (Oki, 2005), ranges in hydraulic conductivity observed within and near the study area (Finstick, 1996), and subsurface geology in the study area (Ferrall, 1976). The numerical model utilized MODFLOW-2005 (Harbaugh, 2005), a quasi-three dimensional cell-centered, finite difference, saturated-flow model.

#### ***2.2.3.1 Model Grid Withdrawals, and Recharge***

The model consisted of 443,602 active 10-m uniform grid cells and two layers, representing caprock and basalt hydrogeologic units. The top of the caprock unit was characterized using 2013 NOAA LiDAR topography data and 2013 U.S. Army Corps of Engineers LiDAR bathymetry data (National Oceanic and Atmospheric Administration (NOAA), 2017b), and the bottom of the unit was characterized using structural contour data that defines the top elevation of the basalt aquifer (Rotzoll and El-Kadi, 2007). Details of the flow in the basalt aquifer unit are beyond the scope of this study. Therefore, such an aquifer was represented by a thin unit that extended an arbitrary 1 m below the base of the caprock and was included exclusively to simulate flow from the basalt into the caprock aquifer. Horizontal hydraulic conductivity for the second unit was defined as 600 m/d based on values reported in modeling studies that simulate local basalt aquifers (Izuka et al., 2018; Rotzoll and El-Kadi, 2007).

Well locations and withdrawal rates available from the State Commission on Water Resource Management were adopted from existing groundwater-flow models representative of the Honolulu aquifer (Rotzoll and El-Kadi, 2007). Only wells pumping from the caprock were considered. Well withdrawal rates were defined as the arithmetic mean of respective pumping rates

from 1996 to 2005. Since pumping rates did not fluctuate significantly between 1996 and 2005, the average was considered an acceptable representation of the simulated period.

Recharge data were acquired from the mean annual water-budget model for the Island of O‘ahu, Hawai‘i (Engott et al., 2017), which is representative of average climate conditions, 1978 to 2007 rainfall, and 2010 land cover. The hydrological processes simulated in the water-budget model are rainfall, fog interception, irrigation, direct runoff, septic system leachate, and evapotranspiration. Note that fog interception does not directly contribute to recharge in the model area.

### ***2.2.3.2 Boundary Conditions and Simulation of SLR***

The landward, seaward, and bottom boundaries were defined as no-flow boundaries and the upper boundary was defined as a recharge boundary for onshore areas and a general-head boundary for offshore areas. Flow from the bottom unit to the upper unit was simulated using a zonally characterized general-head boundary for the bottom unit. Values of head defined for each zone were based on simulations of confined head in southern O‘ahu (Rotzoll and El-Kadi, 2007).

An additional general-head boundary was applied to the upper unit, extending seaward of the 0-m elevation contour, to represent sea-level elevation and coastline position. Increases in sea-level were simulated by raising the general-head boundary from 0 m to 0.32 m, 0.60 m, and 0.98 m for the chosen SLR scenarios, and by migrating the coastline position to corresponding contour lines.

### ***2.2.3.3 Model Calibration***

Calibration accuracy was evaluated by comparing simulated against observed water levels. Several values of horizontal hydraulic conductivity applied to the caprock unit were estimated using the non-linear inverse modeling utility, PEST (Doherty, 2008).

As part of this approach, seven zones were characterized (Fig. 2-3) based on locations of distinct geologic units encountered within the subsurface (Ferrall, 1976). The hydraulic conductivity was defined for two zones prior to executing PEST; the zone labeled HK 50 was assigned a hydraulic conductivity of 1 m/d based on the abundance of cemented and fine grained sediments found offshore (Sherman et al., 1999). The zone labeled HK 30 was assigned a hydraulic conductivity of 65 m/d to replicate results of a drawdown test that had been conducted within the

respective modeled zone (Honolulu Board of Water Supply, 2005). All post-calibration values applied to the model were within the range of values observed inside or just to the west of the study area (Finstick, 1996).

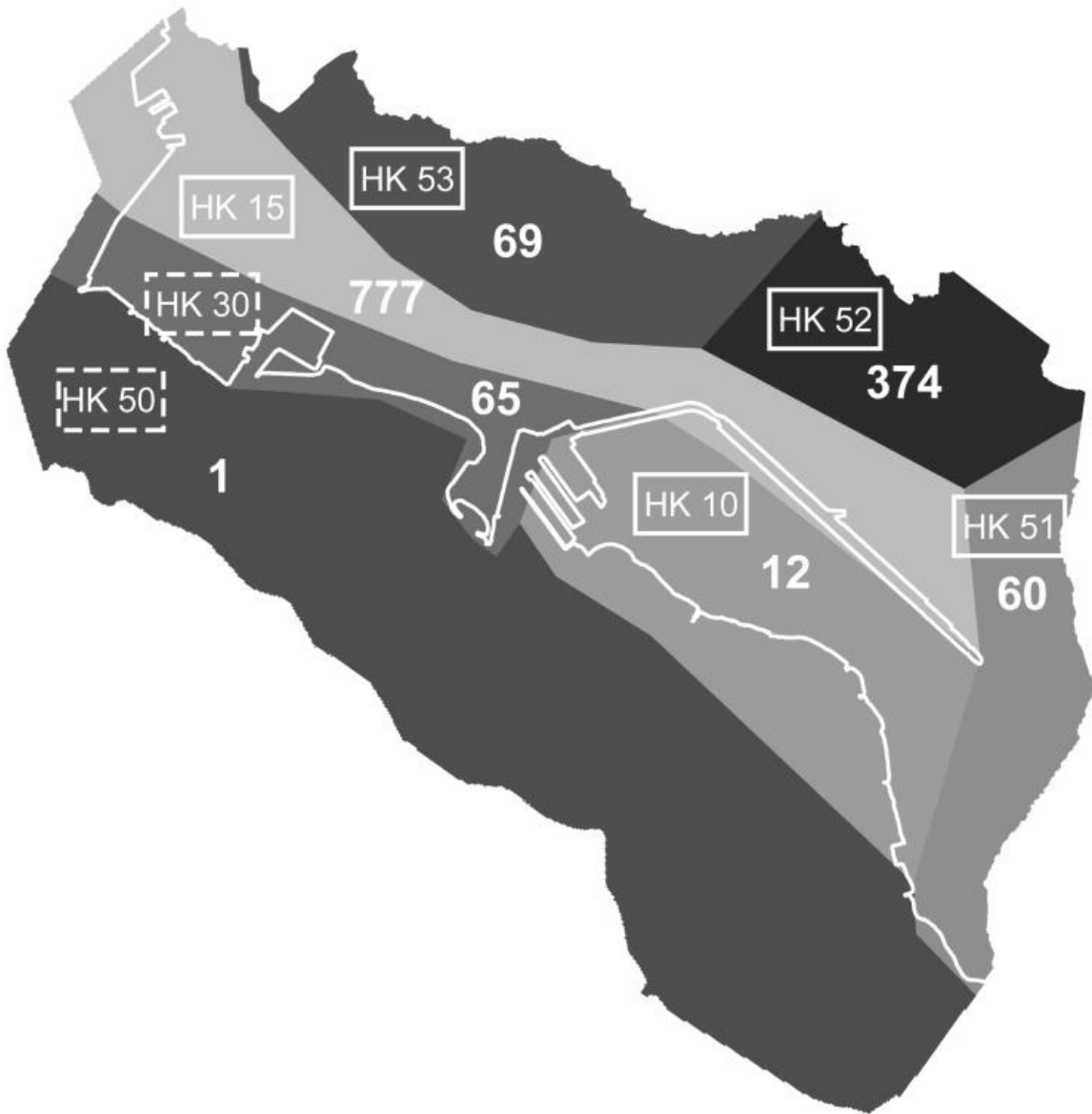


**Figure 2-3 :** Spatial distribution of parameter zones that characterize variations in hydraulic conductivity across the study area. Values of post-calibration hydraulic conductivity are reported in units of m/d; associated zone ID's are shown in white boxes where hydraulic conductivity was calculated using the zonal PEST approach, and in dashed boxes where hydraulic conductivity was defined by other means. The coastline and outer boundary are outlined for reference.

Manual iterative adjustment was employed in the estimation of the conductance parameter of the general-head boundary defined for unit 2, and given a final value of  $0.003 \text{ m}^2/\text{d}$ . The general-

head boundary conductance of unit 1 was pre-defined as  $10 \text{ m}^2/\text{d}$ . Following calibration, the mean residual water level and root-mean-squared error were 0.09 m and 0.12 m, respectively (Fig. 2-4).

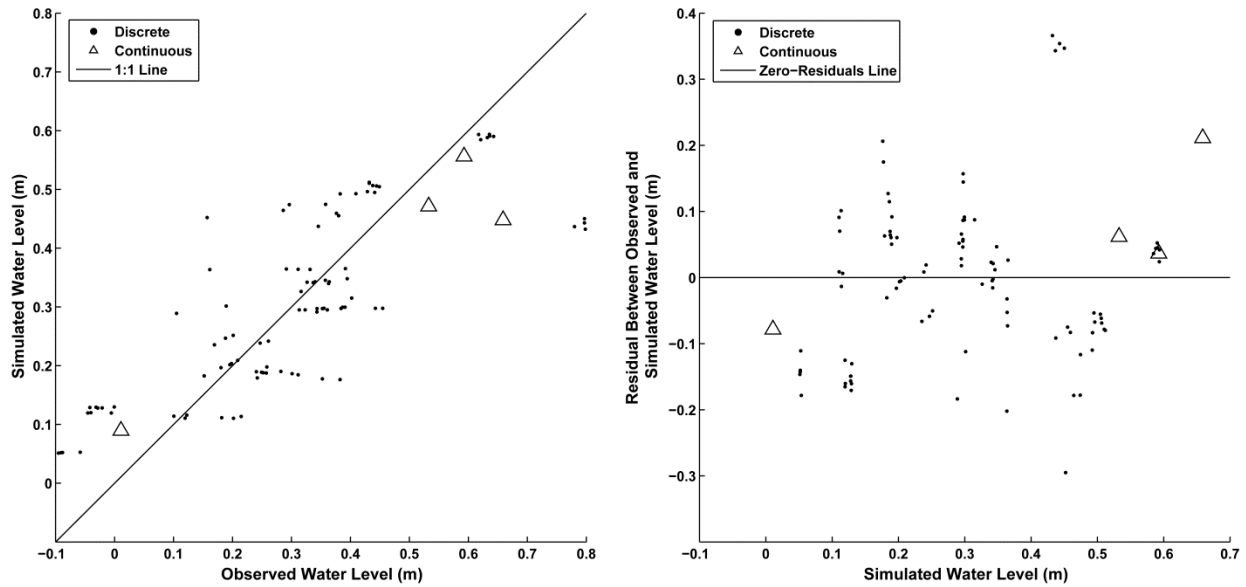


**Figure 2-4 :** a) Calibration plot showing observed relative to computed water levels and b) corresponding plot of residual relative to computed water levels. Discrete water levels are shown as circles and averages of continuous water levels are shown as triangles. Reference lines are included to represent the 1:1 correlation line and the zero-residuals line. The correlation coefficients for continuous and discrete water levels are 0.95 and 0.81, respectively.

#### 2.2.3.4 Model Assumptions and Limitations

In general, numerical models have limitations owing to assumptions inherent in their conceptual design including the governing equations. Simplifications generally lead to overlooking or simplifying certain processes and to ignoring spatial and temporal variability of aquifer parameters. The specific limitations adopted in this study are summarized below.

Simulated steady-state conditions were modeled under the assumption that recharge, pumping, and groundwater flow remain constant. Simulations do not consider small-scale withdrawals that are currently employed across the study area for purposes including construction-site dewatering and mitigation of basement flooding. The simulation is not capable of assessing numerous time-dependent factors including short-term variations in recharge, pumping rates, and boundary flows. The model simulations represent conditions of 30-year average annual recharge and the tide stage relative to mean sea level. They do not include any consideration of anomalous conditions of extreme wet or dry periods or seasonal sea-level anomalies.

The MODFLOW-2005 model assumes a uniform freshwater density, which inhibits the model's capability to simulate the saltwater/freshwater interface, and hence, does not incorporate the influence of density driven fluid flow. Because the caprock aquifer is mainly brackish, the uniform density model was deemed reasonable for use in this study; however, the caprock aquifer does have a freshwater component, thus it would be worthwhile to collect salinity observations across the study area and employ SEAWAT (Langevin et al., 2003) or a similar variable-density groundwater flow model to improve future simulations.

Vertical and horizontal heterogeneity in groundwater environments is prevalent, especially in the caprock aquifer; however, heterogeneities across the study area are poorly understood and thus difficult to include in the design of the conceptual model. Hydrogeologic zones and units were simulated as homogeneous to avoid over-complicating the model, and because detailed hydrologic and geologic information is limited. Thus, heterogeneities in the caprock aquifer were not adequately represented.

Simulations of future conditions assume that GWI occurs when the water table breaches the ground surface; the model does not account for subsequent surface flow, evaporation, or ponding that occurs due to breaching. The model also does not consider flow in the unsaturated zone, which can be relevant for fine materials. Also, what is termed here as unsaturated space is completely dry in the model simulation. With such an assumption, potential risk to utilities is actually underestimated since such areas are not completely dry.

#### **2.2.4 GWI Map Generation**

Digital data surfaces that characterize regions affected by GWI, and regions with severely narrow unsaturated space (defined here as having vertical thickness of less than 0.33 m), can be produced by quantifying vertical proximities between the local terrain and simulated water-table elevations. Local terrain can be simulated by constructing a digital-elevation model (DEM) from regionally specific topographic LiDAR data. Such data is available for many heavily urbanized regions, and can be acquired from NOAA (National Oceanic and Atmospheric Administration (NOAA), 2017b).

For this study, a DEM was produced by merging and hydro-flattening 2013 NOAA DEM tiles. Raw ground return data points describing elevations relative to LMSL were used by NOAA

to generate rasterized DEM tiles with 1-m horizontal resolution. The data have a linear error of 0.15 m; thus, the DEM has a similar linear error across regions defined by high-point density, and slightly higher error across regions defined by low-point density. Hydro-flattening was accomplished to ensure that water-reflected returns were excluded from the DEM by applying an arbitrary constant elevation of -1.5 m to all major waterways, water features, and offshore areas.

Rasterized representations of simulated water tables were constructed by interpolating digital data structures from the xyz point data output of respective MODFLOW simulations. Digital data structures were produced using the triangulated irregular network method of interpolation and subsequently converted into 1x1 m raster grids.

Tidal influence was simulated by applying the 1-D analytical solution for tidal efficiency across a raster grid as a function of the distance of each raster cell from the modeled coastline. The raster grid was produced by calculating the distance of each cell from the 0-m elevation contour and applying the tidal efficiency component of the ocean-oscillation correction equation across the grid to arrive at tidal efficiency values from 0 to 1. The values of each cell were then multiplied by a given tide stage to simulate the tidal surplus. This raster data set was then summed with respective water-table raster data sets to arrive at the tidally influenced water-table height at the given tide stage. The method can be used to simulate any stage within the local tidal range. For this study, the average monthly maximum tidal amplitude (MMT) measured at the Honolulu Tide Station (0.49 m) was chosen for simulation to represent a monthly flood event. The MMT is defined as average maximum monthly tide height measured over the 19-year National Tidal Datum Epoch. The current National Tidal Datum Epoch for the United States is 1983 to 2001.

The final step towards producing GWI maps quantifies the vertical extent of respective SLR-influenced water-table simulations relative to the local terrain. This was accomplished by subtracting each water-table raster grid from the DEM on a cell-by-cell basis. This process produced a series of raster grids in which positive cell values represent locations where the simulated water-table is situated below the modeled terrain and negative cell values where the simulated water-table is situated above the modeled terrain at extents specified by the cell value in meter units.

### **2.2.5 Uncertainty**

Two main sources of error were identified in the uncertainty analysis for vertical disparity between the ground surface and potentiometric surface; these are LiDAR error and calibration MODFLOW error. Vertical error present in the LiDAR data was reported as less than 15 cm (Photo Science Inc., 2013). Error in the MODFLOW simulation was found to be 12 cm based on the root-mean-squared difference between simulated and observed water levels. Water levels and elevations were measured with sub-centimeter accuracy, thus measurement error is assumed to be insignificant compared with the MODFLOW simulation error. The quadrature sum of the two sources of vertical error (LiDAR and MODFLOW simulation) was found to be 20 cm. This measure of vertical uncertainty was used to quantify the lateral uncertainty in GWI rasters, which was accomplished by re-projecting flood and narrow unsaturated space contours (0.33 m relative to the groundwater level) above and below the respective simulated contours considering the 20 cm error. Additional uncertainties are present in the GEOID 12a model, which is used to transform heights between ellipsoidal coordinates and physical height systems. Within the study area, the vertical error in GEOID 12a ranges from 59 to 73.5 cm (Carlson, 2016). The analytical solution that was used to simulate elevated tide stages and to correct discrete groundwater levels considering influence by ocean oscillations assumes uniform tidal and sea-level anomaly attenuation properties across a 1-D transect. Thus, the analytical solution does not account for cross-shore variation of the attenuation properties. Additional conditions that alter the vertical extent of the water table, such as drought, prolonged precipitation and seasonal sea-level anomalies, were not included as part of the vertical uncertainty estimate as simulations are representative of average conditions of annual recharge at the MMT tide stage.

### **2.2.6 Damage Assessment**

To explore the utility of the GWI maps, a damage assessment was carried out that quantifies the extent of municipal infrastructure and taxable real estate threatened by projected increases in water-table elevation.

#### ***2.2.6.1 Taxable Real Estate***

The value of threatened taxable real estate, considering structural assets and property, was assessed for each SLR scenario using the following data sets: 2015 tax data from the City and County of Honolulu's Real Property Assessment Division (City and County of Honolulu (CCH),

2016), geospatial data representing tax parcel locations (State of Hawai‘i Office of Planning, 2016), and geospatial data characterizing building footprint locations (City and County of Honolulu (CCH), 2016). Tax data were merged with geospatial data based on TMK ID to link asset values to their corresponding locations. Merged geospatial data were then compared to GWI raster grids to identify proportions of building areas and property areas affected by GWI. The total value of threatened property was assessed by multiplying each property value by the corresponding percent area affected by GWI and summing all products. The total value of threatened structural assets was quantified similarly; however, structure values representing only the first floor were considered by dividing each structure value by the corresponding number of floors. The sum of the overall threatened property value and overall threatened structure value was calculated to arrive at the total value of threatened taxable real estate.

#### ***2.2.6.2 Municipal Infrastructure***

The potential for roadway inundation was determined for each SLR scenario using a geospatial dataset that characterizes locations of Honolulu City and County Roadway acquired from the State of Hawai‘i Office of Planning (State of Hawai‘i Office of Planning, 2016). The dataset was compared to GWI raster grids to quantify the total length of GWI affected roadway produced by each scenario.

The potential for OSDS inundation was evaluated for each SLR scenario using a geospatial dataset that characterizes active OSDS sites on the island of O‘ahu, acquired from the State of Hawai‘i Department of Health (Whittier and El-Kadi, 2009). The OSDS dataset was compared to GWI raster grids to quantify the number of both fully submerged sites and partially submerged sites lacking the 4.4 m unsaturated space required for cesspool construction according to Administrative Rule, Chapter 11-62 entitled “Wastewater Systems” (Department of Health, 2004). Here we consider fully submerged OSDS sites as potential sources of surface contamination, and partially inundated sites as potential sources of groundwater contamination based on the lack of unsaturated space necessary for sewage filtration. Many existing OSDS sites were constructed prior to the establishment of these requirements, thus their existence has been legally allowed. However, it is prudent to identify potentially inundated sites based on the environmental ramifications that could result from direct seepage of raw sewage into groundwater and floodwater.

## 2.3 Results

### 2.3.1 Monitoring Results

The influence of ocean oscillations and rainfall on water-table elevations at the four monitored well sites was investigated (Fig. 2-5). The corresponding tidal influence parameters were calculated for the four monitored sites (Tab. 2-1). The ocean-oscillation correction equation was derived excluding the anomalous value calculated for Well 3, yielding values of -0.0017 for  $a$ , -0.0002 for  $b$ , and 0.1215 for  $L$  with correlation coefficients of 0.96, 0.41, and 0.95, respectively.

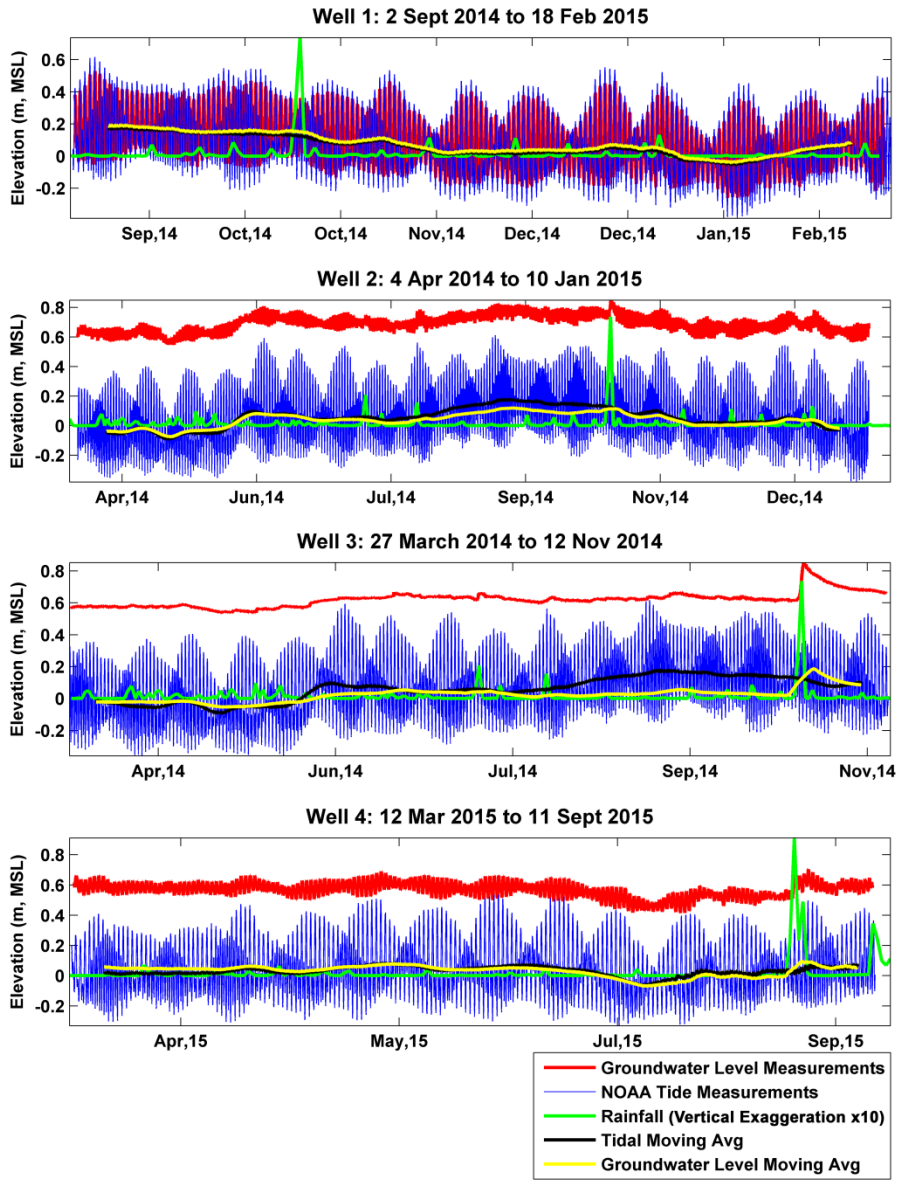


**Figure 2-5 :** Groundwater-level observations at the four monitored well sites. Observations of rainfall in units of meters (x10 vertical exaggeration), the water level at the tide gage, and weekly moving average values of ocean-level and groundwater-level observations (vertically displaced by respective values of offset for clarity).

	<b>Distance to Coast (m)</b>	<b>Tidal Lag (min)</b>	<b>Tidal Efficiency (m/m)</b>	<b>Sea-Level Anomaly Efficiency (m/m)</b>	<b>Offset (m)</b>
<b>Well 1</b>	232	45	0.75	1.02	0.01
<b>Well 2</b>	1042	135	0.13	0.69	0.66
<b>Well 3</b>	867	145	0.002	0.36	0.59
<b>Well 4</b>	1160	130	0.16	1.01	0.53

**Table 2-1** : For each monitored well site, values of site distance from the coastline, vertical offset from LMSL, tidal lag, and tidal and sea-level anomaly efficiency are shown. Tidal lag and offset are correlated to coastal distance, while tidal efficiency is inversely correlated to coastal distance. Heterogeneities in the sediment cause deviation from these trends, and the variation in sea-level anomaly efficiency values.

The influence of tidal oscillations is evident at three of the monitored well sites, with generally higher influence at the site located nearer to the coastline. Water levels observed at Well 3 indicate heavy damping of the tidal signal and sharp increases during rainfall events, specifically during the large rainfall event in September of 2014. The location of Well 3 within a relict river channel suggests that the subsurface is likely comprised of lower permeability, fine grained or weathered sediments, which would explain the elevated water levels during rainfall events owing to reduced rates of infiltration and the damped tidal influence.

The influence of sea-level anomalies is evident at all four of the monitored well sites. Observations from Wells 1 and 4 feature particularly exceptional levels of correlation between long period variations in ocean and groundwater levels; this is based on sea-level anomaly efficiency values and plots of weekly moving average ocean and water-table elevations that approximately mimic each other.

The continued rise in sea level represents an extremely long period ocean oscillation relative to those observed as part of this study; thus, it is expected that corresponding sea-level anomaly efficiencies considering time periods of decades or centuries will be further elevated and will approach 1.0 across the study area. This level of efficiency would produce a nearly 1:1 relationship between magnitudes of SLR and long-term lifting of the coastal water table.

### **2.3.2 Hydrologic Modeling Results**

The simulation of current water-table elevations (Fig. 2-6) illustrates that groundwater levels generally increase with distance from the coastline. Due to the spatial aquifer variability,

the relationship between water-table elevation and shoreline distance is spatially variable. The simulation also illustrates the influence of drawdown at locations where pumping is included in the model. Simulated water levels in the western coastal region of the study area appear to overestimate measured groundwater levels; however these observations consist of anomalously low or negative water-table elevations indicating the presence of localized pumping or karst in the area and the need for further investigation. Simulations showing the influence of SLR on water-table elevations reinforce the assumption that increases in water-table elevations will be approximately equal to magnitudes of SLR.

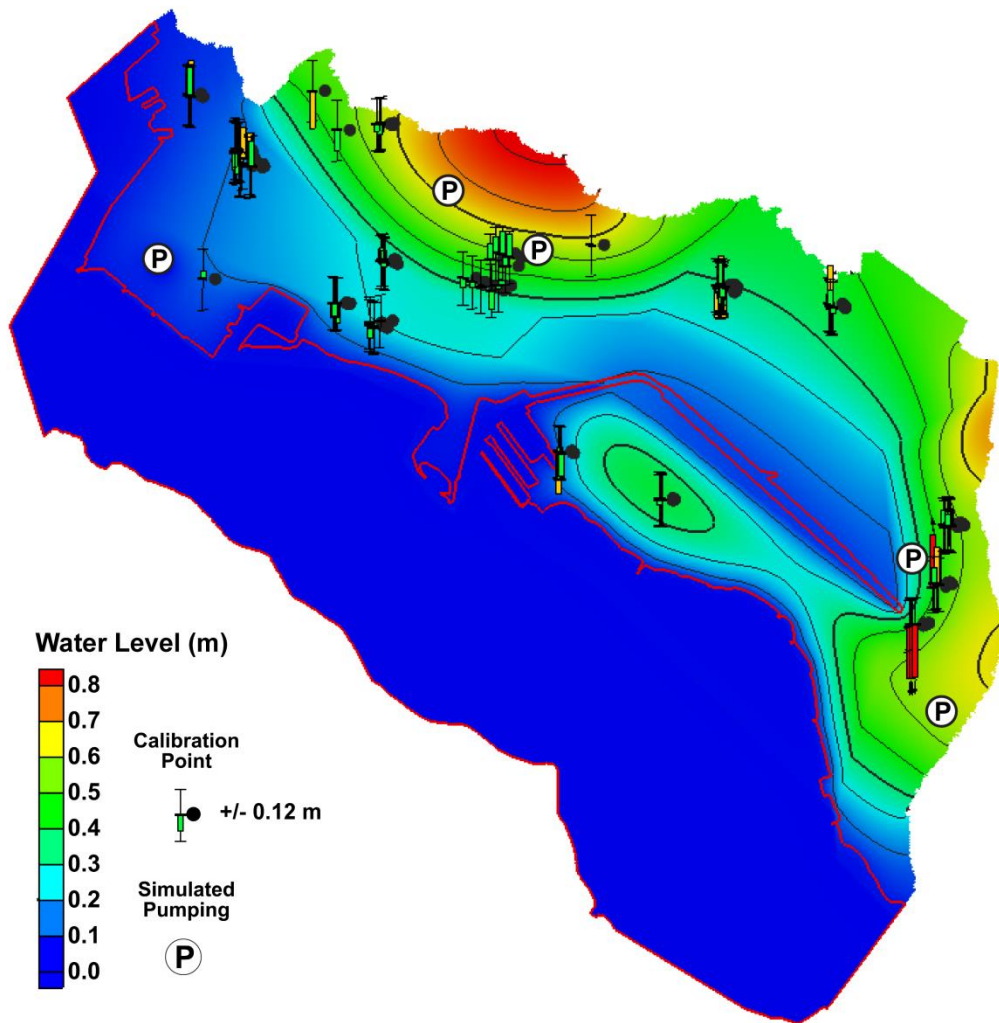


**Figure 2-6 :** Simulated water levels reported in meters relative to LMSL representing current conditions with average annual recharge and a 0-m tide stage. Circles with the letter “P” show the locations of pumping wells. Calibration points are shown to illustrate goodness of fit to observed values. Upward and downward extending bars indicate simulated water levels above and below observed levels respectively. Green bars indicate that computed values are within the model error of 12 cm and orange and red bars indicate computed values in excess of one and two standard deviations, respectively. The red line shows the extent of the coastline and the offshore boundary of study area.

### 2.3.3 Results of GWI Mapping

Raster visualizations illustrate current and future conditions of GWI and narrow unsaturated space (Fig. 2-7). The simulation representing current conditions successfully reproduces water bodies that are present in the study area. However, small pockets of GWI are also simulated in areas not known to flood during the representative tide stage. The simulation was qualitatively compared with images taken of archeological survey trenches that confirm the presence of narrow unsaturated space in multiple regions in which they were simulated.

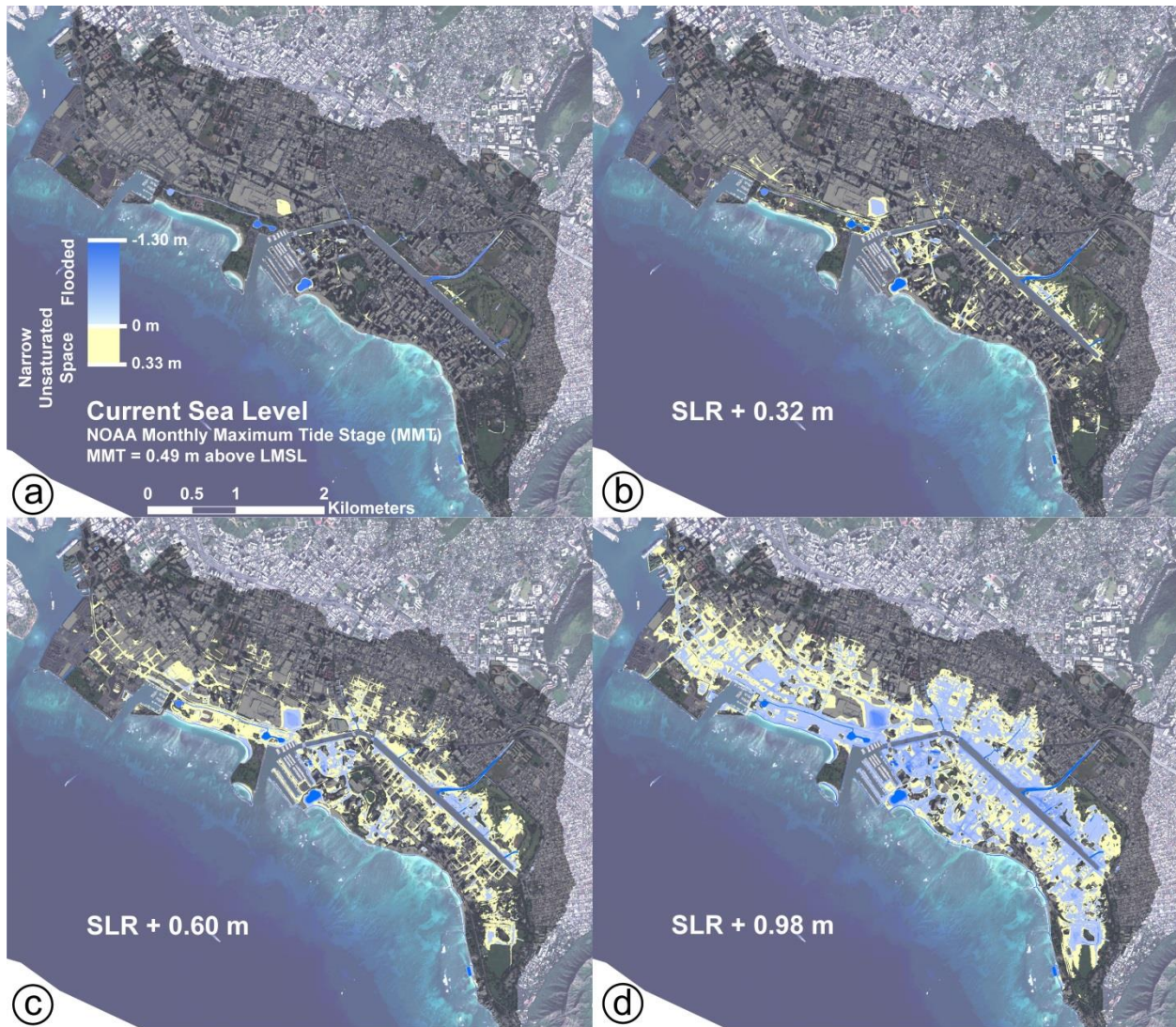


**Figure 2-7** : Raster visualizations of simulated GWI (blue) and narrowed unsaturated space (yellow) for simulations representing a) current conditions and b) 0.32, c) 0.60, and d) 0.98 m increases in sea level for a tide height representative of the MMT datum (0.49 m above LMSL). The study area is indicated by the shadowed region. Estimated vertical error in the distance between terrain and groundwater is +/- 20 cm.

Spatial calculations indicate that 1.1% of the 13 km<sup>2</sup> study area currently hosts unsaturated space narrower than 0.33 m. This extent increases to 5.7% in the + 32 cm scenario, 15.4% in the + 60 cm scenario, and 19.3% in the + 98 cm scenario (Fig. 2-8). The + 98 cm scenario also shows GWI across 23.0% of the study area, which resides mainly in places occupied by heavily used roadways.

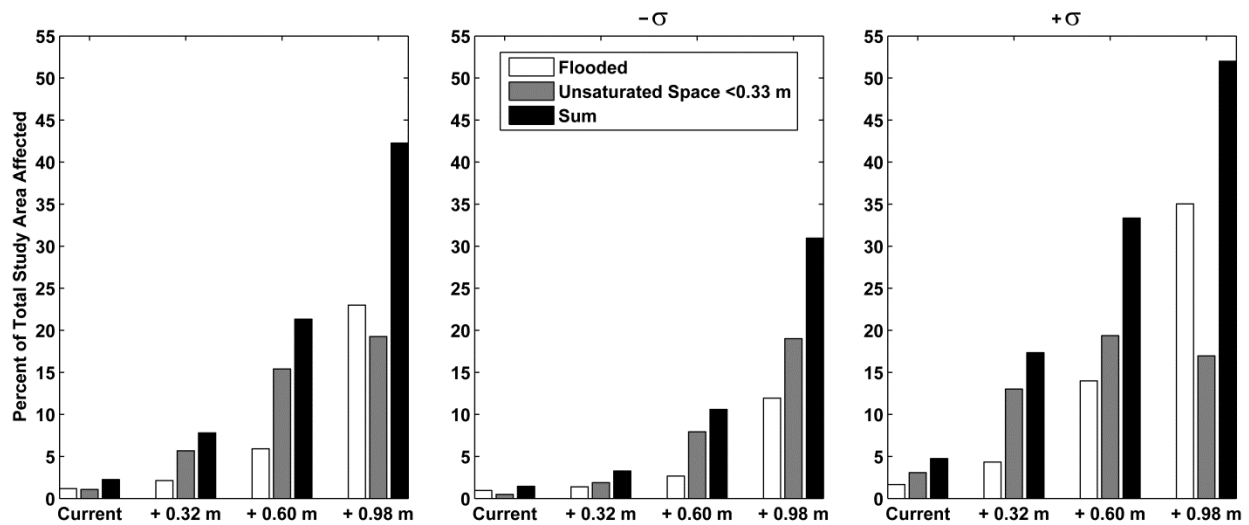


**Figure 2-8** : Spatial calculations of study area percentages considering regions with unsaturated space narrower than 0.33 m, regions with GWI, and the sum of both. Percentages were additionally calculated for scenarios considering the error of +20 cm and -20 cm, denoted here as  $\sigma$ .

### 2.3.4 Vulnerability Assessment

Results of the vulnerability assessment (Tab. 2-2) suggest that more than \$185 million of taxable real estate is currently exposed to flood waters during the MMT stage of the tide. This value increases exponentially over the three respective scenarios, reaching nearly \$5 billion in the + 98 cm scenario. The length of inundated roadway also increases exponentially, covering 0.023 km in the current scenario and increasing to nearly 48 km in the + 98 cm scenario. Results of the OSDS site assessment suggest that 86% of the 259 total active sites present in the study area are not compliant with current construction requirements, with one site shown as being fully submerged. Results considering the + 98 cm scenario indicate that the percentage of non-compliant OSDS sites increases to more than 91%, with 39 sites fully submerged.

Sea Level Rise Projection	Taxable Real Estate (Property and Structures)	Inundated Roadway (km)	Percentage of Total 259 OSDS Sites Likely Inundated	Number of Cesspools Fully Submerged
Current	\$185,319,692	0.02	86%	1
+ 32 cm	\$380,638,276	1.20	90%	1
+ 60 cm	\$1,149,800,027	10.99	91%	5
+ 98 cm	\$4,968,484,196	47.55	91%	39

**Table 2-2:** Results of the damage assessment including taxable parcel and structure real estate considering damages to the ground floor, kilometers of inundated roadway, percentage of the total number of active OSDS sites not compliant with current construction regulations, and the number of OSDS sites fully submerged to the ground surface.

## 2.4 Discussion

This study illustrates the utility of a method to identify localized GWI and municipal vulnerabilities that will result from SLR-induced lifting of tidally influenced coastal water tables. GWI represents a source of flooding separate from that of direct marine flooding, and will occur regardless of shoreline hardening. Because tidal ranges are generally normally distributed, it follows that episodic GWI will initially occur at extreme points in the tide, following which it can be expected to increase in magnitude and frequency as the elevation of built infrastructure is progressively breached at more frequently occurring tide stages.

While the main goals of this case study were focused towards assessing future vulnerabilities, results illuminated two issues of current concern for the representative coastal municipality. First, results reveal a potential prevalence of OSDS inundation by groundwater, and thus direct and widespread seepage of untreated sewage directly into coastal groundwater. Contamination by OSDS sites has become a growing concern as climate-change related temperature increases and unsaturated space narrowing reportedly have the potential to reduce the volume of unsaturated soil and oxygen available to treat wastewater (Cooper et al., 2016). Such reduction in sewage treatment would increase the transport of pathogens and thus jeopardize the health of the public and coastal ecosystems (Cooper et al., 2016). Additionally, this contamination will be present at the ground surface as groundwater progressively breaches the terrain. To prevent future surface exposure of contaminants, it may be necessary to remediate soil at OSDS sites that are projected to be fully submerged.

The second issue of current concern is the likelihood that rainfall induced surficial flooding, commonly experienced in the study area, may result from the prevalence of narrow

unsaturated space. During heavy rainfall events, narrow unsaturated space limits the amount of water that can be accommodated through infiltration. It follows that in regions where unsaturated space is narrow (less than 0.33 m), it is likely that rain induced flooding is partially the result of the full saturation of the soil. Further investigation is required to confirm this; however, if found to be true, regions projected to host narrow unsaturated space in the future can also be expected to experience increased rainfall-induced flooding. This will occur in concurrence with the progressive reduction of water accommodation by storm drains. Thus, it can be assumed that raster visualizations indicate tidally induced chronic GWI in regions shown as flooded, and episodic rainfall-induced flooding in regions shown as having narrow unsaturated space.

Based on the presented scenarios, it is envisioned that as infiltration and drainage are diminished, pools of brackish water containing urban pollutants will become increasingly widespread. Buried infrastructure (i.e., basements, cesspools, utility corridors) not designed to withstand continued submersion will experience inundation. These impacts present engineering challenges to economically maintain a dry city. Practical management approaches toward maintaining a dry city would include the installation of groundwater and storm-water pumping units, and the modification of drainage to reduce inflow of seawater during high tide. Alternatively, vulnerable areas could be redesigned to accommodate a certain amount of flooding. Adapted means of transportation, such as elevated mass-transit systems, may be necessary, considering the prevalence of GWI along heavily utilized roadways shown in accompanying simulations. In any case, it will be necessary that submerged infrastructure be constructed to withstand constant submersion in brackish waters, and that OSDS reliant properties lacking sufficiently thick unsaturated space be connected to municipal sewage treatment systems.

## **2.5 Conclusion**

Over the 21st century, sea level is expected to rise to magnitudes that will result in extensive damage to dense networks of buried and surface infrastructure that exist across heavily developed coastlines. The inundation of low-lying areas and buried infrastructure by tidally influenced groundwater has already become chronically damaging in urban municipalities along the East Coast of the United States. In preparation for more extreme and frequent flood events, the identification of vulnerabilities is a necessary step toward designing workable solutions.

This case study illustrates the need to consider coastal groundwater fluctuations in the simulation of SLR-induced flooding and presents a regionally flexible method in which to do so. The method is specifically geared for use in heavily developed coastal regions owing to the generally increased availability and public accessibility of required data sets. The production of flood simulations combines groundwater monitoring, quasi-3 dimensional hydrologic modeling (MODFLOW-2005), 1-D analytical evaluation of tidal influence, and terrain modeling. The model output consists of raster data sets that specify the elevation of the water-table either above or below the simulated terrain, which can be seamlessly integrated into geospatial platforms to conduct various hazard analyses.

For proof of concept, this study applies the method to the Waikīkī area of Honolulu, Hawai‘i. Here we construct flood simulations that consider current conditions and future elevations of sea level projected by the IPCC 5th assessment report considering RCP 8.5 for the years 2050, 2075 and 2100, and a tide stage representative of the mean maximum monthly tide elevation (0.49 m above LMSL). Tidal influence was estimated across the study area based on continuous water-level monitoring in three wells.

The hydrologic model simulation of current water-table elevations was well calibrated using data from monitoring wells in addition to 95 discrete water-level measurements compiled from Department of Health Leaky Underground Storage Tank reports. The calibrated model produced a root-mean-squared residual of 12 cm between observed and simulated groundwater levels. Following calibration, the influence of SLR on water tables was simulated by specifying the modeled ocean elevations for future scenarios of SLR.

Results indicate that approximately 1.1% of the 13 km<sup>2</sup> study area presently has narrow unsaturated space of less than 0.33 m. SLR of 0.98 m raises this extent to 19.3% and produces GWI over 23.0% of the study area. It follows that under 0.98 m of SLR, nearly half (~42%) of the region will likely experience either chronic GWI during elevated stages of the tide, or episodic flooding induced by heavy rainfall. The corresponding hazard assessment indicates that the currently narrow state of unsaturated space likely causes inundation of 86% of 259 active OSDS sites located across the study area, and threatens to fully submerge 39 OSDS sites by the end of the century. This suggests that sewage-based contamination is currently ongoing across the study area. If contamination is indeed ongoing and remains unchecked, serious public health threats

could ensue as groundwaters progressively breach the surface and come into contact with local residents and the millions of visitors who travel to Waikīkī each year.

## **Chapter 3 : Comparison of a Simple Hydrostatic and a Data-Intensive 3D Numerical Modeling Method of Simulating Sea-Level Rise Induced Groundwater Inundation for Honolulu, Hawai‘i, USA**

Published as: Habel, S., Fletcher, C.H., Rotzoll, K., El-Kadi, A.I., Oki, D.S., 2019. Comparison of a simple hydrostatic and a data-intensive 3D numerical modeling method of simulating sea-level rise induced groundwater inundation for Honolulu, Hawai‘i, USA. *Environ. Res. Commun.* 1, 041005. doi:10.1088/2515-7620/ab21fe

*Abstract* - Groundwater inundation (GWI) is a particularly challenging consequence of sea-level rise (SLR), as it progressively inundates infrastructure located above and below the ground surface. Paths of flooding by GWI differ from other types of SLR flooding (i.e., wave overwash, storm-drain backflow) such that it is more difficult to mitigate, and thus requires a separate set of highly innovative adaptation strategies to manage. To spur consideration of GWI in planning, data-intensive numerical modeling methods have been developed that produce locally specific visualizations of GWI, though the accessibility of such methods is limited by extensive data requirements. Conversely, the hydrostatic (or “bathtub”) modeling approach is widely used in adaptation planning owing to easily accessed visualizations (i.e., NOAA SLR Viewer), yet its capacity to simulate GWI has never been tested. Given the separate actions necessary to mitigate GWI relative to marine overwash, this is a significant gap. Here we compare a simple hydrostatic modeling method with a more deterministic, dynamic and robust 3D numerical modeling approach to explore the effectiveness of the hydrostatic method in simulating equilibrium aquifer effects of multi-decadal sea-level rise, and in turn GWI for Honolulu, Hawai‘i. We find hydrostatic modeling in the Honolulu area and likely other settings may yield similar results to numerical modeling when referencing the local mean higher-high water tide datum (generally typical of flood studies). These findings have the potential to spur preliminary understanding of GWI impacts in municipalities that lack the required data to conduct rigorous groundwater-modeling investigations.

### **3.1 Introduction**

Sea-level rise (SLR) presents inevitable challenges for low-lying coastal municipalities (Hallegatte et al., 2013; Hinkel et al., 2014). Even as SLR projections evolve, many researchers

have concluded that flooding will grow progressively damaging within decades (Kulp and Strauss, 2017; Sweet et al., 2018). This is especially true for regions where rates of SLR exceed the global mean (i.e., East and Gulf Coasts of the U.S.) (Sweet et al., 2017). High-tide flooding is already problematic at these locations resulting in drainage failure, road closure, and the deterioration of municipal infrastructure (Sweet and Park, 2014).

To avoid overwhelming losses from flooding and infrastructure failure, adaptive-management consideration ideally would be given to SLR flood scenarios in municipal planning, policy writing, and project implementation (de Moel et al., 2014; Hinkel et al., 2014). This is progressing in several municipalities where locally pertinent SLR flood maps guide planning (Climate Ready Boston, 2016; Hawai‘i Climate Change Mitigation and Adaptation Commission, 2017; Horton et al., 2015; Mitchell et al., 2013; Office of Resilience, Department of Regulatory and Economic Resources, Miami-Dade County, 2016; Rutgers University, n.d.; The New York State Sea Level Rise Task Force, 2010). However, assessment has not progressed in regions lacking the necessary resources to produce such maps, even where similar vulnerabilities to SLR exist. Moreover, the absence of flood simulations has been cited as one of the main impediments to adaptation planning and policy development (Bierbaum et al., 2013).

Groundwater inundation (GWI) has been identified as one of the more problematic components of SLR flooding, because the water table can evade coastal barriers designed to mitigate surface-water inundation as it is lifted through the ground surface (Rotzoll and Fletcher, 2013). Damage to municipal infrastructure will ensue as groundwater rises above critical elevation thresholds; first somewhat discreetly as buried assets become submerged, and then more obviously as groundwater breaches the ground surface (Habel et al., 2017) The GWI component of flooding will occur contemporaneous with, and in some cases ahead of, non-storm marine components (i.e., wave overwash, storm-drain backflow) and will require a separate set of planning and engineering efforts to manage (Habel et al., 2017). Despite the expected significance of GWI in SLR flooding, GWI has not been widely recognized as a critical element of long-range planning.

Studies undertaken in Honolulu, Hawai‘i have been among the first to specifically simulate the GWI component of SLR flooding, using 1D analytical (Rotzoll and Fletcher, 2013) and 3D numerical (Habel et al., 2017) methods. These methods use the diffusion equation to simulate groundwater levels in the coastal zone, and further determine where GWI is likely to develop by

identifying locations where surface topography will fail to accommodate SLR induced increases in water-table height.

GWI has also been simulated using the hydrostatic method, also known as the “bathtub” or “single-surface” approach (Cooper et al., 2013; Cooper and Chen, 2013; Kane et al., 2015). However, this method is more commonly used to identify vulnerability to direct marine flooding by characterizing locations that lie below projected sea level in a digital-elevation model, when referenced to the local mean higher-high water (MHHW) datum (Marcy et al., 2011; Strauss et al., 2012). Elevations are generally referenced to the MHHW datum for consideration of the average daily maximum threshold of local nearshore sea level (National Oceanic and Atmospheric Administration (NOAA), 2017a). Incentive for widespread use of the hydrostatic method lies in the availability of high-resolution Light Detection and Ranging (LiDAR) data (LiDAR Online, 2017; National Ecological Observatory Network (NEON), n.d.; National Oceanic and Atmospheric Administration (NOAA) Digital Coast, 2017; OpenTopography, 2017; U.S. Army Corps of Engineers (USACE) National Coastal Mapping Program (NCMP), 2017; United States Geological Survey (USGS), n.d.). In the U.S., interpretive maps using LiDAR are publicly available (i.e., NOAA SLR Viewer: <https://coast.noaa.gov/slr/>). Use of the hydrostatic method to simulate GWI has thus far been done implicitly only; assuming locations without direct connection to the marine environment, but that nonetheless fall below a reference datum, must represent some combination of GWI and storm-drain backflow. Until now, this assumption has not been tested.

Although the hydrostatic method is favored for its simplicity, it has been criticized as potentially overestimating areal flood extent by including locations lacking direct marine connection (Gilmer and Ferdaña, 2012; Henman and Poulter, 2008). Some studies consider these locations artifacts of model output, and a number of studies have taken steps to exclude them from final flood simulations (Gesch, 2009; Henman and Poulter, 2008; Marcy et al., 2011; Poulter and Halpin, 2008). However, available mapping tools, such as the NOAA SLR Viewer, include and identify disconnected areas to address the likelihood of flooding by flow pathways not resolved in the elevation data (i.e., under bridges or covered channels) (Marcy et al., 2011; Strauss et al., 2012). Although excluding disconnected areas is appropriate for cases in which marine connection is the main process of inundation related to sea-level rise, excluding these areas for cases in which groundwater inundation is important may yield biased results (Bjerklie et al., 2012; Habel et al., 2017; Rotzoll and El-Kadi, 2008).

Here, we assess the hydrostatic method with comparisons to the more comprehensive and data-intensive 3D numerical method. We explore the effectiveness of the simple hydrostatic method in simulating GWI to determine under which conditions its use might be acceptable. Ultimately, our intent is to evaluate a cost-effective and simple method to enable improved assessment of flood impacts related to SLR among municipalities that lack the capacity to conduct rigorous groundwater-modeling investigations.

### **3.1.1 Study Area**

The study area is located on the southeastern coastal plain of O‘ahu, Hawai‘i (Fig. 3-1) encompassing the primary urban corridor of Honolulu. Groundwater here is part of a larger freshwater-lens system in which the uppermost 100 to 200 m of the aquifer is unconfined (Macdonald et al., 1983; Rotzoll et al., 2010), and influenced directly by rainfall and near-shore sea-level fluctuations produced by tides, wave set-up, and longer period sea-level variations (Gonneea et al., 2013; Habel et al., 2017; Ponte, 1994; Wu et al., 1996; Yin et al., 2001).

Groundwater in the unconfined aquifer is not potable owing to elevated salinity and urban contamination, and therefore is only extracted for use in small-scale irrigation and cooling towers (Whittier et al., 2010). Flow in the unconfined aquifer is driven by the pressure gradient from the underlying confined aquifer into the unconfined aquifer, and through surficial recharge by rainfall, leakage of water-conveyance infrastructure, and small-scale irrigation (Engott et al., 2017). The subsurface geology comprises post-erosional volcanics, alluvial debris, artificial fill, and reefal carbonates related to Quaternary sea-level high stands (Ferrall, 1976; Finstick, 1996; Izuka et al., 2018; Munro, 1981; Stearns and Vaksvik, 1935).

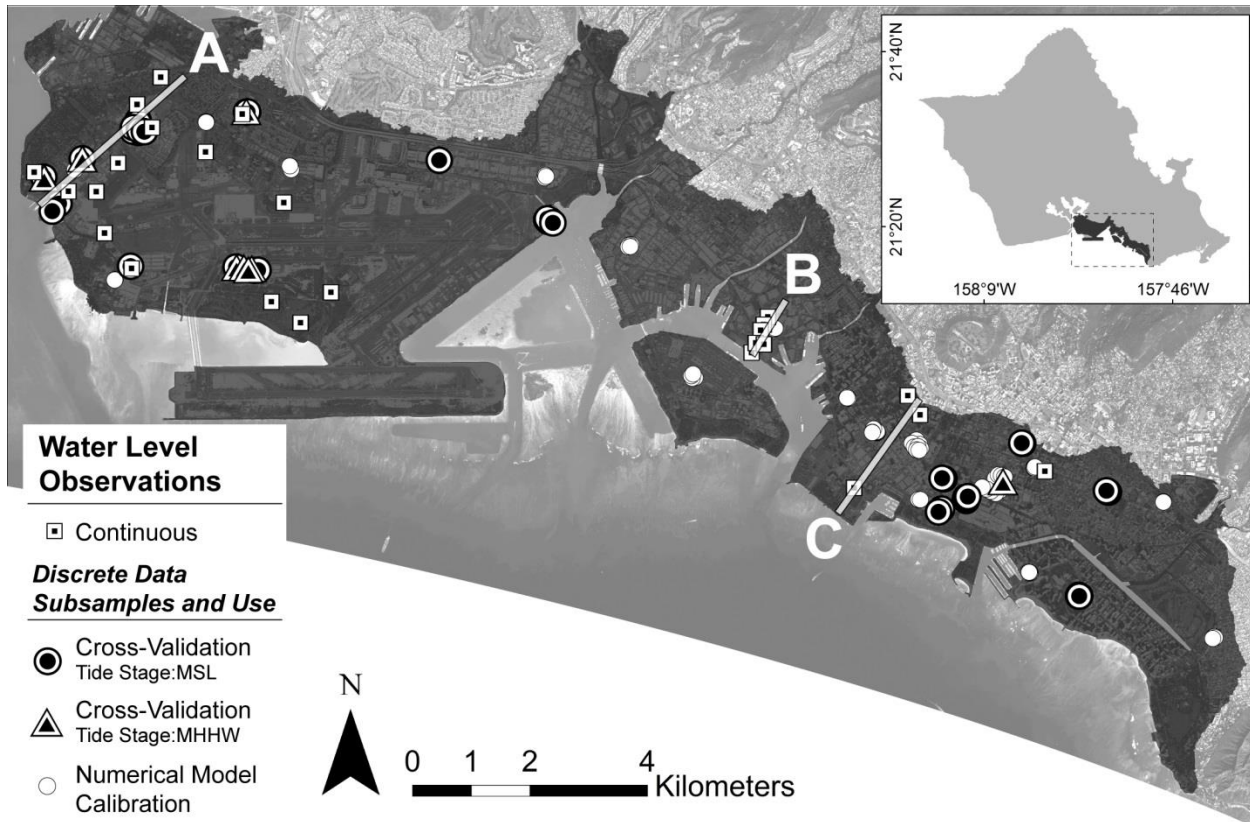


**Figure 3-1** : Primary Urban Center of Honolulu on the island of O‘ahu, Hawai‘i. The shaded area shows the study region including locations of water-level observations. Transects A, B, and C illustrate where groundwater-level simulations are compared in cross sections.

### 3.1.2 Sea-Level Rise Projections

The IPCC Fifth Assessment Report (Church et al., 2013) estimates that global mean sea level could reach magnitudes ranging from 0.52 to 0.98 m by 2100 (relative to 1986–2005) under Representative Concentration Pathway 8.5, the “business as usual scenario.” However, studies incorporating ice-shelf hydrofracturing and ice-cliff collapse mechanisms, triggered under high-emissions scenarios, indicate the potential for higher SLR late this century (i.e., Kopp et al., 2017). Additionally, owing to global gravitational effects (i.e., ice fingerprinting), SLR particular to the Hawaiian Islands will likely exceed the global mean (Kopp et al., 2015, 2014; Spada et al., 2013). For the purpose of this comparison study, when simulating GWI, we consider a SLR magnitude of 1 m, consistent with the intermediate scenario of Sweet et al. (2017).

### 3.2 Methods

Model accuracy is assessed by comparing simulated present-day groundwater levels produced using the hydrostatic and 3D numerical methods to groundwater-level observations

compiled within the study area from monitoring wells. We consider Honolulu's mean sea-level (MSL) tide stage and MHHW tide stage (0.33 m + MSL) in model construction (National Oceanic and Atmospheric Administration (NOAA), 2017a).

The approach used to characterize areas vulnerable to GWI was adopted from similar studies (Cooper et al., 2015; Habel et al., 2017; Rotzoll and Fletcher, 2013) such that GWI is characterized in locations where groundwater elevations exceed the ground-surface elevations. Ground-surface elevations were simulated using a digital-elevation model (DEM) that was constructed by merging rasterized 2013 NOAA DEM tiles. The tiles were produced by NOAA using LiDAR ground-return elevation data referenced to local mean sea level (LMSL) (National Oceanic and Atmospheric Administration (NOAA), 2017b). The elevation data have 0.15 m and 1 m vertical and horizontal resolutions, respectively (Photo Science Inc., 2013).

### **3.2.1 Groundwater Elevation Data and Subsets**

Observations of groundwater elevations were compiled for use in 3D model calibration and to test the accuracy of model simulations. Groundwater-level data available for this study included 247 discrete water-level observations obtained from Hawai'i Department of Health Leaky Underground Storage Tank records (State of Hawai'i Department of Health, 2019), and 73 sets of continuous water-level observations compiled from local hydrologic studies. For model calibration, 193 discrete water-level measurements were spatially subsampled and 49 continuous records were temporally subsampled from the original dataset, and the remaining measurements were used for cross-validation analysis.

Cross-validation compares simulated groundwater levels with two observation subsets representative of the MSL and MHHW scenarios. Compared to oscillations in ocean water levels, groundwater-level oscillations are attenuated, decreasing in amplitude and increasing in temporal lag as oscillations propagate inland. The influence of ocean oscillations was quantified for each set of continuous observations using the methods of Habel et al. (2017) in which temporal lag was evaluated by cross correlating tidal signals at the Honolulu tide station with tidal signals observed in the groundwater data, and tidal efficiency was calculated using linear least-squares regression of lag-corrected groundwater time series to tidal-signal data. To accommodate the tidal-response phenomenon, data in each subset were chosen with consideration of the tidal elevation such that the tide was within 4 cm of the respective MSL or MHHW tidal scenario at the lag-corrected time of data collection. Subsamples consist of 43 discrete measurements representing the MSL scenario,

11 discrete measurements representing the MHHW scenario, and 24 continuous observations used to represent both scenarios. All discrete observations were corrected for anomalous sea-surface height using the methods of Habel et al. (2017). The 24 continuous measurements were processed to represent MSL by calculating average recorded water levels during times with negligible rainfall and non-anomalous sea-surface levels. Measurements were processed to represent MHHW by calculating the average reconstructed tidal influence produced during the MHHW tide stage. Reconstructions of tidal influence were produced using UTIDE (Codiga, 2011).

### **3.2.2 Summary of Modeling Methods**

#### ***3.2.2.1 Hydrostatic Model Construction***

In hydrostatic modeling, the groundwater hydraulic gradient and attenuated tidal response with distance inland are ignored (i.e., Marcy et al., 2011; Strauss et al., 2012). Thus, we set the water table to an elevation equal to simulated sea level, referenced to the MSL datum. For example, for cases in which sea level is simulated at an elevation of 0 m, the water table inland is assumed to be located at an elevation of 0 m across the entire study area. For a simulated SLR of 1 m, the water table everywhere is assumed to be at an elevation of 1 m.

#### ***3.2.2.2 3D Numerical Model Construction***

Groundwater simulation using the 3D numerical method with MODFLOW 2005 (Harbaugh, 2005) follows Habel et al. (2017), but has been extended to represent a larger study area encompassing the Primary Urban Center of Honolulu. The numerical model simulates steady-state conditions of the water table at current mean sea level and a 1-m increase in sea level. Simulated subsurface hydrogeologic conditions are based on conditions determined in regional studies (Ferrall, 1976; Finstick, 1996; Munro, 1981; Oki, 2005; Rotzoll and El-Kadi, 2007). The model was calibrated using discrete and continuous water-level measurements discussed previously (Fig. 3-1).

The extended model consists of 48,483 active, 100-m uniform grid cells and three layers, representing unconsolidated caprock (model layer 1), consolidated caprock (model layer 2), and basalt (model layer 3) hydrogeological units, respectively. The inland boundary is defined by the 0-m elevation structural contour (Fig. 3-2) that represents the uppermost extent of the basalt aquifer (Rotzoll and El-Kadi, 2007). The seaward boundary is defined by the 200-m depth contour of 2013 U.S. Army Corps of Engineers LiDAR bathymetry data (National Oceanic and Atmospheric

Administration (NOAA), 2017b). The top of the unconsolidated caprock unit (model layer 1) is defined by mosaicked 2013 NOAA LiDAR topography data and 2013 U.S. Army Corps of Engineers LiDAR bathymetry data (National Oceanic and Atmospheric Administration (NOAA), 2017b), with a specified thickness of 10 m based on the approximate depth in which consolidated caprock material has been encountered (Ferrall, 1976; Finstick, 1996; Munro, 1981). The consolidated caprock unit (model layer 2) extends from the base of the unconsolidated caprock unit to the uppermost extent of the basalt unit (model layer 3) as defined by elevation data that represents the uppermost extent of the basalt aquifer (Rotzoll and El-Kadi, 2007). Details of the flow in the basalt aquifer unit are beyond the scope of this study. Therefore, the basalt aquifer is represented by a thin unit that extends an arbitrary 1 m below the base of the consolidated caprock unit and was included exclusively to simulate flow from the basalt into the caprock aquifer in which model layers 1 and 2 represent the caprock aquifer.

The model domain is bounded on the bottom and the sides by no-flow boundaries (with the exception of the inland boundary for the bottom unit); the onshore upper-boundary is a specified recharge boundary; the inland lateral boundary of the bottom unit (model layer 3) is a specified head boundary to simulate flow from the basalt unit to the upper caprock units (Fig. 3-2). Specified-head values were based on simulations of confined groundwater flow in southern O‘ahu (Rotzoll and El-Kadi, 2007). Seaward of the 0-m land-surface elevation contour, current sea-level conditions were simulated using a specified general-head boundary at the ocean bottom with a conductance of  $10 \text{ m}^2/\text{d}$ . A 1-m increase in sea level was simulated by re-evaluating the general-head boundary seaward of the 1-m elevation contour, and by increasing the elevation of hydraulic head from 0 m to 1 m; conductance was not changed.

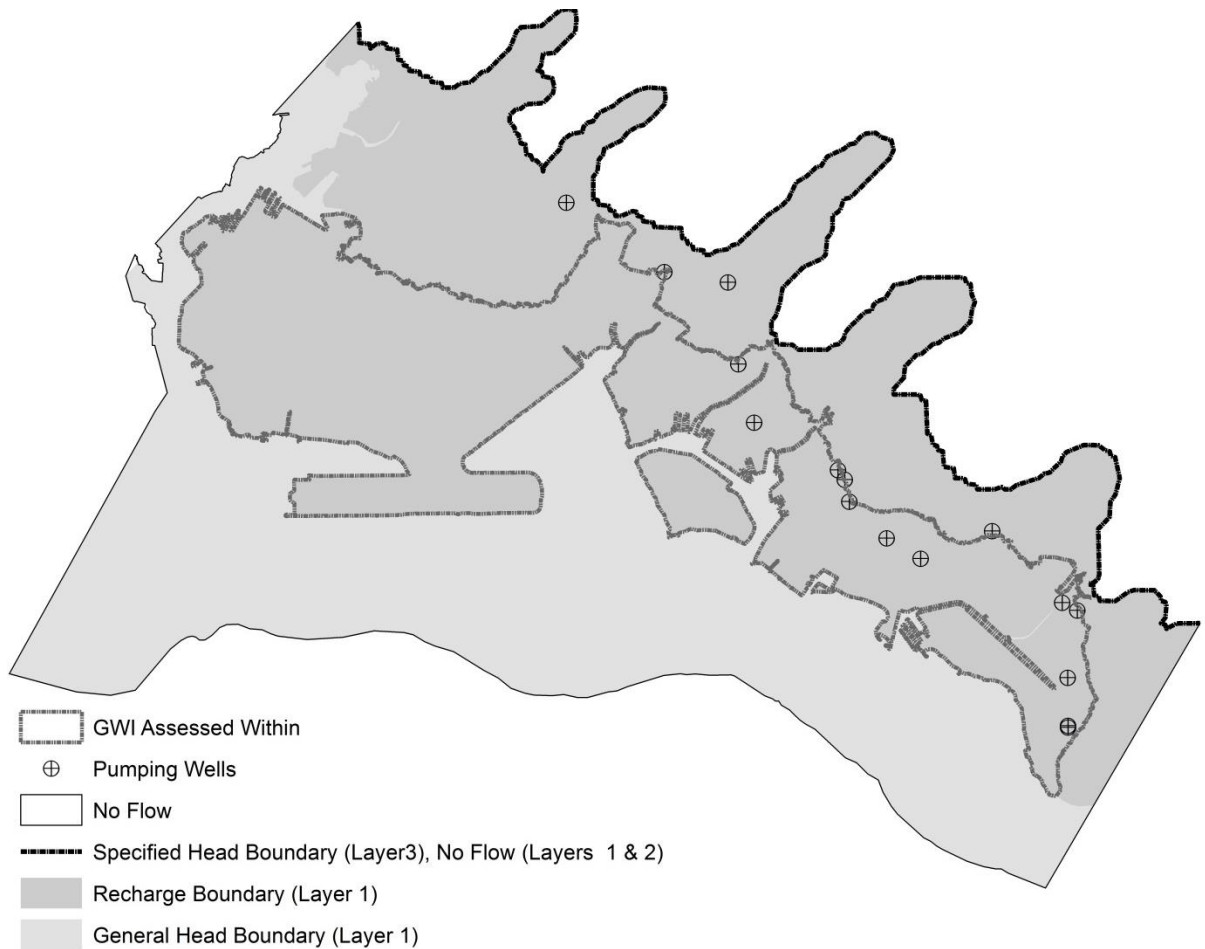


**Figure 3-2** : Diagram of model construction illustrating the application of boundary conditions. The area within which GWI was assessed is shown, and extends from the 10 m land surface elevation contour to the coastline; the area was chosen for analysis based on hosting adequate water level observations for calibration.

Well locations (Fig. 3-2) and withdrawal rates available from the State Commission on Water Resource Management were adopted from existing groundwater-flow models representative of the Honolulu aquifer (Rotzoll and El-Kadi, 2007) and only those wells pumping from the caprock were considered following the application of Habel et al. (2017). Well withdrawal rates were defined as the arithmetic mean of respective pumping rates from 1996 to 2005. Recharge data were acquired from the mean annual water-budget model for the Island of O‘ahu, Hawai‘i (Engott et al., 2017), which simulated hydrological processes including rainfall, fog interception, irrigation, direct runoff, return flows from septic systems, and evapotranspiration. Note that fog interception does not directly contribute to recharge in the model area.

Hydraulic-conductivity values for model layer 1 representing the unconsolidated caprock unit were estimated using the nonlinear inverse modeling utility, PEST in which Tikhonov preferred homogeneous regularization was used (Doherty, 2008). As part of this approach, pilot

points were established on 500-m grid across the study area, totaling 361 points. All post-calibration values applied to the unconsolidated caprock unit were within the range of values previously observed for the study area, ranging from 0.001 to 854 m/d (Finstick, 1996) with an average value of 135.2 m/d and standard deviation of 288.5 m/d.

Manual iterative adjustment was employed in the estimation of a hydraulic-conductivity parameter value of 1 m/d for model layer 2 representing consolidated caprock. A hydraulic conductivity of 600 m/d was specified for model layer 3 representing the basalt unit and was based on values employed in modeling studies that simulate local basalt aquifers (Izuka et al., 2018; Rotzoll and El-Kadi, 2007). A vertical anisotropy ( $K_h/K_v$ ) of 3.0 was specified for all layers.

Following model calibration, the simulated mean residual water level and root-mean-squared error were 0.04 m and 0.12 m, respectively.

The specific limitations of the modeling method are summarized in Habel et al. (2017) in which the main limitations include:

- The model is steady-state and thus does not assess time-dependent hydrological processes such as variations in recharge, pumping rates, boundary flows and groundwater storage, and aperiodic short-term changes in sea level by phenomena such as storm-surges, tsunamis, etc.;
- MODFLOW-2005 assumes a uniform density of water, and thus does not incorporate the influence of density-driven fluid flow such as mixed seawater and freshwater flows;
- The model does not consider flow that occurs in the unsaturated zone or surface-water flow, evaporation from surface-water sources, and ponding or routing of waters that occurs once groundwater has breached the ground surface;
- The model does not consider dynamic changes in landscape (i.e., erosion) produced by SLR.

### ***3.2.2.3 Tidal Application***

For the hydrostatic method, tidal influence was assessed by elevating the groundwater level to the tide stage elevation being simulated, thus natural attenuation of the tidal signal in an inland direction was not considered and water levels were not adjusted when simulating the MSL tide stage. As such, this method would tend to overestimate the inundation derived from groundwater when considering tides as it neglects attenuated head responses to tidal forcing.

For the 3D numerical method, tidal influence was evaluated by performing regression analyses to compute analytical solutions that assign tidal efficiency as an exponential function of distance from the coastline following the assessment in Habel et al. (2017). Tidal efficiencies representing six subzones were calculated by comparing tidal amplitudes recorded at the NOAA Honolulu Tide station (National Oceanic and Atmospheric Administration (NOAA), 2017a) to those observed at continuous monitoring wells. The six subzones represent the eastern, middle, and western extent of the study area, in which the western extent was further divided into four subzones. Subdivisions were made in the western extent to represent unique patterns of observed tidal efficiencies that correlated with distinct geologic strata that constitute the shallow geology (i.e, fill, beach deposits, lagoon and reef deposits, and Honolulu Volcanics) (Sherrod et al., 2007). Average post-calibration hydraulic conductivities within each subzone defined for the unconsolidated caprock unit are 198.6 m/d (eastern), 88.8 m/d (middle), 64.2 m/d (western-fill), 87.1 m/d (western-beach deposits), 184.7 m/d (western-lagoon and reef deposits), and 157.0 m/d (western-Honolulu Volcanics). Tidal efficiencies are expressed as increases in piezometric head considering the tidal half amplitude ( $h_0$ ) as follows:  $h(x)/h_0=e^{-0.002x}$  (eastern),  $h(x)/h_0=e^{-0.005x}$  (middle),  $h(x)/h_0=0.55e^{-0.0007x}$  (western-fill),  $h(x)/h_0=0.43e^{-0.001x}$  (western-beach deposits),  $h(x)/h_0=0.44e^{-0.0004x}$  (western-lagoon and reef deposits), and  $h(x)/h_0=0.43e^{-0.0002x}$  (western-Honolulu Volcanics) in which  $h(x)$  is the increase in piezometric head (m), and  $x$  is the distance from the shoreline (m). Based on the estimated diffusivities for these units, the computed tidal efficiencies are reasonable and consistent with the hydraulic properties. Similar to Habel et al. (2017), the analytical solutions were applied within the respective boundaries of each of the six subzones to a raster grid as a function of the distance of each grid cell to the modeled coastline. Raster values representing tidal efficiency were calculated by setting  $h_0$  to 0.33 (the MHHW tide elevation above the MSL datum in meters), which were subsequently summed with water-table raster data from the model output to generate the tidally influenced water-table height considering the MHHW tide stage.

### 3.3 Results

#### 3.3.1 Test of Model

As part of cross-validation analysis, error statistics were calculated for the 3D numerical and hydrostatic methods based on the residual values between simulated and observed groundwater levels representing MSL and MHHW scenarios under current conditions (Tab. 3-1).

Tide Stage: MSL Model Type	RMSE (cm)	$\mu$ (cm)	Median (cm)	Skew	$\sigma$ (cm)	Min (cm)	Max (cm)
Hydrostatic	40	-33	-34	0.33	14	-57	-1
3D Numerical	9	-2	-3	0.05	9	-24	16

Tide Stage: MHHW Model Type	RMSE (cm)	$\mu$ (cm)	Median (cm)	Skew	$\sigma$ (cm)	Min (cm)	Max (cm)
Hydrostatic	20	-8	-7	0.15	18	-50	32
3D Numerical	10	3	5	-0.44	9	-18	20

**Table 3-1** : Comparison of error statistics calculated for model residuals. Simulations considering MSL and MHHW scenarios are analyzed. Calculations include root mean squared error (RMSE), mean ( $\mu$ ), median, skew, standard deviation ( $\sigma$ ), minimum and maximum residual values.

In simulating MSL, the RMSE and systematic error (bias) of hydrostatic residuals reveal profoundly low estimates of groundwater level. This finding is reinforced by the negative maximum residual, indicating that at every comparison point, the method underestimates groundwater level. Performance improves markedly when simulating MHHW. This is evident from the significant reduction in RMSE and bias; however, the bias remains negative indicating overall underestimation of groundwater level. As expected, the RMSE representing the 3D numerical model is similar to that calculated in Habel et al. (2017) considering both tidal scenarios.

Simulated groundwater levels are illustrated in cross-section along shore-normal transects (Fig. 3-3). Cross-section locations represent regions that feature different hydraulic gradients with distinctive subsurface geologies. Transect A represents a calcium carbonate platform comprising mainly Pleistocene skeletal limestone; Transect B represents alluvium and fill; Transect C represents limestone and fill and rises relatively abruptly in elevation. Results indicate that,

although the hydrostatic simulations do not thoroughly align with the more robust model, the RMSE overlaps with results of the 3D numerical simulations (other than on transect C landward of approximately 1500 m). This is true for both evaluated tide scenarios, however, for the hydrostatic simulations the RMSE of the MHHW scenario is half that of the MSL scenario.

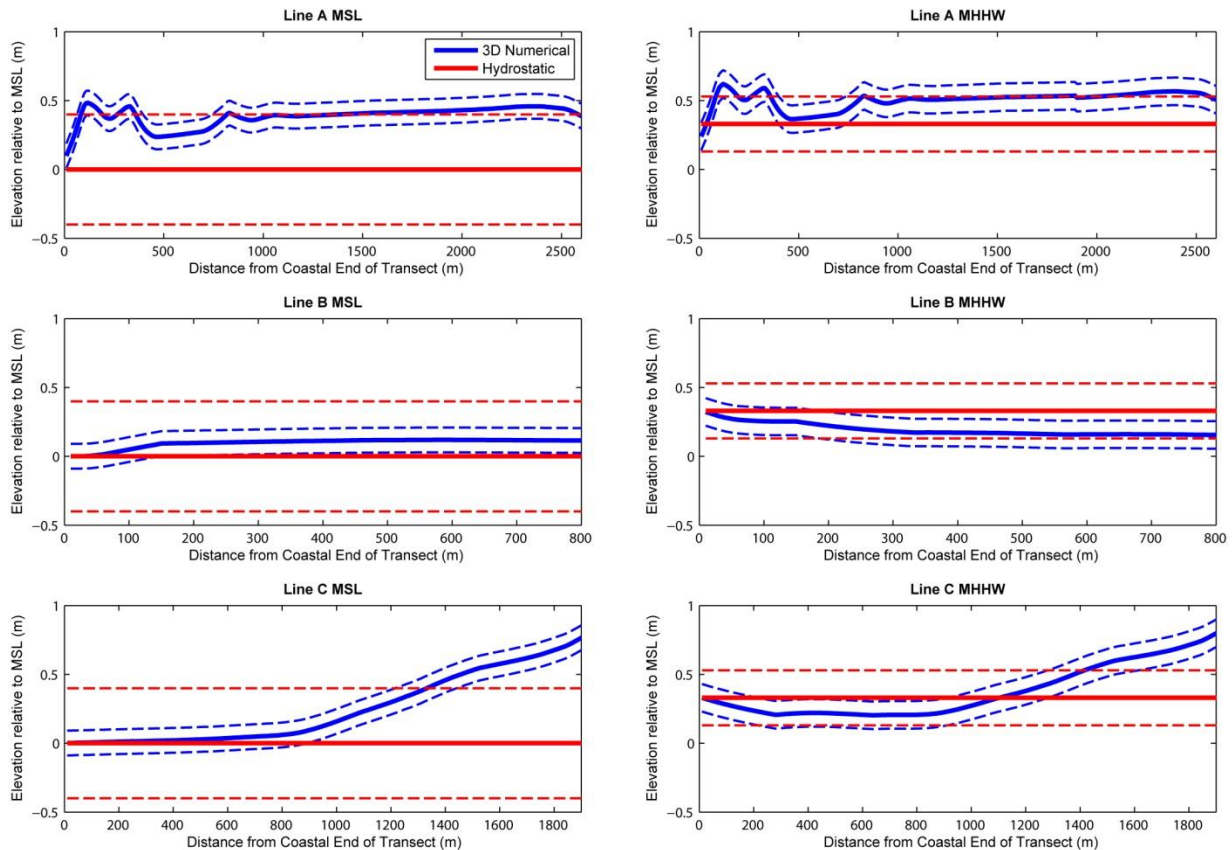


**Figure 3-3** : Composite water-table simulations considering the influence of MSL (left column) and MHHW (right column) generated using hydrostatic (red) and 3D numerical (blue) simulations, along shore-normal transects (see Figure 3-1 for location). Dotted lines denote RMSE departure from observed water levels. Lines A, B and C represent differing hydrogeologic conditions within the study area. Note that water levels along transect A dip at the inland extent due to the backshore presence of Pearl Harbor.

### 3.3.2 SLR Flood Simulations

Illustrations of GWI considering a 1-m SLR scenario are presented in Fig. 3-4. The hydrostatic method reproduces 65 percent (MSL) and 88 percent (MHHW) of the inundated area depicted by the 3D numerical method. In the MHHW case, 14 percent of the area inundated by the hydrostatic method lies outside of the 3D numerical-method inundation area. Thus, the total inundated area simulated using the hydrostatic method comes within 2 percent of the total inundated area simulated using the 3D numerical method. However, the flooded footprint of the

two methods for the MHHW case differs by 26 percent as indicated by the uniquely flooded areas for the two methods (no overlap between two methods).

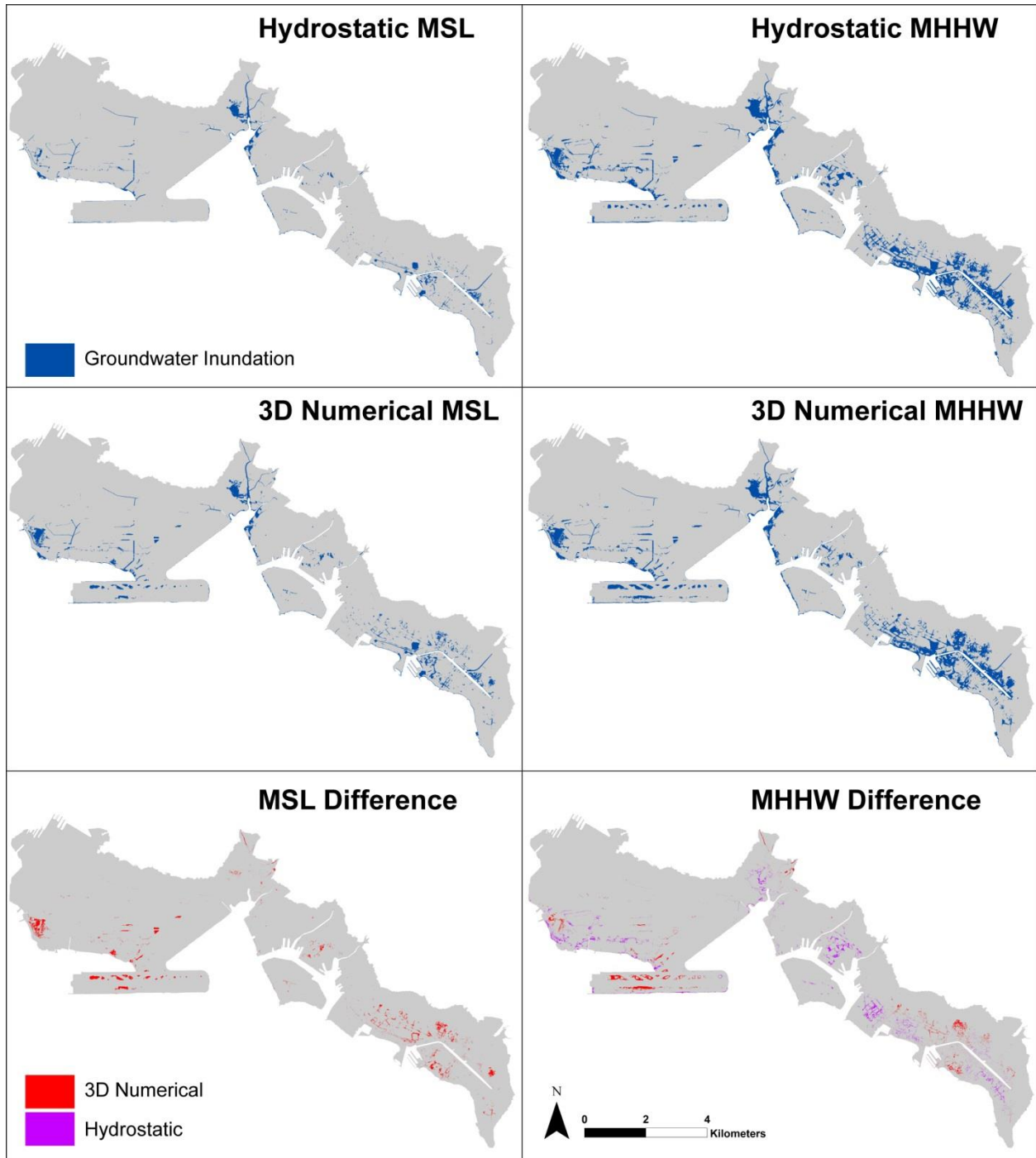


**Figure 3-4 :** Simulations of 1 m SLR at MSL (left) and MHHW (right) showing GWI (blue). Top – Hydrostatic method. Middle – 3D numerical method. Bottom – Uniquely flooded area (no overlap between two methods).

### 3.4 Discussion

As anticipated, our results reinforce 3D numerical modeling as the more robust of the two methods. Data assimilation by the 3D method provides for better representation of observed water levels. However, when referenced to MHHW, we find the hydrostatic approach produces simulations that are usefully accurate, with specific caveats.

Improved hydrostatic simulation of MHHW relative to MSL results from two offsetting and unrealistic assumptions inherent in the method. These are 1) that an aquifer has a hydraulic gradient equal to zero, and 2) that tidal signals do not attenuate as they move through an aquifer. These assumptions produce errors that are oppositely sensed. This explains why the hydrostatic method underestimates groundwater elevations (RMSE of 40 cm, Bias of -33 cm) in the MSL scenario, as only the negative bias of the first assumption is introduced. This results from the fact that in most areas in the MSL case the actual groundwater hydraulic gradient is oriented toward the coast.

Commonly used hydrostatic simulations conveniently and fortuitously are referenced to local MHHW (i.e., NOAA SLR Viewer). When referenced to MHHW, the hydrostatic method can produce reasonable estimations of groundwater elevation in low-lying coastal regions, especially given the limited effort required for model construction. Municipalities can employ the method as a first-cut approach towards revealing vulnerabilities to GWI.

However, the two methods produce localized differences in flood simulation (Fig. 3-4) that result from the ability of the 3D method to capture heterogeneous hydrological conditions (i.e., recharge, and conductivity) that influence tidal efficiency and head. These differences illustrate the inability of the hydrostatic method to produce high-quality simulations that can be used as the basis for fine-scale decision making. Thus, we do not recommend use of the hydrostatic method alone for such endeavors. Rather, we advise it be used as an indicator of exposure to GWI at the municipal scale that could be used to inform decisions of whether methods of greater accuracy and precision are necessary. We recognize these findings apply specifically to the Honolulu area, since tidal ranges, topography, and hydraulic gradients vary regionally. However, because the minimum elevation of coastal groundwater generally exceeds that of local mean sea level in coastal regions (Turner et al., 1997), it is reasonable to assume that where a coastal plain aquifer exists, the hydrostatic method (specifically considering a MSL tide stage) provides, at worst, a minimum estimate of groundwater elevation, and in turn GWI.

Use of the 3D numerical approach is more appropriate when a) modeling coastal regions that feature particularly complicated conditions such as those that host extensive extraction/injection wells; b) conducting modeling efforts that consider specific tidal scenarios (i.e., lower stages of the tide, extreme high tide); or c) developing engineering techniques to mitigate flooding from GWI (i.e., implementation of extraction wells). We also note that, although the 3D numerical approach is more rigorous and widely applicable than the hydrostatic approach, the numerical approach may be unreliable if sufficient data are not available to constrain and evaluate model performance.

We also recognize that neither modeling approach presented here simulates dynamical coastal processes (i.e., coastal erosion, sediment accretion or changes in land cover) (Anderson et al., 2018; Lentz et al., 2015) that drive evolution of the landscape as sea level rises (FitzGerald et al., 2008). Hence, our conclusions are most appropriately applied to regions, or environments that are less impacted by dynamical coastal processes (i.e., heavily developed shorelines that have been structurally hardened).

### **3.5 Summary and Conclusion**

Numerous coastal municipalities around the world face impacts from SLR flooding. The impacts are wide ranging and include disruptions in daily commerce, progressive failure of critical infrastructure, and intensified socio-economic burdens. In an effort to manage SLR impacts, informed, adaptive management is crucial and necessitates specific consideration of the various components of flooding including GWI. The GWI component is often overlooked in vulnerability studies, yet it is arguably the more challenging to manage as it includes complete saturation of the ground that is difficult to mitigate. This type of flooding can evade coastal barriers (i.e., seawalls) and overwhelm traditional drainage conveyances, rendering them ineffective.

To spur consideration of GWI in policy and planning, a data-intensive 3D numerical method was developed by Habel et al. (2017) to specifically simulate SLR induced GWI; however, its accessibility is limited by data requirements to produce robust simulations. Here we investigate applicability of the more simple and accessible hydrostatic method in simulating GWI. The hydrostatic method is commonly used to produce flood simulations considering a direct marine source; however its applicability towards simulating GWI had not previously been explored.

Comparison of the hydrostatic method to 3D numerical modeling reveals each method's ability to replicate present day groundwater levels at MSL and MHHW stages of the tide, and

similarities of GWI simulations considering 1 m SLR. For Honolulu the hydrostatic method produces groundwater level and GWI simulations that are comparable to the more physically based method, specifically when referencing the local MHHW tide stage (generally typical of flood studies). Hydrostatic simulations produce a RMSE of 20 cm during the MHHW tide stage, compared to 10 cm produced by the 3D numerical method. Further, hydrostatic simulation of GWI in a scenario of 1 m SLR at MHHW reproduces 88% of the inundated area simulated using the 3D numerical method. However, because neither method has been designed to simulate dynamic landscape changes their use should be limited to settings or environments that are less impacted by dynamic coastal processes that accompany change as a result of SLR.

Though use of data-assimilating numerical modeling methods are more appropriate in cases where high accuracy simulations are necessary, we find that use of the hydrostatic method (specifically when referencing the local MHHW tide stage) is suitably accurate as a first-cut approach in identifying municipal vulnerabilities to GWI.

## **Chapter 4 : Compound Flooding Related to Sea-Level Rise and Urban Infrastructure**

*In review for publication as:* Habel, S., Fletcher, C.H., Thompson, P. Compound Flooding Related to Sea-Level Rise and Urban Infrastructure. Scientific Reports.

*Abstract* - A method is developed that identifies sea-level rise impacts in Honolulu's Primary Urban Core. The method includes simulation of flood scenarios consisting of high-resolution raster datasets featuring flood-water depth generated by three mechanisms: 1) direct marine flooding, 2) storm-drain backflow, and 3) groundwater inundation. Damage associated with compound flooding has not been previously studied, despite present-day impacts during king-tide events. This represents a significant literature gap pertaining to sea-level rise flood simulation and associated impacts, as the design of effective adaptation measures will require consideration of these disparate mechanisms. Annual exceedance frequencies of simulated flood thresholds are established using a statistical model that considers predicted tide and projections of SLR. We find that critical infrastructure (i.e., roads, drainage, cesspools) already experience sporadic failure during king-tide events. Such failure will be amplified over coming decades, approximately doubling in extent by the 2030s. Our results underscore the need for timely implementation of adaptation methods to avoid societal impacts related to chronic flooding. The design of such methods will require site-specific strategies that account for compound flooding.

### **4.1 Introduction**

The PUC of Honolulu has been the subject of several studies regarding sea-level rise (SLR) induced flooding. These studies include the following:

Rotzoll and Fletcher (2013) were among the first to simulate SLR-induced groundwater inundation (GWI). This flood mechanism is produced by a rise of the groundwater table with sea level, which can lead to flooding from below. The study employed coastal groundwater-elevation data and measurements of tidal influence in combination with a digital-elevation model (DEM) to assess vulnerability to GWI within the PUC.

Habel et al. (2017) expanded upon the methods of Rotzoll and Fletcher (2013) by employing a 3D numerical model calibrated with discrete and continuous water-level

observations to simulate SLR induced GWI (Habel et al., 2017). This method allowed simulated groundwater levels to vary in the cross-shore direction. Habel et al. (2017) found that among much of Honolulu’s low-lying coastal areas, groundwater is already near to the ground surface such that GWI is likely already causing impacts to submerged infrastructure (i.e., cesspools, basements, and others).

Anderson et al. (2018) provided the method for flood analyses detailed in a report released by the Hawai‘i Climate Change Mitigation and Adaptation Commission (2017) (Anderson et al., 2018; Hawai‘i Climate Change Mitigation and Adaptation Commission, 2017). As part of the study by Anderson et al. (2018), dynamical physical processes were modeled including erosion and wave run-up. These simulations supplemented the widely employed hydrostatic (bathtub) modeling method that simulates passive flooding (Marcy et al., 2011; Strauss et al., 2012). The hydrostatic method was used to implicitly represent flooding likely to result from a combination of phenomena including passive direct marine inundation (MI), storm-drain backflow (DBF), and groundwater inundation (GWI); however, the three mechanisms were not uniquely simulated.

Thompson et al. (2019) developed a statistical model that provides frequencies at which sea level will exceed given thresholds in Honolulu over the 21st century (Thompson et al., 2019). The model considers secular local mean sea-level (LMSL) rise, annual LMSL variability, and the annual 99th percentile of astronomical tidal height. Projections of exceedance frequencies can be used in combination with flood mapping methods to provide a powerful tool for agencies that conduct adaptation planning. Such a tool can also be used to estimate when intermittent flooding is expected to progress to chronic flooding. The Thompson et al. (2019) study defines chronic flooding as the point in which a defined flood threshold is exceeded more than 50 days per year for 9 in 10 years. The study reported the potential for rapid transitions in threshold exceedance in which the transition from intermittent to chronic can occur within as little as a decade.

The objective of the present study is to provide simulations of multiple SLR-induced flood mechanisms (Fig. 4-1) expected to impact the PUC by uniquely combining elements of the studies described above to simulate overlapping flood modes. We refer to this as compound flooding. These methods are developed to establish a foundation for planning and policymaking.

We simulate flood conditions for four established elevation thresholds; these include three thresholds expected to produce disruptive and damaging coastal flooding (Sweet et al., 2018), and a fourth threshold defined by Thompson et al. (2019) that represents the sea-level elevation at which exceedance is known to produce tidally induced flood impacts in Honolulu. Using the methods of Thompson et al. (2019), we assess the annual frequency of exceedance in coming decades. Note that each flood mechanism will require a separate engineering strategy to manage. Flood mechanisms simulated here include, 1) direct marine inundation (MI), flooding that occurs where topographic elevations are situated below a given flood threshold in which marine waters can move unimpeded over the land surface; 2) drainage backflow (DBF), flooding that occurs as ocean levels and coastal groundwater are elevated above gravity-flow drainage networks, resulting in reverse flow and flooding along low-lying areas such as streets and basements (much of Honolulu area employs gravity flow drainage infrastructure to discharge storm-water runoff into marine waters. Many of these networks are fractured or otherwise unsealed such that surrounding coastal groundwater can add to the discharge); and 3) groundwater inundation (GWI), flooding that occurs as the water table is lifted above the elevation of the ground surface and/or buried infrastructure. Groundwater in the study area is part of a freshwater-lens system in which the uppermost extent of the aquifer is unconfined (Macdonald et al., 1983; Rotzoll et al., 2010) and influenced directly by rainfall and near-shore sea-level fluctuations produced by tides, wave set-up, and longer period sea-level variations (Gonneea et al., 2013; Habel et al., 2017a; Ponte, 1994; Wu et al., 1996; Yin et al., 2001).

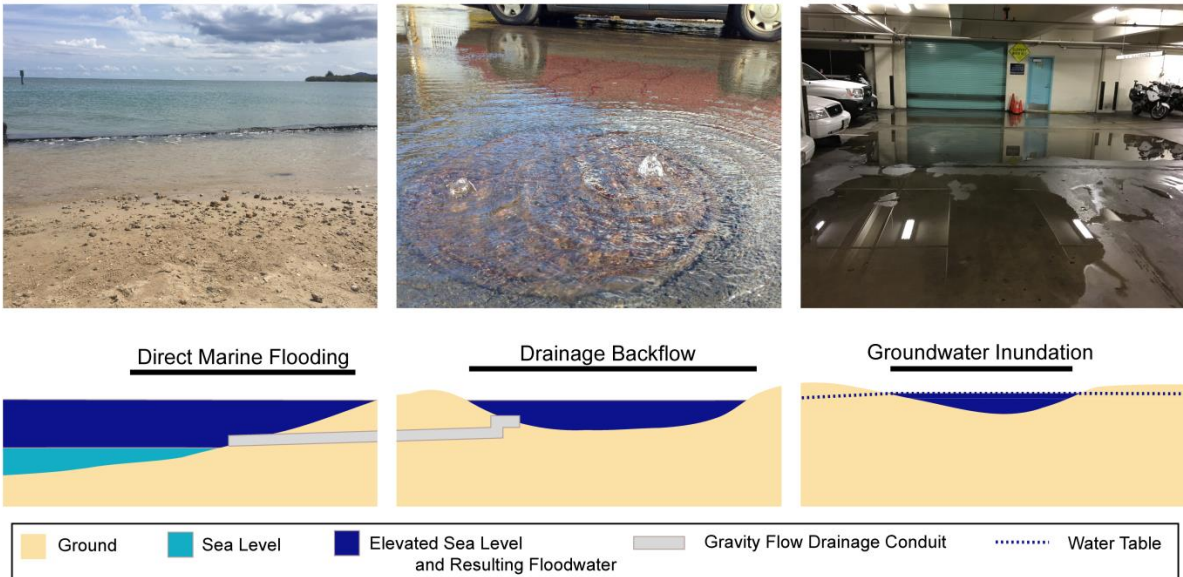


**Figure 4-1** Observations and illustrations of direct marine flooding, drainage backflow, and groundwater inundation within Honolulu. Note that each mechanism of flooding has already been observed during periods of extreme tide in various locations within the study area. Photo Credit, Hawai‘i and Pacific Islands King Tide Project (University of Hawai‘i Sea Grant, 2019).

Here we do not consider dynamic coastal processes such as coastal erosion or wave run-up, nor changes in land cover. Honolulu’s coastline within the PUC is unique relative to the more natural coastlines featured among the Hawaiian Islands in that it is heavily developed and armored such that erosion will likely be managed by continued armoring. Further, we acknowledge that this study does not include simulation of rainfall-induced flooding.

Utilizing the generated flood simulations, we conduct an assessment of critical infrastructure failure likely to occur as sea level reaches established flood thresholds. The assessment includes: length of roadway that features dangerous driving conditions and/or is impassable by 4-wheel drive vehicles, number of drainage inlets that have no capacity for storm water and instead act as conduits for additional flooding, and number of cesspools that are non-functional at filtering effluent and/or are fully flooded to the ground surface.

#### 4.1.1 Study Area

The study area encompasses the Primary Urban Core (PUC) of Honolulu on the southeastern coastal plain of O‘ahu, Hawai‘i (Fig. 4-2). The city represents a major hub for tourism, international business, and military defense; about 76% of O‘ahu’s employment is concentrated within the PUC (Hawai‘i Climate Change Mitigation and Adaptation Commission, 2017). The Honolulu metropolitan area features the 4th highest population density in the United

States behind Los Angeles, New York City, and San Francisco (Dillinger, 2019), in which 9% of its population reside in the floodplain (NOAA Office for Coastal Management, 2019).

The PUC hosts the majority of O‘ahu’s critical infrastructure, including Daniel K. Inouye International Airport, Hickam Field, Honolulu Harbor, Ke‘ehi Lagoon, Honolulu Power Plant, five solid waste collection locations, Hawai‘i bio-waste system, the Māpunapuna industrial area, and a sewage treatment plant. Further, the area includes locations popular to residents and visitors including Ala Moana Mall, the Honolulu Convention center, and the Waikīkī area. The Waikīkī area is especially vital to the State’s economy as it represents the core of Hawai‘i’s tourism industry, hosting 49,000 jobs and 39% of total statewide visitor spending (Hawai‘i State Department of Business Economic Development & Tourism, 2018).

Owing to the high density of population and economic assets, Honolulu faces the highest potential economic loss in the State, representing 66% of the total statewide losses resulting from approximately 1 m of sea level rise (Hawai‘i Climate Change Mitigation and Adaptation Commission, 2017). Much of this vulnerability stems from limited tidal ranges that have allowed a dense network of development to take place in close proximity to the shoreline and has resulted in Honolulu having some of the lowest elevation flood thresholds in the United States (Sweet et al., 2017). Further, the area hosts a shallow grade such that small increments of SLR will cause relatively large lateral shifts in impacted area (Kane et al., 2015).

Large swaths of the dense urban network in Honolulu have been heavily developed atop land that was filled over the 19th and 20th centuries as part of large-scale land reclamation projects that dramatically altered shoreline locations and topography. Filling of low-lying areas such as shallow coral reef, marshes, and salt ponds was undertaken in Kaka‘ako, Kewalo, downtown Honolulu, Waikīkī, and Sand Island, and the runway of the Daniel K. Inouye International Airport (Department of Transportation, n.d.; Honolulu Dredging Construction Company, n.d.; Wiegel, 2008).

These large-scale reclamation projects were spurred by rapid growth in tourism and the military-based economy, such that the PUC has now become intensely developed to the point that nearly the entire coastline is altered by engineering projects. Many of the areas identified

as being most vulnerable to SLR-related economic impacts are located on fill (land reclamation projects) (Hawai‘i Climate Change Mitigation and Adaptation Commission, 2017).

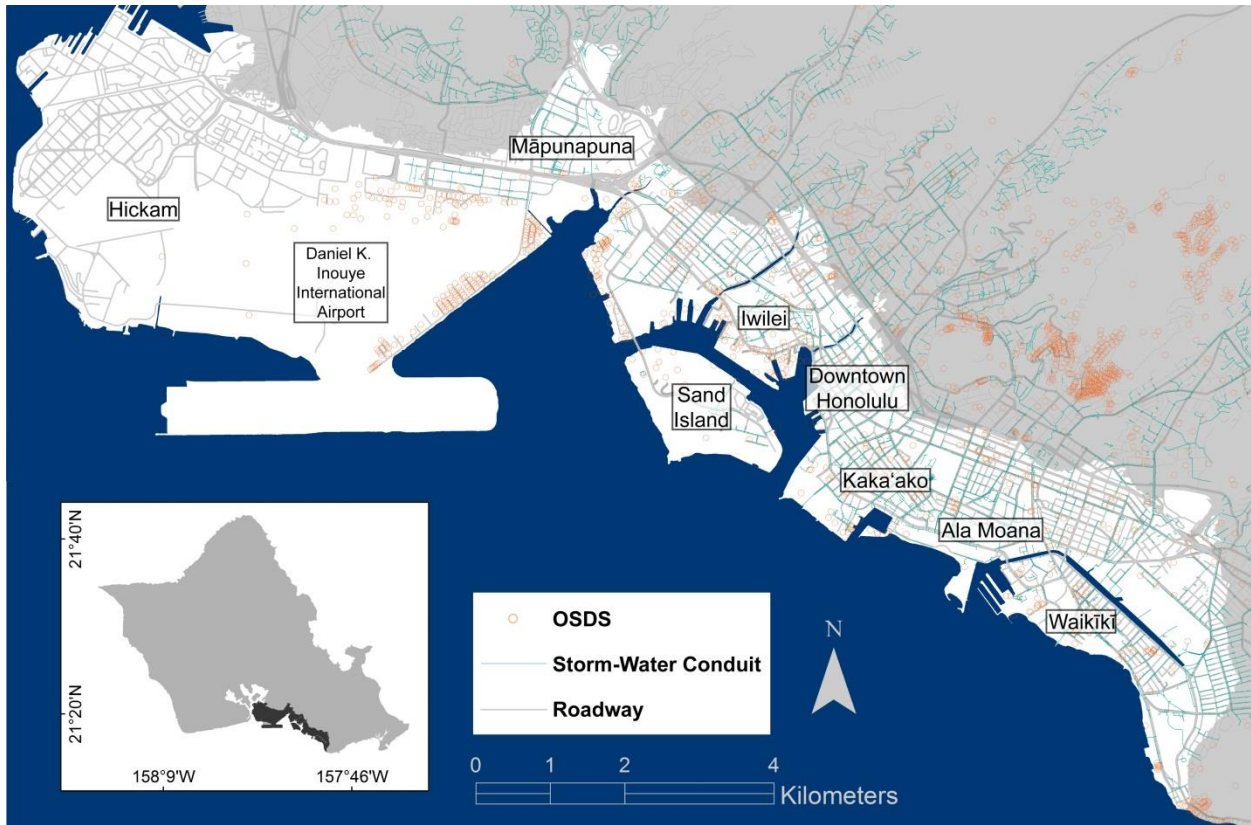


**Figure 4-2:** Study area showing the extent in white. Infrastructure locations including Class V on-site sewage disposal systems (OSDS) (cesspools), storm-water conduits, and roadways are shown.

#### 4.1.2 Sea-Level Rise Projections

The most useful projections of SLR for local planning efforts account for changes in both LMSL and forecasted local high-tide flooding. Thompson et al. (2019) use the National Oceanic and Atmospheric Administration (NOAA) set of SLR scenarios reported by Sweet et al. (2017) to represent the secular component of sea-level change. The study by Sweet et al. (2017) provided six scenarios of SLR discretized by 0.5-m increments that are associated with emissions-based, conditional probabilistic scenarios and global-model projections (Sweet et al., 2017).

In this study, we consider the median intermediate local SLR projection provided by Sweet et al. (2017) that assumes a non-linear rate of rise and reaches 0.4 m in Honolulu by 2050 and 1.19 m by 2100. The intermediate scenario is considered here for the purpose of supporting general adaptation planning. However, we suggest the use of more extreme SLR projections (i.e.,

intermediate-high, high, and extreme) when designing projects that are highly sensitive to flood impacts such as centralized critical infrastructure with no capacity to accommodate flooding (Hawai'i Climate Change Mitigation and Adaptation Commission, 2017).

## **4.2 Methods**

### **4.2.1 Identification of Flood Thresholds**

Coastal flood severity thresholds have been established by Sweet et al. (2018) for forecasting purposes and to ensure public safety; these thresholds vary by location and are generally calibrated to NOAA tide gauge stations (William V. Sweet et al., 2018). The thresholds are defined as minor, moderate and major to respectively describe disruptive, damaging, and destructive coastal flooding, respectively. Sweet et al. (2018) define local elevation thresholds as a function of local tide ranges along U.S. coastlines to establish a nationally consistent definition of flooding and impacts for the purpose of quantifying and communicating risk. Flood thresholds calculated for Honolulu are 0.52 m, 0.82 m, and 1.19 m for minor, moderate, and major thresholds, respectively, relative to the local mean higher high water (MHHW) tidal datum.

Note that NOAA thresholds have not been officially established for the Honolulu tide gauge as the thresholds have not yet been reached, and in-turn, calibrated relative to flood impacts. However, flood thresholds derived for Honolulu were considered valid as part of the study by Sweet et al. (2018) since topographic characteristics and tidal ranges are represented by locations in which NOAA thresholds have been derived (i.e., stations in South Florida).

Tidally induced flood impacts are known to occur among exceptionally low-lying regions of Honolulu. An additional flood threshold was defined by Thompson et al. (2019) for the purpose of evaluating the progressive increase in exceedance of water levels known to produce tidally induced flood impacts in these areas. The study qualitatively established a 0.35 m threshold relative to MHHW by comparing photo documentation of flooding to water levels recorded at the Honolulu Harbor Tide Gauge. Since tide gauge records began in 1905, this threshold has been exceeded on 37 distinct days, in which fifteen of those days occurred during the summer of 2017 (Thompson et al., 2019).

## **4.2.2 Flood-Frequency Prediction**

Methods for determining increases in flood frequencies considering SLR were adopted from the method of Thompson et al. (2019) that projects frequencies at which a defined flood threshold will be exceeded by sea level over the 21st century. The method uses a hierarchical statistical model that describes annual counts of exceedance days (or number of days in which a defined threshold is exceeded for at least one hour) as beta-binomially distributed random variables, which allows for exceedance probability on a given day to vary year-to-year as a function of annual mean sea level and the amplitude of the highest tides.

## **4.2.3 Flood Mapping**

### ***4.2.3.1 DEM Construction***

To define ground elevations on which water levels can be compared, and thus, depth of flooding evaluated, a digital-elevation model (DEM) was constructed by merging and hydroflattening 2013 NOAA DEM tiles. The tiles were constructed by NOAA using raw LiDAR ground return data points that characterize elevations relative to LMSL (National Oceanic and Atmospheric Administration (NOAA), 2017b).

Hydroflattening was accomplished by characterizing areas in which water returns were likely by applying an arbitrary constant elevation of -1.5 m to all major waterways, water features, and offshore areas. Note that all major waterways are thus assumed to be connected to groundwater. The tiles have 1 m horizontal and 0.15 m vertical resolution, respectively (Photo Science Inc., 2013). In the results section, flood scenarios were generated considering mechanisms described below and sea-level elevations equal to the 0.35 m threshold established by Thompson et al. (2019), and the minor, moderate, and major flood thresholds established by Sweet et al. (2018). Note that more than one flood mechanism can be featured in the same location. In such cases, it is assumed that flooding will remain unless all mechanisms featured in that area are mitigated. For example, if GWI and direct marine flooding are featured in an area, and only the direct marine source is mitigated, GWI would remain.

To ground-truth the flood-mapping method, simulations produced considering the 35 cm threshold were qualitatively compared to flooding observed within the study area during 2017 king-tide events (University of Hawai'i Sea Grant, 2019).

#### ***4.2.3.2 Direct Marine Inundation***

Locations vulnerable to the direct marine source of flooding were identified using a variant of the hydrostatic modeling method (Cooper and Chen, 2013). The hydrostatic method characterizes flood vulnerability by identifying areas within a DEM that host elevations below that of chosen flood thresholds (Marcy et al., 2011; Strauss et al., 2012). Here we amend the method by excluding flooded areas that lack surficial connection to the coastline as it is inferred that the topography would obstruct direct surficial flow from a marine source. The coastline used to determine surficial connectivity was digitized using DEM elevation contours of the respective simulated flood thresholds. The contribution of groundwater to flooding was not considered in the simulation of direct marine inundation.

#### ***4.2.3.3 Drainage Backflow***

Locations vulnerable to flooding from DBF were also identified using a variant of the hydrostatic modeling method. Here we amend the method by excluding flooded areas that lack surficial connection to drainage infrastructure. Geospatial data that characterize locations of drainage inlets were used to identify locations where drainage would facilitate flow from a marine source (State of Hawai‘i Office of Planning, 2016). Flood areas that did not overlap drainage infrastructure were excluded as it is inferred that flooding would not be facilitated by drainage infrastructure. The contribution of groundwater to flooding was not considered in the simulation of DBF.

#### ***4.2.3.4 Groundwater Inundation***

Simulations of groundwater levels were produced using a 3D numerical model (MODFLOW). Methodologies employed in model construction were adopted from chapter 2 as published in Habel et al. (2017) and expanded according to chapter 3 as published in Habel et al. (2019). The model simulates steady-state conditions of head considering increases in sea level equal to defined flood thresholds, applied as 0.52, 0.82, and 1.19 m, respectively. Regional studies were used to characterize subsurface hydrogeology of the study area (Ferrall, 1976; Finstick, 1996; Munro, 1981; Oki, 2005; Rotzoll and El-Kadi, 2007).

The model was calibrated using 247 discrete water-level observations obtained from Hawai‘i Department of Health Leaky Underground Storage Tank records, and 73 sets of continuous water-level measurements compiled from local hydrogeologic studies. Further

information regarding groundwater model construction and limitations is included in the supplementary material at the end of this chapter.

Locations vulnerable to GWI were identified by comparing simulated water-table elevations to the DEM in which flood depth and depth to groundwater were assessed by evaluating elevation differences between the water table and ground surface (i.e., DEM). Flood depths were calculated in locations where water-table elevations exceed ground-surface elevations and depths to groundwater were calculated in locations in which ground-surface elevations exceed water-table elevations.

#### **4.2.4 Damage Assessment**

To illustrate the utility of flood simulations in conducting vulnerability analyses, a damage assessment was conducted. As part of the assessment we quantify critical infrastructure failure considering sea levels equal to respective flood threshold elevations and considering the three flood mechanisms simulated. Here we calculate the following impacts.

The length of roadway featuring dangerous driving conditions produced by flood depth is identified where simulated depth of flooding is greater than 0.15 m along roadways. This water depth is based on the depth in which water would enter the intake systems of small vehicles causing them to stall, thus impeding the flow of traffic (Pregolato et al., 2017).

The length of roadway impassable by 4-wheel drive vehicles is identified where simulated depth of flooding is greater than 0.6 m along roadways. This water depth is based on the depth in which water would enter the intake systems of 4-wheel drive vehicles causing them to stall (Pregolato et al., 2017). A roadway is considered impassable once 4-wheel drive vehicles can no longer pass.

Drainage inlets that have no capacity to transport storm water were identified. These inlets act as conduits for additional flooding by DBF. Inlet failure is characterized in locations where the elevation of a drainage inlet is equal to or less than simulated water levels. Drainage inlet elevations were extracted from the DEM.

Cesspools that are non-functional at filtering effluent were identified. Non-functioning cesspools are identified using the methods of Habel et al. (2017) such that cesspool locations

lacking 4.4 m of unsaturated space, required by the State Department of Health, indicate partial inundation of the cesspool and inability of the system to properly treat effluent (Department of Health, 2004).

We identify cesspools fully flooded to the ground surface. Fully flooded cesspools were also identified using the methods of Habel et al. (2017) in which the cesspool locations featuring elevations below that of simulated water levels are identified as being fully submerged.

Geospatial data sets that characterize locations of drainage inlets, roadway, and on-site sewage disposal systems were used to conduct the assessment of infrastructure failure (State of Hawai‘i Office of Planning, 2016).

## **4.3 Results**

### **4.3.1 Results of Mapping Analysis**

Maps were produced that illustrate locations in which flooding will occur as the result of MI, DBF, and GWI due to sea level exceedance of the minor (0.52 m MHHW) and moderate flood thresholds (0.82 m MHHW) (Fig. 4-3). Maps were not produced considering the major flood threshold (1.19 m MHHW) because the intent is to focus attention on near-term scenarios, although calculations of flooded area and infrastructure failure at the major threshold were completed (Tab. 4-1 and 4-2). As part of flood mapping, the three mechanisms are superimposed in the following order, MI, DBF, GWI, such that MI is the top layer featured. To avoid overcomplicating the mapping product, we report results relating to concurrent (compound) flood mechanisms in an associated table (Tab. 4-1) as areas and percentages of total inundation.

Flood simulations indicate that four main areas of Honolulu are especially vulnerable to compound flood mechanisms. These areas are Waikīkī and surrounding neighborhoods, Māpunapuna, Iwilei, and the southwest corner of Hickam. The Waikīkī and Māpunapuna areas host the majority of flooded area. The deepest flooding is shown to occur in Māpunapuna over a relatively limited area, while flooding in Waikīkī is shown to host shallower water depths that are more widespread. At the minor threshold, the assessment of infrastructure failure indicates that each assessed infrastructure type experiences failure within or near these flooded areas, with the exception of partially flooded cesspools which are distributed across the PUC and represent nearly 90% of all active cesspools in the study area. At the moderate threshold, infrastructure

failure multiplies in extent considering dangerous or impassable lengths of roadway, flooded cesspools, and failed drainage.

This assessment does not represent a full accounting of infrastructure that will be impacted by considered flood mechanisms. To maximize efficiency of design, planning, and workflow, agencies could conduct their own assessments considering assets they manage and further, to integrate their results with the results of other agencies and utilities to thoroughly inform adaptation planning efforts. For example, such collaboration will likely be necessary when adapting a roadway since multiple types of infrastructure are typically aligned adjacent to most roads and thus will also need to be adapted at the same time by respective managing agencies (i.e., departments of transportation, public works, water supply, energy, cable, waste management, and others).

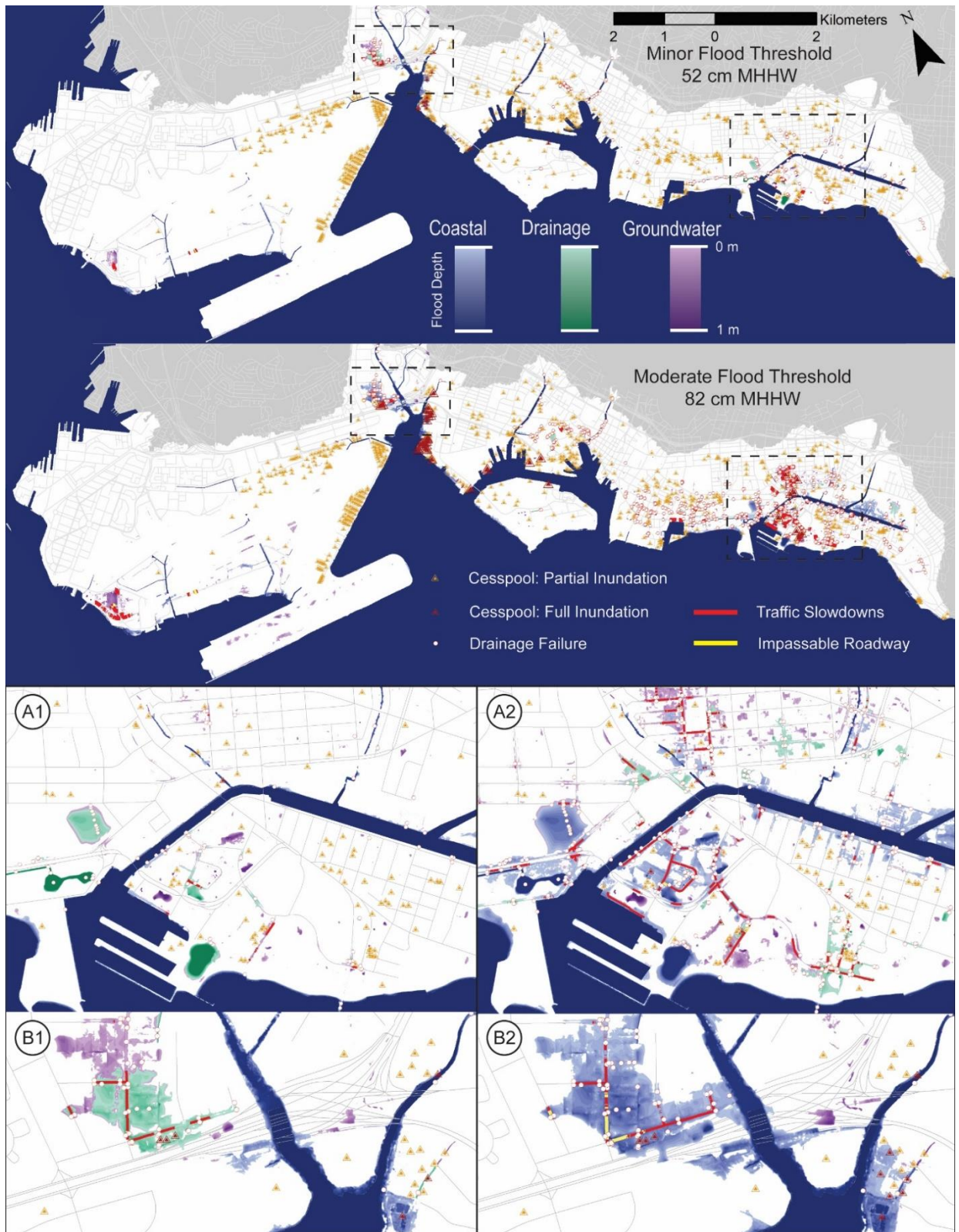


**Figure 4-3:** Upper figures show flooding and infrastructure failure across the PUC considering minor and moderate flood thresholds. The bottom two subsets show the Waikiki (A1 and A2) and the Māpunapuna industrial area (B1 and B2). A1 and B1 illustrate flooding at the minor threshold and A2 and B2 illustrate flooding at the moderate threshold.

Flood Type	GWI Only		MI Only		DBF Only		Compound GWI and MI		Compound GWI and DBF		Compound MI and DBF		Compound GWI, MI, DBF		Total Area Inundated (km <sup>2</sup> )
	Area Inundated (km <sup>2</sup> )	% of Total	Area Inundated (km <sup>2</sup> )	% of Total	Area Inundated (km <sup>2</sup> )	% of Total	Area Inundated (km <sup>2</sup> )	% of Total	Area Inundated (km <sup>2</sup> )	% of Total	Area Inundated (km <sup>2</sup> )	% of Total	Area Inundated (km <sup>2</sup> )	% of Total	
<b>2017</b>	0.19	26.33	0.02	2.39	0.00	0.40	0.31	41.98	0.07	10.10	0.00	0.65	0.13	18.15	0.73
<b>Minor</b>	0.24	23.32	0.03	2.66	0.01	0.84	0.38	36.65	0.17	16.14	0.01	0.95	0.20	19.43	1.04
<b>Moderate</b>	0.63	24.74	0.06	2.31	0.10	3.74	0.50	19.56	0.19	7.52	0.08	3.17	0.99	38.95	2.54
<b>Major</b>	1.19	15.19	0.28	3.61	0.04	0.55	1.37	17.55	0.18	2.35	0.47	6.05	4.27	54.71	7.81

**Table 4-1:** Areas of flooding by individual and compound flood mechanisms within the study area encompassing Honolulu’s Primary Urban Core consisting of direct marine inundation (MI), drainage backflow (DBF), and groundwater inundation (GWI) at four flood thresholds: 2017 flood observations, minor, moderate, and major flood thresholds (Sweet et al., 2018).

Flood Threshold	Traffic Slowdowns (km)	Roadway Impassable (km)	Failed Storm Drains	Non-Functional Cesspools	Fully Flooded Cesspools
<b>2017</b>	0.61	0.00	110	619	11
<b>Minor</b>	1.33	0.03	200	620	18
<b>Moderate</b>	9.19	0.40	860	629	38
<b>Major</b>	53.88	4.66	2340	633	112

**Table 4-2:** Failed infrastructure: length of roadway (km) featuring traffic slowdowns because of dangerous driving conditions; length of roadway impassable by 4-wheel drive vehicles; number of drainage inlets that have no capacity for storm water and instead act as conduits for additional flooding; number of cesspools that are non-functional at filtering effluent and/or are fully flooded to the ground surface.

#### **4.3.1.1 Flood Threshold 2017**

Simulations were produced and qualitatively compared to flooding observed during king tide events in 2017 that produced record high water levels at the Honolulu tide station (National Oceanic and Atmospheric Administration (NOAA), 2017a; Thompson et al., 2019). Imagery from the 2017 king tide event were used to validate model results (Fig. 4-4).



**Figure 4-4:** Qualitative comparison of the 35 cm flood scenario in the Māpunapuna industrial area and observations during 2017 king tide events. Note that only the DBF and GWI mechanisms are shown; direct MI not observed.

#### 4.3.1.2 Minor Flood Threshold

Considering the minor flood threshold, we find that a total of approximately 1 km<sup>2</sup> will be inundated within the study area. Calculation of area impacted by specific mechanisms indicate that GWI will cover the largest area, as the majority of the flooding will be caused solely by GWI or by compound flooding of GWI and one of the other two mechanisms. Compound flooding by GWI and MI will inundate approximately 37% of the total flooded area, over 23% will be inundated solely by groundwater, and approximately 16% of the area will be inundated by combined GWI and DBF. The majority of the flooded area, approximately 73%, is vulnerable to compound flooding by at least two flood types. The area impacted by all three flood types represents more than 19% of the total flooded area. Note that the area flooded solely by MI accounts for less than 3% of the total inundation area, which is noteworthy given that it is generally the main mechanism envisioned by stakeholders when contemplating SLR generated flooding.

Infrastructure failure featured at the minor flood threshold includes 200 locations where drainage inlets will lose all capacity for drainage and begin acting as conduits for flooding. Flooding will cause 1.3 km of roadway across 22 separate roadway segments to be impassable by small vehicles. This includes three intersections concentrated mainly in the Māpunapuna industrial area, Waikīkī, Iwilei and southwest Hickam. A total of 620 failed cesspools are distributed across the study area. Of these, 18 will be flooded to the ground surface and the remaining 602 will be partially inundated. Most failed cesspools are located at the western extent of Iwilei and in Māpunapuna.

#### ***4.3.1.3 Moderate Flood Threshold***

Moderate flooding more than doubles the impacted area compared to minor flooding. Calculations of compound flood area (Tab. 4-1) indicate that the area impacted by all three flood types represents nearly 39% of the total flooding, which is double that featured by the minor threshold. GWI will also have a large impact, as nearly 25% will be caused solely by GWI. The area flooded solely by marine inundation remains at less than 3%.

Upon reaching the moderate flood threshold, infrastructure failure will be significantly magnified. Drainage failure will increase to 860 locations, a fourfold jump from the minor threshold; the length of dangerous roadway conditions will increase to 9.19 km, a nearly sevenfold jump from the minor threshold; and cesspools flooded to the ground surface will more than double. Locations that will host fully submerged cesspools are mainly centered in the Waikīkī area and surrounding neighborhoods, eastern and western Iwilei, and Māpunapuna. Compared to the minor threshold, there is a small increase in failed cesspools (629), a number that already represents roughly 90% of the total number of active cesspools in the study area.

#### ***4.3.1.4 Major Flood Threshold***

While the focus of this study is on near-term flood scenarios, calculation of impacts represented by the major flood threshold is included to illustrate the trajectory of expected flooding and infrastructure failure. Calculations illustrate two main findings; critical infrastructure and flood area multiply relative to the moderate threshold, and more than half of the total area flooded will be impacted by all three flood types. Thus, an increasing level of adaptation effort will be required to manage flooding if infrastructure is to remain at current elevations.

### 4.3.2 Frequency Analysis

Calculations following the methods of Thompson et al. (2019) illustrate the frequency at which sea levels are projected to exceed the minor and moderate flood thresholds (Fig. 4-5). For each decade, the average and maximum number of exceedance days per year are shown.

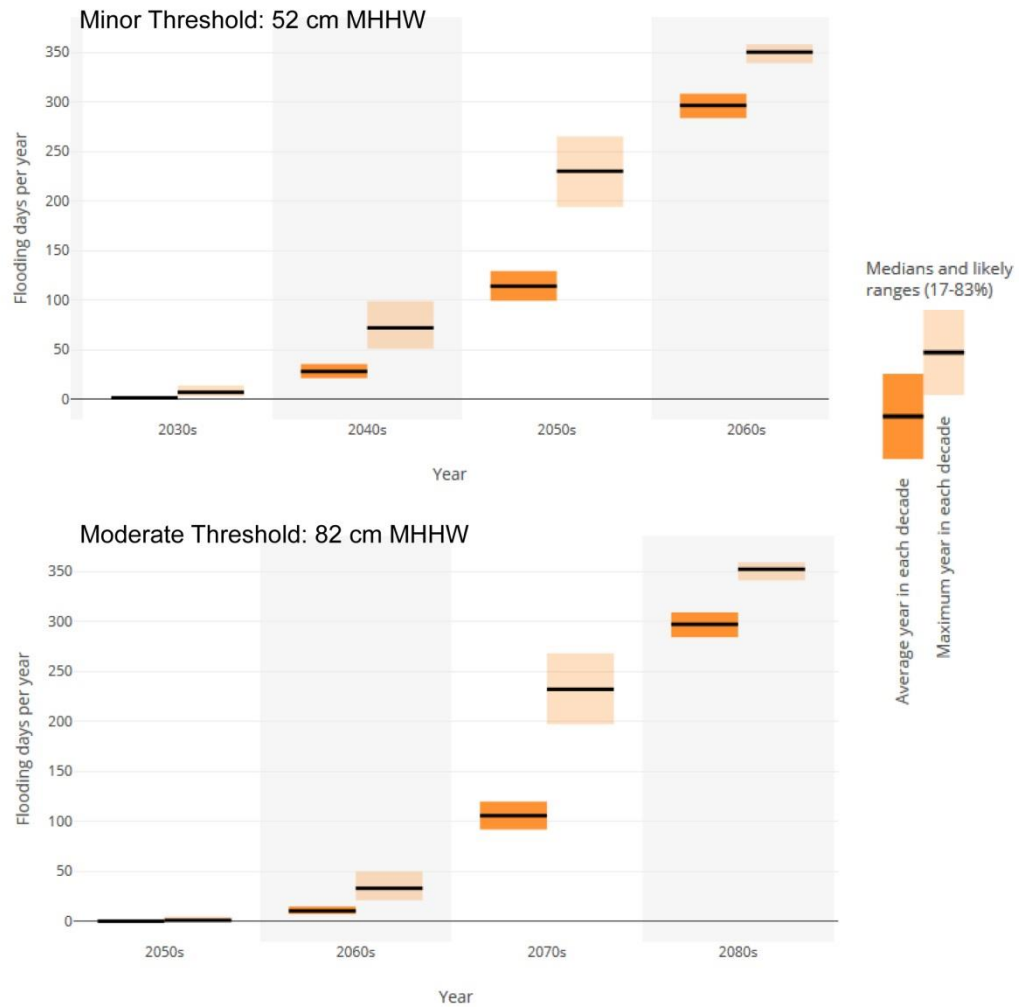


**Figure 4-5:** Days per year of exceedance for minor and moderate flooding per decade.

Exceedance of the minor flood threshold begins in the 2030s. By the 2040s this threshold is exceeded 28 days during the average year and as often as 72 days per year. By the 2050s exceedance occurs 114 days per year and beyond the 2050s exceedance is almost a daily phenomenon. Considering that the construction lifespan of an average building is generally 50 years (EN 1990, 2002), a structure constructed today would have an intended lifespan beyond the decade in which the minor flood scenario will become nearly a daily occurrence.

Exceedance of the moderate flood threshold begins in the 2050s. By the 2060s this threshold is exceeded 10 days during the average year, and by the 2070s exceedance occurs 105 days during the average year. Beyond the 2070s exceedance of the moderate flood threshold is nearly a daily phenomenon.

#### **4.4 Discussion**

Infrastructure design over the past century has relied heavily on coastal armoring, land reclamation, and channelized gravity-flow drainage to support urban expansion along the oceanfront. These projects were designed considering historical tide and flood levels. As sea level has risen, high-tide flooding has become increasingly common and extreme precipitation events have become more intense such that historically determined extreme conditions are more frequently surpassed. Thus, planning guidelines and development policies from the 20th century are now out-of-date. We can expect the progressive failure of critical infrastructure over the course of coming decades.

The three types of flooding simulated in this study are already problematic within the PUC. The most notable flood events were observed during the summer of 2017, when a combination of anomalously high mean sea levels and seasonally high tides contributed to record water levels reaching more than 35 cm above the MHHW datum at the Honolulu Tide Station (National Oceanic and Atmospheric Administration (NOAA), 2017a; Thompson et al., 2019). These events are a glimpse into the future.

Several types of infrastructure impacts were observed: roadway near the Honolulu International Airport was inundated by direct marine flooding; GWI impacted basements in urban Honolulu; drainage backflow produced flooding in underground parking garages and contributed to traffic congestion in western Waikīkī. Impacts resulting from the 2017 event, although relatively mild compared to impacts in other urban settings, revealed the advent of infrastructure failure within the PUC.

The minor and moderate flood thresholds simulated as part of this study have not yet been reached locally and represent an additional elevation of 0.17 and 0.47 m, respectively, beyond the 0.35 m threshold. We find that as water levels reach the minor threshold by the 2030s and moderate flood threshold by the 2050s, flooded area and infrastructure failure will escalate.

Exceedance of these thresholds will become nearly a daily phenomenon beyond the 2050s and 2070s, respectively.

The potential of roadway failure is a serious concern as the reduction in performance of transport systems has been identified as having some of the most detrimental impacts to society (Arkell and Darch, 2006; Hooper et al., 2014). Transportation systems are the main support for safety, commerce, and the economy, which has become increasingly reliant on the mobility of commodities, services, and people (Rodrigue and Notteboom, 2012).

To mitigate sea-level rise related impacts, simulations included as part of this study can be used to prioritize infrastructure upgrades, ideally as part of normal maintenance schedules by identifying locations in which initial failures are likely to occur. Flood scenarios identify initial roadway failure mainly in localized areas in Māpunapuna, Western Waikīkī, and Iwilei. Here we have focused on roadway failure owing to water depth and the inability of cars to traverse, although it is understood that damages such as rutting and potholing of roadways will likely also result from the presence of shallow water tables (Knott et al., 2017). Assessment of such damages is outside the scope of this study and is recommended for future work.

Failure of drainage infrastructure will partially contribute to roadway failure as drainage is generally located adjacent to transportation networks. DBF will become progressively widespread during high-tide events. During heavy rainfall events, there will be reduced means for the transport of storm water owing to the reduction of drainage capacity, especially during elevated tidal stages. Some municipalities have invested in one-way valves and pump systems to prevent drainage backflow (Burnett, 2015; Georgetown Climate Center, 2019). However, these systems can be costly and potentially ineffective as one-way valves are not designed to impede GWI that seeps in from unsealed or cracked pipes and, further, because pumps can be overwhelmed when their capacity is met.

Each of the three flood components we model presents its own challenges, complicating adaptation solutions where compound flooding occurs. Of the three components, GWI will flood the most extensive area in the PUC and will likely be the most difficult to manage. In locations such as the Netherlands and New Orleans, Louisiana the combination of flood mechanisms, including GWI, is managed by a mixture of hard structures (i.e., seawalls, levees) and pumping

to decrease the elevation of flood waters (Fischetti, 2001; Pellenbarg, 1997). However, responding to GWI in this manner has been found to cause subsidence and increase susceptibility to flooding, especially in areas of unconsolidated sediment (Fischetti, 2001; Holzer, 1984).

An additional and very serious concern regarding GWI involves the widespread contamination of groundwater across the PUC. Poor land-use and waste-management practices (i.e., contaminant spills, leaking underground storage tanks, cesspool use in areas lacking adequate unsaturated space) have contributed to a high level of contamination in groundwater and nearshore coastal waters in the PUC (State of Hawai'i Department of Health, 2019; Whittier and El-Kadi, 2014, 2009) (Fig.4-6). In areas susceptible to GWI, these contaminants potentially can reach the ground surface. As part of the suite of adaptation strategies considered for the PUC, focused efforts will be required to limit public contact with, and/or heavily remediate contaminated groundwater.



**Figure 4-6:** a) Hawai'i State Department of Health website (State of Hawai'i Department of Health, 2019) showing the number of leaking underground storage tanks identified across the State; b) photo showing a construction trench in which contaminated groundwater containing liquid petroleum hydrocarbon was unearthed.

Widespread failure of cesspool infrastructure likely contributes to the contamination of groundwater, which suggests the need for alternative methods of effluent treatment. Efforts are currently underway to phase out the use of cesspools by 2050 (The State of Hawai'i, 2017); however, if cesspools are allowed to remain in use up to the year 2050, ongoing contamination

will occur in concert with the progression of GWI at the ground surface. Further, with the finding that at least 18 presently active cesspools will be fully flooded by the 2040s given NOAA intermediate projections of SLR, total failure of these systems will begin to occur in highly vulnerable locations prior to the 2050 deadline. Thus, if elimination of cesspool systems cannot be accomplished within the next one or two decades, measures can be taken to prioritize removal and remediation of sites most likely to cause health concerns to the public. Finally, efforts to eliminate cesspools have largely involved replacement of cesspools with septic systems; however, in areas that will lack unsaturated space under future SLR projections, septic tanks would similarly be ineffective at treating effluent and should potentially be avoided.

Upcoming community planning projects provide an opportunity to prioritize adaptation strategies that address failing infrastructure. Honolulu is currently in the process of installing its first elevated rail transit system in which Transit Oriented Development (TOD) is being designed within 1.6 km radii of each rail station. TOD areas currently being designed encompass many of the most vulnerable areas identified here, with the exception of Waikīkī. The design of TODs is intended to host high-density mixed-use development that reduces parking requirements and enhances walkability, reducing the population's dependence on motor vehicles (The City and County of Honolulu, 2008). These projects present the opportunity to organize area-wide flood-mitigation strategies that can be tailored for each area. Nine distinct TOD areas being designed within the PUC are projected to experience flood impacts as soon as the 2030s (i.e., Lagoon Drive that encompasses the Māpunapuna area, Middle Street, Iwilei, Kapālama, Chinatown, Downtown, Civic Center, Kaka'ako, and Ala Moana). Lagoon Drive TOD area hosts the particularly vulnerable area of Māpunapuna that currently experiences chronic flooding. In development planning documentation for this area, the need for flood management is acknowledged (City and County of Honolulu Department of Planning and Permitting, 2017); however, drainage improvements are the only mention of adaptation measures, which will likely be an inadequate strategy owing to the extent of compound flooding projected in this area. In general, for the purpose of increasing resilience in the PUC, TOD design will require that adaptation is considered a priority. If flood prevention is included simply as an afterthought or includes consideration of only current extreme flood scenarios, the opportunity to improve resilience will be missed.

Overall, owing to the costly and complicated system of potentially ineffective methods typically considered to mitigate flooding, a more feasible approach may require vertical retreat. Such an approach would have the benefit of potentially mitigating each flood mechanism simultaneously by elevating above flood datums. Such an approach can be combined with installation of green multi-use infrastructure to accommodate flood water for the purpose of adding redundancy to the overall system of flood management. Green infrastructure can also be designed to partially remove contaminants before entering nearshore waters (Hughes et al., 2014).

As discussed, effective methods will likely include a combination of measures that entail vertical retreat and remediation of coastal groundwater, in part by removing failing sewage transport and treatment systems. With multiple projects in development, planners have the opportunity to incorporate adaptive strategies to address flooding for some of the most vulnerable parts of the PUC.

#### **4.5 Summary and Conclusion**

Government offices of Hawai'i have recognized the need to implement adaptive measures to mitigate flood impacts induced by SLR. By identifying locations and depths in which flooding is likely to occur and by combining results with annual exceedance frequencies, infrastructure can be adapted in an efficient manner such that critical municipal needs can continue to be met.

Here we produce a streamlined method of simulating locations and depths of flooding generated by three SLR-induced mechanisms. The method was produced by combining and adapting elements of previous flood-mapping efforts and frequency analyses specific to the study area. Frequencies of annual threshold exceedance are established using the methods of Thompson et al. (2019) that consider predicted tide and projections of SLR. Flood mechanisms assessed include direct marine flooding, drainage backflow, and groundwater inundation, which have not been explicitly simulated and assessed as a combined suite prior to this study.

Flood simulations are produced considering four flood thresholds; 0.35 m, representing known instances of nuisance flooding, and three others established by Sweet et al. (2018) expected to produce minor, moderate and major flood impacts in the Honolulu area. With the

combined method, near term scenarios of compound flooding are produced that consist of high-resolution, site-specific raster datasets featuring water depth generated by the three flood types. Because the majority of the PUC shoreline has been hardened, we do not include consideration of dynamic coastal processes (i.e., coastal erosion, wave run-up, changes in land cover).

To illustrate the utility of the method, we conduct a preliminary damage assessment by superimposing geospatial data that characterize locations of drainage, roadways, and cesspools, on flood simulations. We find that infrastructure failure is already occurring during periods of high tide, as illustrated by backflow of gravity drainage, by traffic slowdowns along submerged roadway, and by partial inundation of active cesspools. Considering the NOAA intermediate SLR scenario, the 2030s will feature localized stretches of roadway that become impassable to 4-wheel drive vehicles (i.e., emergency response vehicles) and drainage failure that is increasingly widespread. From the 2030s to 2050s infrastructure failure of each type assessed will multiply and the amount of area inundated concurrently by three types of flooding will increase fivefold. Here we show that flood-management strategies will require site-specific engineering projects that consider multiple flood types. Any failure to attend to each flood type individually will render flood management ineffective and may lead to a false sense, by key decision makers, that SLR adaptation has been achieved.

## **4.6 Appendix**

### **4.6.1 Supplementary Information on the Geohydrology of the Study Area**

The study area is situated to the southwest of the Ko‘olau volcanic range and atop a geologic unit referred to as caprock. The unit is composed of a combination of post-erosional volcanics, alluvial debris, and carbonate reef and lagoonal deposits that formed during Pleistocene sea-level variations (Finstick, 1996; Oki et al., 1998; Stearns and Vaksvik, 1935), and lies atop basalt flanks of the Ko‘olau Volcano.

Groundwater within the study area occurs mainly as a freshwater lens located in the basalt aquifer, and secondarily in the caprock aquifer (Gingerich and Oki, 2000). The lens floats atop saltwater due to density differences between saltwater and freshwater. Groundwater migrates down-gradient from areas of recharge to areas of coastal discharge (Souza and Voss, 1987) in which flow is partially obstructed owing to the lower permeability of caprock relative to basalt (Stearns, 1935). Groundwater levels in the caprock aquifer are influenced by various phenomena

including rainfall and marine oscillations (Gonneea et al., 2013; Ponte, 1994; Wu et al., 1996; Yin et al., 2001). Groundwater withdrawal from the caprock aquifer is minimal owing to the lack of potable water, and is mainly for use in cooling towers and for small-scale irrigation.

#### **4.6.2 Supplementary Information on Groundwater-Level Simulation**

The following data and methods were adopted from a study by Habel et al. (2017) and modified in accordance with Habel et al. (2019) unless otherwise noted (Habel et al., 2017, 2019).

##### ***4.6.2.1 Groundwater-Level Data***

Groundwater-level observations used in 3D model calibration and simulation of tidal influence included 247 discrete water-level observations obtained from Hawai‘i Department of Health Leaky Underground Storage Tank records (State of Hawai‘i Department of Health, 2019), and 73 sets of continuous water-level observations compiled from local hydrologic studies. Discrete groundwater-level observations were corrected for tidal influence and anomalous sea-surface height using the methods of Habel et al (2017).

##### ***4.6.2.2 3D Model Construction***

The method employs MODFLOW 2005 (Harbaugh, 2005), a 3D finite-difference flow model, to simulate steady-state conditions of the water table considering various magnitudes of sea-level rise. Subsurface hydrogeologic conditions were simulated based on conditions determined in regional studies (Ferrall, 1976; Finstick, 1996; Munro, 1981; Oki, 2005; Rotzoll and El-Kadi, 2007). The model consists of 48,483 active 100-m uniform grid cells and three layers that represent unconsolidated caprock (model layer 1), consolidated caprock (model layer 2), and basalt (model layer 3). The top of model layer 1 (unconsolidated caprock unit) is defined by mosaicked 2013 NOAA LiDAR topography data and 2013 US Army Corps of Engineers LiDAR bathymetry data (National Oceanic and Atmospheric Administration (NOAA), n.d.) and given a specified thickness of 10 m based on the approximate depth in which consolidated caprock material has been encountered in drilling studies (Ferrall, 1976; Finstick, 1996; Munro, 1981). Model layer 2 (consolidated caprock unit) extends from the base of layer 1 to the uppermost extent of model layer 3 (basalt unit), which was defined using elevation data that represents the uppermost extent of the basalt aquifer (Rotzoll and El-Kadi, 2007). Simulation of groundwater flow in the basalt aquifer is beyond the scope of this study; thus, model layer 3 is represented by a thin unit that extends an

arbitrary 1 m below the top of the layer and was included to simulate flow from the basalt into the caprock aquifer represented by model layers 1 and 2.

The inland boundary of the model is defined by the 0-m elevation contour representing the uppermost extent of the basalt aquifer (Rotzoll and El-Kadi, 2007). The seaward boundary is defined by the 200-m depth contour of 2013 US Army Corps of Engineers LiDAR bathymetry data (National Oceanic and Atmospheric Administration (NOAA), n.d.). With the exception of the inland boundary of layer 3, the model domain is bounded on the sides and base by no-flow boundaries; the upper-boundary is a specified recharge boundary. The inland lateral boundary of model layer 3 is a specified-head boundary that simulates flow from the basalt unit to the upper layers, in which specified-head values were based on simulations of confined groundwater flow in southern O‘ahu (Rotzoll and El-Kadi, 2007). Locations and withdrawal rates of pumped well locations available from the State Commission on Water Resource Management were adopted from existing groundwater-flow models representative of the Honolulu aquifer (Rotzoll and El-Kadi, 2007); only wells pumping from the caprock aquifer were considered. Withdrawal rates were defined using the arithmetic mean of respective pumping rates from 1996 to 2005. Recharge data were adopted from a mean annual water-budget model representing the Island of O‘ahu, Hawai‘i (Engott et al., 2017) that simulates processes including rainfall, fog interception, evapotranspiration, direct runoff, irrigation and return flow from septic systems. Seaward of the 0-m land-surface elevation contour, conditions of mean sea level were simulated using a specified general-head boundary at the ocean bottom with a conductance of  $10 \text{ m}^2\text{d}^{-1}$  and a general-head elevation of 0 m.

#### ***4.6.2.3 Model Calibration***

Model calibration was accomplished using discrete and continuous water-level measurements described previously. All groundwater-level observations were used for 3D model calibration, unlike the methods of Habel et al. (2019) in which groundwater-level observation datasets were subsampled for use in cross-validation analysis. The nonlinear inverse modeling utility, PEST, using Tikhonov preferred homogeneous regularization was employed to estimate hydraulic-conductivity values for model layer 1 representing the unconsolidated caprock unit (Doherty and Hunt, 2010); pilot points were established on 500-m grid across the study area, totaling 361 points. All post-calibration values applied to the unconsolidated caprock unit were within the range of values previously observed for the study area, ranging from 0.001 to 854 m/d

(Finstick, 1996) with an average value of 117.4 m/d and standard deviation of 271.0 m/d, which are comparable to values calculated in chapter 3 of 135.2 m/d and 288.5 m/d, respectively. Manual iterative adjustment was employed to estimate the hydraulic-conductivity value for layer 2, which was set to 1 m d<sup>-1</sup>. For layer 3 the hydraulic conductivity was set to 600 m d<sup>-1</sup> based on values employed in modeling studies that simulate local basalt aquifers (Izuka et al., 2018; Rotzoll and El-Kadi, 2007). Vertical anisotropy (Kh/Kv) was set to 3.0 for all layers.

The simulated mean residual water level and root-mean-squared error were 0.04 m and 0.12 m, respectively, following model calibration.

#### ***4.6.2.4 Simulation of SLR***

Increases in mean sea level were simulated by setting the general head to a value equal to that of the simulated sea-level increase. For example, an increase in mean sea level of 1 m is simulated by setting the value of general head to 1 m. Further, the landward extent of the general-head boundary was re-evaluated using the land-surface elevation contour equal to that of the simulated sea-level increase.

#### ***4.6.2.5 Limitations of the Groundwater Model***

Limitations of the modeling method have been summarized in Habel et al (2017) in which main limitations include:

- The model is steady state and thus does not assess time-dependent processes (i.e., variations in boundary flows, recharge, pumping rates, and groundwater storage, aperiodic short-term changes in sea level by phenomena such as tsunamis, storm-surges, etc.);
- MODFLOW-2005 assumes uniform density of water, and thus does not assess the influence of density-driven fluid flow including mixed seawater and freshwater flows;
- The model does not consider the following: flow that occurs in the unsaturated zone, surface-water flow, evaporation from surface-water sources, ponding or routing of waters that occur once groundwater breaches the ground surface, dynamic changes in landscape (i.e., erosion);

#### ***4.6.2.6 Calculation of Tidal Influence***

Groundwater-level oscillations are attenuated relative to oscillations in ocean water levels, increasing in temporal lag and decreasing in amplitude as they propagate inland. The influence of ocean oscillations was quantified for each set of continuous observations. Temporal lag was

evaluated by cross correlating tidal signals at the NOAA Honolulu Tide station with those observed in the groundwater data (National Oceanic and Atmospheric Administration (NOAA), 2017a). Tidal efficiency was calculated using linear least-squares regression of lag-corrected groundwater time series to tidal-signal data.

#### ***4.6.2.7 Application of Tidal Influence to Simulated Groundwater Levels***

Analytical solutions representing tidal influence on groundwater were evaluated for six subzones by performing regression analyses that assign tidal efficiency as an exponential function of distance from the coastline. Subzones represent the eastern (Waikīkī and surrounding neighborhoods), middle (Iwilei and surrounding neighborhoods), and western (Hickam area) extent of the study area. The western extent was further divided into four subzones to represent unique patterns of observed tidal efficiencies that correlated with distinct geologic strata that comprise the subsurface geology (i.e., fill, beach deposits, lagoon and reef deposits, and Honolulu Volcanics) (Sherrod et al., 2007). Tidal influence is expressed as increases in piezometric head considering the tidal half amplitude ( $h_0$ ) by the following analytical solutions in which  $h(x)$  is the increase in piezometric head (m), and  $x$  is the distance from the shoreline (m):

$$\begin{aligned}
 h(x)/h_0 &= e^{-0.002x} \text{ (eastern)} \\
 &= e^{-0.005x} \text{ (middle)} \\
 &= 0.55e^{-0.0007x} \text{ (western-fill)} \\
 &= 0.43e^{-0.001x} \text{ (western-beach deposits)} \\
 &= 0.44e^{-0.0004x} \text{ (western-lagoon and reef deposits)} \\
 &= 0.43e^{-0.0002x} \text{ (western-Honolulu Volcanics)}
 \end{aligned}$$

The computed tidal efficiencies are considered reasonable and consistent with the hydraulic properties based on the estimated diffusivities for these units.

The six analytical solutions were applied to a raster grid within respective subzone boundaries as a function of the distance of each grid cell to the simulated coastline. Raster values representing tidal efficiency were calculated by setting  $h_0$  to 0.33 (MHHW tide elevation relative to the MSL datum in meters). These values were summed with water-table raster data from the groundwater model output to generate the tidally influenced water-table height considering the MHHW tide stage.

## References Cited

- Anderson, T.R., Fletcher, C.H., Barbee, M.M., Romine, B.M., Lemmo, S., Delevaux, J.M., 2018. Modeling multiple sea level rise stresses reveals up to twice the land at risk compared to strictly passive flooding methods. *Sci. Rep.* 8, 14484. doi:10.1038/s41598-018-32658-x
- Arkell, B., Darch, G., 2006. Impacts of climate change on London's transport systems. *Proc. ICE–Municipal Eng.* 159, 231–237.
- Balaraman, K., 2016. Sewage Floods Likely to Rise [WWW Document]. *Clim. Wire*. URL <http://www.scientificamerican.com/article/sewage-floods-likely-to-rise/#> (accessed 10.20.16).
- Bierbaum, R., Smith, J.B., Lee, A., Blair, M., Carter, L., Chapin III, F.S., Fleming, P., Ruffo, S., Stults, M., McNeeley, S., 2013. A comprehensive review of climate adaptation in the United States: more than before, but less than needed. *Mitig. Adapt. Strateg. Glob. Chang.* 18, 361–406.
- Bjerklie, D.M., Mullaney, J.R., Stone, J.R., Skinner, B.J., Ramlow, M.A., 2012. Preliminary investigation of the effects of sea-level rise on groundwater levels in New Haven, Connecticut. Open-File Report 2012-1025.
- Budhu, M., Adiyaman, I.B., 2009. Mechanics of land subsidence due to groundwater pumping. *Int. J. Numer. Anal. Methods Geomech.* 34, 1459–1478. doi:10.1002/nag.863
- Burnett, J., 2015. Billions Spent On Flood Barriers, But New Orleans Still A 'Fishbowl' : NPR [WWW Document]. *Natl. Public Radio. All Things Considered*. URL <https://www.npr.org/2015/08/28/432059261/billions-spent-on-flood-barriers-but-new-orleans-still-a-fishbowl> (accessed 4.8.19).
- Carlson, E., 2016. Pacific Region Geodetic Advisor for NOAA's National Geodetic Survey. Email communication (May 5, 2016).
- Church, J.A., Clark, P.U., Cazenave, A., Gregory, J.M., Jevrejeva, S., Levermann, A., Merrifield, M.A., Milne, G.A., Nerem, R.S., Nunn, P.D., 2013. Sea level change. *Climate Change 2013: The Physical Science Basis. Contribution of Working Group I to the Fifth*

- Assessment Report of the Intergovernmental Panel on Climate Change. PM Cambridge University Press.
- City and County of Honolulu (CCH), 2016. CCH Data Download Site: Structures\_Facilities [WWW Document]. URL [http://gis.hicentral.com/datadictionary/Structure\\_Nga.htm](http://gis.hicentral.com/datadictionary/Structure_Nga.htm) (accessed 10.20.16).
- City and County of Honolulu Department of Planning and Permitting, 2017. Airport Area Transit-Oriented Development Plan: Public Review Draft.
- Climate Ready Boston, 2016. Climate Ready Boston: Final Report.
- Codiga, D.L., 2011. Unified Tidal Analysis and Prediction Using the UTide Matlab Functions. Technical Report 2011-01. Graduate School of Oceanography, University of Rhode Island, Narragansett, RI.
- Cooper, H.M., Chen, Q., 2013. Incorporating uncertainty of future sea-level rise estimates into vulnerability assessment: A case study in Kahului, Maui. *Clim. Change* 121, 635–647. doi:10.1007/s10584-013-0987-x
- Cooper, H.M., Chen, Q., Fletcher, C.H., Barbee, M.M., 2013. Assessing vulnerability due to sea-level rise in Maui, Hawai'i using LiDAR remote sensing and GIS. *Clim. Change* 116, 547–563. doi:10.1007/s10584-012-0510-9
- Cooper, H.M., Zhang, C., Selch, D., 2015. Incorporating uncertainty of groundwater modeling in sea-level rise assessment: a case study in South Florida. *Clim. Change* 129, 281–294. doi:10.1007/s10584-015-1334-1
- Cooper, J.A., Loomis, G.W., Amador, J.A., 2016. Hell and High Water: Diminished Septic System Performance in Coastal Regions Due to Climate Change. *PLoS One* 11, e0162104.
- de Moel, H., Vliet, M. van, Aerts, J.C.J.H., 2014. Evaluating the effect of flood damage-reducing measures: a case study of the unembanked area of Rotterdam, the Netherlands. *Reg. Environ. Chang.* 14, 895. doi:10.1007/s10113-013-0420-z

- DeConto, R.M., Pollard, D., 2016. Contribution of Antarctica to past and future sea-level rise. *Nature* 531, 591–597.
- Department of Business: Economic Development and Tourism, 2003. The Economic Contribution of Waikīkī [WWW Document]. URL [http://files.hawaii.gov/dbedt/economic/data\\_reports/e-reports/econ\\_waikiki.pdf](http://files.hawaii.gov/dbedt/economic/data_reports/e-reports/econ_waikiki.pdf) (accessed 10.20.16).
- Department of Health, 2004. Hawai‘i Administrative Rules, Title 11, Department of Health, Chapter 62, Wastewater Systems.
- Department of Transportation, H.D., n.d. Planning Process & Principles — Honolulu Harbor 2050 Master Plan [WWW Document]. URL <https://honoluluharbormp.com/planning> (accessed 2.23.19).
- Dillinger, J., 2019. Highest Population Densities by US Metropolitan Areas - WorldAtlas.com [WWW Document]. worldatlas. URL <https://www.worldatlas.com/articles/the-most-crowded-city-in-the-united-states.html> (accessed 5.11.19).
- Doherty, J., 2008. Groundwater data utilities: Brisbane. *Aust. Watermark Numer. Comput.*
- Doherty, J.E., Hunt, R.J., 2010. Approaches to highly parameterized inversion: a guide to using PEST for groundwater-model calibration. US Department of the Interior, US Geological Survey.
- EN 1990, 2002. Eurocode - Basis of structural design (Authority: The European Union Per Regulation 305/2011, Directive 98/34/EC, Directive 2004/18/EC).
- Engott, J.A., Johnson, A.G., Bassiouni, M., Izuka, S.K., Rotzoll, K., 2017. Spatially distributed groundwater recharge for 2010 land cover estimated using a water-budget model for the Island of O‘ahu, Hawai‘i, Scientific Investigations Report. Reston, VA.  
doi:10.3133/sir20155010
- Ferrall, C.C., 1976. Subsurface geology of Waikīkī, Moili‘ili and Kaka‘ako with engineering application. University of Hawai‘i, Mānoa.

- Finstick, S.A., 1996. Subsurface geology and hydrogeology of downtown Honolulu with engineering and environmental implications. Water Resources Research Center, University of Hawai'i at Mānoa.
- Firing, Y.L., Merrifield, M.A., 2004. Extreme sea level events at Hawai'i: Influence of mesoscale eddies. *Geophys. Res. Lett.* 31.
- Fischetti, M., 2001. Drowning New Orleans. *Sci. Am.* 285, 76–85.
- FitzGerald, D.M., Fenster, M.S., Argow, B.A., Buynevich, I. V, 2008. Coastal impacts due to sea-level rise. *Annu. Rev. Earth Planet. Sci.* 36.
- Georgetown Climate Center, 2019. Miami Beach Stormwater Infrastructure Adaptation | Adaptation Clearinghouse [WWW Document]. Adapt. Clear. URL <https://www.adaptationclearinghouse.org/resources/miami-beach-stormwater-infrastructure-adaptation.html> (accessed 4.9.19).
- Gesch, D.B., 2009. Analysis of Lidar Elevation Data for Improved Identification and Delineation of Lands Vulnerable to Sea-Level Rise. *J. Coast. Res.* 49–58. doi:10.2112/SI53-006.1
- Gillis, J., 2016. Flooding of Coast, Caused by Global Warming, Has Already Begun. *New York Times*.
- Gilmer, B., Ferdaña, Z., 2012. Developing a Framework for Assessing Coastal Vulnerability to Sea Level Rise in Southern New England, USA. Springer, Dordrecht, pp. 25–36. doi:10.1007/978-94-007-4223-9\_4
- Gingerich, S.B., Oki, D.S., 2000. Ground water in Hawai'i Fact Sheet 126-00. US Geological Survey.
- Gonnea, M.E., Mulligan, A.E., Charette, M.A., 2013. Climate-driven sea level anomalies modulate coastal groundwater dynamics and discharge. *Geophys. Res. Lett.* 40, 2701–2706.
- Gornitz, V., Couch, S., Hartig, E.K., 2001. Impacts of sea level rise in the New York City metropolitan area. *Glob. Planet. Change* 32, 61–88. doi:10.1016/S0921-8181(01)00150-3
- Gregory, K., 2013. Where streets flood with the tide, a debate over city aid. *New York Times*.

- Habel, S., Fletcher, C.H., Rotzoll, K., El-Kadi, A.I., 2017. Development of a model to simulate groundwater inundation induced by sea-level rise and high tides in Honolulu, Hawai‘i. *Water Res.* 114, 122–134. doi:10.1016/j.watres.2017.02.035
- Habel, S., Fletcher, C.H., Rotzoll, K., El-Kadi, A.I., Oki, D.S., 2019. Comparison of a simple hydrostatic and a data-intensive 3D numerical modeling method of simulating sea-level rise induced groundwater inundation for Honolulu, Hawai‘i, USA. *Environ. Res. Commun.* 1, 041005. doi:10.1088/2515-7620/ab21fe
- Hallegatte, S., Green, C., Nicholls, R.J., Corfee-Morlot, J., 2013. Future flood losses in major coastal cities. *Nat. Clim. Chang.* 3, 802–806. doi:10.1038/nclimate1979
- Harbaugh, A.W., 2005. MODFLOW-2005, the US Geological Survey modular ground-water model: the ground-water flow process. US Geological Survey Reston, VA, USA.
- Hawai‘i Climate Change Mitigation and Adaptation Commission, 2017. Hawai‘i Sea Level Rise Vulnerability and Adaptation Report. Prepared by Tetra Tech, Inc. and the State of Hawai‘i Department of Land and Natural Resources, Office of Conservation and Coastal Lands, under the State of Hawai‘i Department of Land and Natural.
- Hawai‘i State Department of Business Economic Development & Tourism, 2018. Hawai‘i State Data Book, Tables 7.33 and 7.34.
- Henman, J., Poulter, B., 2008. Inundation of freshwater peatlands by sea level rise: uncertainty and potential carbon cycle feedbacks. *J. Geophys. Res. Biogeosciences* 113.
- Hinkel, J., Lincke, D., Vafeidis, A.T., Perrette, M., Nicholls, R.J., Tol, R.S.J., Marzeion, B., Fettweis, X., Ionescu, C., Levermann, A., 2014. Coastal flood damage and adaptation costs under 21st century sea-level rise. *Proc. Natl. Acad. Sci.* 111, 3292–3297. doi:10.1073/pnas.1222469111
- Holzer, T.L., 1984. Man-induced Land Subsidence: Groundwater Failure Induced by Groundwater Withdrawal from Unconsolidated Sediment. *Geol. Soc. Am. Rev. Eng. Geol.* 6.

- Honolulu Board of Water Supply, 2005. John A. Burns School of Medicine Kaka'ako, O'ahu, Hawai'i Kaka'ako Cold Seawater Cooling System Injection Well UIC Application UO-2287.
- Honolulu Dredging Construction Company, I., n.d. Our History - Progress powered by over 10 decades [WWW Document]. URL <http://www.hdcc.com/about-2/about-3/> (accessed 2.23.19).
- Hooper, E., Chapman, L., Quinn, A., 2014. Investigating the impact of precipitation on vehicle speeds on UK motorways. *Meteorol. Appl.* 21, 194–201.
- Horton, R., Little, C., Gornitz, V., Bader, D., Oppenheimer, M., 2015. New York City Panel on Climate Change 2015 Report Chapter 2: Sea Level Rise and Coastal Storms. *Ann. N. Y. Acad. Sci.* 1336, 36–44. doi:10.1111/nyas.12593
- Horton, R.E., 1933. The role of infiltration in the hydrologic cycle. *Eos, Trans. Am. Geophys. Union* 14, 446–460.
- Hughes, R.M., Dunham, S., Maas-Hebner, K.G., Yeakley, J.A., Schreck, C., Harte, M., Molina, N., Shock, C.C., Kaczynski, V.W., Schaeffer, J., 2014. A Review of Urban Water Body Challenges and Approaches: (1) Rehabilitation and Remediation. *Fisheries* 39, 18–29. doi:10.1080/03632415.2013.836500
- Izuka, S.K., Engott, J.A., Rotzoll, K., Bassiouni, M., Johnson, A.G., Miller, L.D., Mair, A., 2018. Volcanic aquifers of Hawai'i—Hydrogeology, water budgets, and conceptual models, Scientific Investigations Report. doi:10.3133/sir20155164
- Kane, H.H., Fletcher, C.H., Frazer, N.F., Barbee, M.M., 2015. Critical elevation levels for flooding due to sea-level rise in Hawai'i. *Reg. Environ. Chang.* 15, 1679.
- Knott, J.F., Elshaer, M., Daniel, J.S., Jacobs, J.M., Kirshen, P., 2017. Assessing the Effects of Rising Groundwater from Sea Level Rise on the Service Life of Pavements in Coastal Road Infrastructure. *Transp. Res. Rec. J. Transp. Res. Board* 2639, 1–10. doi:10.3141/2639-01

- Kopp, R.E., DeConto, R.M., Bader, D.A., Hay, C.C., Horton, R.M., Kulp, S., Oppenheimer, M., Pollard, D., Strauss, B.H., 2017. Evolving understanding of Antarctic ice-sheet physics and ambiguity in probabilistic sea-level projections. *Earth's Futur.* 5, 1217–1233.
- Kopp, R.E., Hay, C.C., Little, C.M., Mitrovica, J.X., 2015. Geographic variability of sea-level change. *Curr. Clim. Chang. Reports* 1, 192–204.
- Kopp, R.E., Horton, R.M., Little, C.M., Mitrovica, J.X., Oppenheimer, M., Rasmussen, D.J., Strauss, B.H., Tebaldi, C., 2014. Probabilistic 21st and 22nd century sea-level projections at a global network of tide-gauge sites. *Earth's Futur.* 2, 383–406. doi:10.1002/2014EF000239
- Kulp, S., Strauss, B.H., 2017. Rapid escalation of coastal flood exposure in US municipalities from sea level rise. *Clim. Change* 142, 477–489. doi:10.1007/s10584-017-1963-7
- Langevin, C.D., Shoemaker, W.B., Guo, W., 2003. SEAWAT-2000: A Version of MODFLOW-2000 with the Variable-Density Flow Process and the Integrated MT3DMS Transport Process, US Geological Survey Open-File Report.
- Lentz, E.E., Stippa, S.R., Thieler, E.R., Plant, N.G., Gesch, D.B., Horton, R.M., 2015. Evaluating Coastal Landscape Response to Sea-Level Rise in the Northeastern United States-Approach and Methods.
- Li, L., Barry, D.A., 2000. Wave-induced beach groundwater flow. *Adv. Water Resour.* 23, 325–337.
- LiDAR Online, 2017. Lidar Online: Worldwide LiDAR data and geoservices [WWW Document]. URL <https://www.lidar-online.com/> (accessed 7.3.17).
- Macdonald, G.A., Abbott, A.T., Peterson, F.L., 1983. *Volcanoes in the sea: the geology of Hawai'i*. University of Hawai'i Press.
- Marcy, D., Brooks, W., Draganov, K., Hadley, B., Haynes, C., Herold, N., McCombs, J., Pendleton, M., Ryan, S., Schmid, K., Sutherland, M., Waters, K., 2011. New Mapping Tool and Techniques for Visualizing Sea Level Rise and Coastal Flooding Impacts, in: *Solutions to Coastal Disasters 2011*. American Society of Civil Engineers, Reston, VA, pp. 474–490. doi:10.1061/41185(417)42

- Mitchell, M., Herschner, C.H., Herman, J.D., Schatt, D.E., Eggington, E., Resources, and C. for C., Management., 2013. Recurrent flooding study for Tidewater Virginia. Virginia Institute of Marine Science. College of William and Mary. doi:10.21220/V5TG79
- Munro, K., 1981. The subsurface geology of Pearl Harbor with engineering application. University of Hawai'i, Geology and Geophysics.
- National Ecological Observatory Network (NEON), n.d. Open data to understand changing ecosystems [WWW Document]. 2017. URL <http://www.neonscience.org/data/airborne-data> (accessed 7.3.17).
- National Oceanic and Atmospheric Administration (NOAA), 2017a. Tide Station 1612340 Station Info [WWW Document]. URL <http://tidesandcurrents.noaa.gov/inventory.html?id=1612340> (accessed 10.20.16).
- National Oceanic and Atmospheric Administration (NOAA), 2017b. Digital Coast [WWW Document]. URL <https://coast.noaa.gov/digitalcoast/> (accessed 10.20.16).
- National Oceanic and Atmospheric Administration (NOAA), 2016. Station Data Inventory: BERETANIA PUMP STATION 7, HI US, GHCND:USC00510211 [WWW Document]. URL [http://www.ncdc.noaa.gov/cdo-web/datasets/NORMAL\\_MLY/stations/GHCND:USC00510211/detail](http://www.ncdc.noaa.gov/cdo-web/datasets/NORMAL_MLY/stations/GHCND:USC00510211/detail) (accessed 10.20.16).
- National Oceanic and Atmospheric Administration (NOAA), n.d. United States Interagency Elevation Inventory [WWW Document]. 2017. URL <https://coast.noaa.gov/inventory/> (accessed 7.3.17).
- National Oceanic and Atmospheric Administration (NOAA) Digital Coast, 2017. Data Access Viewer [WWW Document]. URL <https://www.coast.noaa.gov/dataviewer/#/lidar/search/> (accessed 7.3.17).
- National Research Council (NRC), 2011. National security implications of climate change for U.S. naval forces. National Academies Press, Washington. D.C.

- Nerem, R.S., Chambers, D., Choe, C., Mitchum, G.T., 2010. Estimating Mean Sea Level Change from the TOPEX and Jason Altimeter Missions. *Mar. Geod.* 33.  
doi:10.1080/01490419.2010.491031
- New Jersey Department of Environmental Protection (NJDEP), 2013. Christie administration announces post–superstorm Sandy flood mitigation studies by New Jersey universities [WWW Document]. URL [http://www.state.nj.us/dep/newsrel/2013/13\\_0091.htm](http://www.state.nj.us/dep/newsrel/2013/13_0091.htm)
- Nicholls, R.J., 1995. Coastal megacities and climate change. *GeoJournal* 37, 369–379.
- NOAA Office for Coastal Management, 2019. Flood Exposure Snapshot: Honolulu County, Hawai‘i [WWW Document]. URL <https://coast.noaa.gov/snapshots/#/process?action=flood&state=15&county=003&bounds=-178.74211461107046,20.857703426083507,-157.25181440948913,28.80739311549053> (accessed 5.11.19).
- Office of Resilience, Department of Regulatory and Economic Resources, Miami-Dade County, F., 2016. Assessment of Available Tools to Create a More Resilient Transportation System.
- Oki, D.S., 2005. Numerical simulation of the effects of low-permeability valley-fill barriers and the redistribution of ground-water withdrawals in the Pearl Harbor area, O‘ahu, Hawai‘i. Scientific Investigations Report 2005-5253. US Geological Survey.
- Oki, D.S., Souza, W.R., Bolke, E.L., Bauer, G.R., 1998. Numerical analysis of the hydrogeologic controls in a layered coastal aquifer system, O‘ahu, Hawai‘i, USA. *Hydrogeol. J.* 6, 243–263.
- OpenTopography, 2017. OpenTopography: High-Resolution Topography Data and Tools [WWW Document]. URL <http://opentopo.sdsc.edu/datasets> (accessed 7.3.17).
- Pellenburg, N.P., 1997. Groundwater Management in the Netherlands: Background and Legislation. *ILRA Work. Groundw. Manag.* 137–149.
- Photo Science Inc., 2013. Airborne Topographic LiDAR Report: O‘ahu, Hawai‘i. Post Flight Aerial Acquisition and Calibrated Report to USGS. Contract No. G10PC00026.

- Ponte, R.M., 1994. Understanding the relation between wind-and pressure-driven sea level variability. *J. Geophys. Res. Ocean.* 99, 8033–8039.
- Poulter, B., Halpin, P.N., 2008. Raster modelling of coastal flooding from sea-level rise. *Int. J. Geogr. Inf. Sci.* 22, 167–182. doi:10.1080/13658810701371858
- Pregolato, M., Ford, A., Wilkinson, S.M., Dawson, R.J., 2017. The impact of flooding on road transport: A depth-disruption function. *Transp. Res. Part D Transp. Environ.* 55, 67–81. doi:10.1016/J.TRD.2017.06.020
- Prothero, A., 2013. What South Florida’s Spring Tide (Or King Tide) Looks Like [WWW Document]. WLRN-TV. URL <http://wlrn.org/post/what-south-floridas-spring-tide-or-king-tide-looks> (accessed 10.20.16).
- Rodrigue, J.-P., Notteboom, T., 2012. Transportation and economic development, in: *The Geography of Transport Systems*.
- Rotzoll, K., El-Kadi, A.I., 2008. Estimating hydraulic properties of coastal aquifers using wave setup. *J. Hydrol.* 353, 201–213. doi:10.1016/j.jhydrol.2008.02.005
- Rotzoll, K., El-Kadi, A.I., 2007. Numerical ground-water flow simulation for Red Hill fuel storage facilities, NAVFAC Pacific, O’ahu, Hawai’i, University of Hawai’i & Water Resources Research Center, prepared for TEC Inc., Honolulu, Hawai’i.
- Rotzoll, K., Fletcher, C.H., 2013. Assessment of groundwater inundation as a consequence of sea-level rise. *Nat. Clim. Chang.* 3, 477–481.
- Rotzoll, K., Oki, D.S., El-Kadi, A.I., 2010. Changes of freshwater-lens thickness in basaltic island aquifers overlain by thick coastal sediments. *Hydrogeol. J.* 18, 1425–1436. doi:10.1007/s10040-010-0602-4
- Rutgers University, n.d. NJADAPT [WWW Document]. URL <http://www.njadapt.org/> (accessed 7.8.17).

- Savonis, M.J., Burkett, V.R., Potter, J.R., 2008. Impacts of climate change and variability on transportation systems and infrastructure: Gulf coast study, Phase I. US Climate Change Science Program.
- Sherman, C.E., Fletcher, C.H., Rubin, K.H., 1999. Marine and meteoric diagenesis of Pleistocene carbonates from a nearshore submarine terrace, O‘ahu, Hawai‘i. *J. Sediment. Res.* 69.
- Sherrod, D.R., Sinton, J.M., Watkins, S.E., and Brunt, K.M., 2007. Geologic Map of the State of Hawai‘i: U.S. Geological Survey Open-File Report 2007-1089, US geological survey open-file report.
- Souza, W.R., Voss, C.I., 1987. Analysis of an anisotropic coastal aquifer system using variable-density flow and solute transport simulation. *J. Hydrol.* 92, 17–41.
- Spada, G., Bamber, J.L., Hurkmans, R., 2013. The gravitationally consistent sea-level fingerprint of future terrestrial ice loss. *Geophys. Res. Lett.* 40, 482–486.
- Spanger-Siegfried, E., Fitzpatrick, M., Dahl, K., 2014. Encroaching tides: How sea level rise and tidal flooding threaten US east and gulf coast communities over the next 30 years. Cambridge, MA.
- State of Hawai‘i Department of Health, 2019. Environmental Health Warehouse [WWW Document]. URL <http://eha-web.doh.hawaii.gov/ehw/>
- State of Hawai‘i Office of Planning, 2016. Hawai‘i Statewide GIS Program: Download GIS Data [WWW Document]. URL <http://planning.hawaii.gov/gis/download-gis-data/> (accessed 10.20.16).
- Stearns, H.T., 1935. Pleistocene shore lines on the islands of O‘ahu and Maui, Hawai‘i. *Geol. Soc. Am. Bull.* 46, 1927–1956.
- Stearns, H.T., Vaksvik, K.N., 1935. Geology and ground-water resources of the island of O‘ahu, Hawai‘i. Maui Publishing Company, Limited.

- Sterling, R., Nelson, P., 2013. City resiliency and underground space use. *Adv. Undergr. Sp. Dev.* Singapore ACUUS.
- Strauss, B.H., Ziemiński, R., Weiss, J.L., Overpeck, J.T., 2012. Tidally adjusted estimates of topographic vulnerability to sea level rise and flooding for the contiguous United States. *Environ. Res. Lett.* 7, 14033.
- Sweet, W. V., Kopp, R.E., Weaver, C.P., Obeysekera, J., Horton, R.M., Thieler, E.R., Zervas, C., 2017. Global and Regional Sea Level Rise Scenarios for the United States. NOAA Technical Report NOS CO -OPS 083. Silver Spring, Maryland.
- Sweet, W. V, Dusek, G., Obeysekera, J., Marra, J.J., 2018. Patterns and projections of high tide flooding along the US coastline. NOAA Tech. Rep. NOS CO-OPS 86.
- Sweet, W. V, Park, J., 2014. From the extreme to the mean: Acceleration and tipping points of coastal inundation from sea level rise. *Earth's Futur.* 2, 579–600.
- Sweet, W.V., 2014. Sea level rise and nuisance flood frequency changes around the United States. NOAA Technical Report NOS CO-OPS 073.
- The City and County of Honolulu, 2008. A Bill For an Ordinance Relating to Transit-Oriented Development. Honolulu Hawai'i City Council, Honolulu.
- The New York State Sea Level Rise Task Force, 2010. New York State Sea Level Rise Task Force: Report to the Legislature. New York.
- The State of Hawai'i, 2017. Act 125, HB1244 Relating to Cesspools. House of Representatives Twenty-Ninth Legislature.
- Thompson, P.R., Widlansky, M.J., Merrifield, M.A., Becker, J.M., Marra, J.J., 2019. A statistical model for frequency of coastal flooding in Honolulu, Hawai'i during the 21st century. *J. Geophys. Res. Ocean.* 2018JC014741. doi:10.1029/2018JC014741
- Turner, I.L., Coats, B.P., Acworth, R.I., 1997. Tides, waves and the super-elevation of groundwater at the coast. *J. Coast. Res.* 46–60.

- U.S. Army Corps of Engineers (USACE) National Coastal Mapping Program (NCMP), 2017. Joint Airborne Lidar Bathymetry Technical Center of Expertise [WWW Document]. URL <http://shoals.sam.usace.army.mil/Mapping.aspx> (accessed 5.9.17).
- United States Geological Survey (USGS), n.d. EarthExplorer [WWW Document]. 2017. URL <https://earthexplorer.usgs.gov/> (accessed 7.3.17).
- University of Hawai‘i Sea Grant, 2019. Hawai‘i and Pacific Islands King Tides Project – Hawai‘i Sea Grant [WWW Document]. URL <http://seagrant.soest.hawaii.edu/coastal-and-climate-science-and-resilience/ccs-projects/hawaii-pacific-islands-king-tides-project/> (accessed 4.14.19).
- US Army Corps of Engineers (USACE), 2013. Coastal Risk Reduction and Resilience: Using the Full Array of Measures.
- Veiga, C., 2014. Miami Beach to spend up to \$400 million to deal with flooding issues. Miami Her.
- Visher, F. N., Mink, J. F., 1964. Ground-water resources in southern O‘ahu, Hawai‘i. U.S. Geological Survey Water-Supply Paper 1778.
- Whittier, R.B., El-Kadi, A., 2014. Human health and environmental risk ranking of on-site sewage disposal systems for the Hawaiian Islands of Kauai, Molokai, Maui, and Hawai‘i, Final report prepared for State of Hawai‘i Department of Health, Safe Drinking Water Branch.
- Whittier, R.B., El-Kadi, A.I., 2009. Human and Environmental Risk Ranking of Onsite Sewage Disposal Systems, Final, Department of Geology & Geophysics, University of Hawai‘i at Mānoa.
- Whittier, R.B., Rotzoll, K., Dhal, S., El-Kadi, A.I., Ray, C., Chang, D., 2010. Groundwater source assessment program for the State of Hawai‘i, USA: Methodology and example application. *Hydrogeol. J.* 18, 711–723.

- Wiegel, R.L., 2008. Waikīkī Beach, O‘ahu, Hawai‘i: History of its transformation from a natural to an urban shore. *Shore and Beach* 76, 3.
- Wu, J., Zhang, R., Yang, J., 1996. Analysis of rainfall-recharge relationships. *J. Hydrol.* 177, 143–160.
- Yin, B., Hou, Y., Cheng, M., Su, J., Lin, M., Li, M., El-Sabh, M.I., 2001. Numerical study of the influence of waves and tide-surge interaction on tide-surges in the Bohai Sea. *Chinese J. Oceanol. Limnol.* 19, 97–102.